FORMULATION OF CONTROL ALGORITHMS FOR GRID INTERACTIVE INVERTERS IN POWER QUALITY ENHANCED MICROGRID SYSTEM

A Project Report

submitted by

LINO ABRAHAM

in partial fulfilment of the requirements
for the award of the degree of

MASTER OF TECHNOLOGY

DEPARTMENT OF ELECTRICAL ENGINEERING
INDIAN INSTITUTE OF TECHNOLOGY MADRAS.

MAY 2013

THESIS CERTIFICATE

This is to certify that the thesis titled **FORMULATION OF CONTROL ALGORITHMS FOR GRID INTERACTIVE INVERTERS IN POWER QUALITY ENHANCED MICROGRID SYSTEM**, submitted by **LINO ABRAHAM**, to the Indian Institute of Technology, Madras, for the award of the degree of **Master of Technology**, is a bona fide record of the research work done by him under my supervision. The contents of this thesis, in full or in parts, have not been submitted to any other Institute or University for the award of any degree or diploma.

Dr. Mahesh Kumar
(Project Guide)
Professor
Dept. of Electrical Engineering
IIT-Madras, 600 036

Place: Chennai

Date: 1st May 2013

ACKNOWLEDGEMENTS

It gives me great pleasure in expressing my sincere and heartfelt gratitude to my project guide Prof. Mahesh Kumar for his excellent guidance, motivation and constant support throughout my project . I consider myself extremely fortunate to have had a chance to work under his supervision. In spite of his hectic schedule he was always approachable and took his time off to discuss problems and give his advice and encouragement. It has been a very learning and enjoyable experience to work under him.

I am also grateful for the laboratory facilities provided by him in the Power Quality Simulation Laboratory, ESB 342, Department of Electrical Engineering, which facilitated my simulation work.

My appreciation to my fellow research scholars in the Power Simulation Laboratory, especially Chandan and Sijo for spending their invaluable time with me, in discussing about the project and answering my queries, goes well beyond words. I would also extend my thanks to Nagesh, Manojkumar, K. Sathish Kumar ,Narasa Reddy, Suma, Onkar and Venu for their support during my work.

I would like to extend my thanks to my friends Arun, Cyril, and Shenil for their companionship and encouragement which made my stay in the IIT Madras campus, a memorable one.

This work could not have come to this stage without the support and encouragement from my family. My heartfelt thanks to all of them.

ABSTRACT

KEYWORDS: Microgrid;Grid Interactive Inverter;Grid Connected Mode;Islanded Mode;Power Quality;

Microgrid is a solution for power generation schemes, comprising of local generation and storage facilities. Microgrid is interfaced on to the utility grid with a grid interactive inverter. Microgrid can operate either in grid connected mode or in islanded mode. Maintaining power quality is another challenge which is faced by modern power system. The increased application of power electronics has turned most of the power system loads into non-linear loads. Therefore it is essential to compensate this unbalanced and nonlinear load. Developing control algorithms which adds nonlinear load compensation capability into the microgrid systems will make microgrids more efficient.

It has been observed that various transformations in power engineering has been made used to formulate control algorithms for microgrid systems. Therefore a study on various transformation has been made, and the transformed voltages for when various voltage profiles in *abc* reference frames are transformed have been studied. A generalized $\alpha\beta 0$ and *dq0* transformation has been developed for the ease of obtaining transformation matrices. Control strategies has been developed using these transformations and a comparison study has been conducted among the different control strategies.

A dual voltage source inverter scheme is prposed for microgrid system, which enhances the power quality and reliability of the microgrid system. The scheme comprises of two inverters namely the main inverter and the auxiliary inverter. This scheme enables the microgrid to exchange power generated by the distributed energy resources to the loads and in addition to this compensate unbalanced and nonlinear load. The grid connected mode and islanded mode of operations of the the scheme are studied.

TABLE OF CONTENTS

LIST OF TABLES

LIST OF FIGURES

ABBREVIATIONS

DER	Distributed Energy Resources
DG	Distributed Generator
PV	Photovoltaic
WES	Wind Energy System
CB	Circuit Breaker
PSCAD	Power System Computer Aided Design
PI	Proportional and Integral
DC	Direct Current
PCC	Point of Common Coupling
VSI	Voltage Source Inverter
PWM	Pulse Width Modulation
THD	Total Harmonic Distortion
PLL	Phase Locked Loop
VCO	Voltage Controlled Oscillator
DVSI	Dual Voltage Source Inverter

NOTATION

v_a, v_b, v_c	Instantaneous voltages in *abc* frame, V
v_α, v_β, v_0	Instantaneous voltages in $\alpha\beta 0$ frame, V
v_d, v_q, v_0	Instantaneous voltages in *dq0* frame, V
v_{ta}, v_{tb}, v_{tc}	PCC Voltages in phase-a, b and c respectively, V
i_{la}, i_{lb}, i_{lc}	Instantaneous load currents in phase-a, b and c respectively, A
$i_{\mu ga}, i_{\mu gb}, i_{\mu gc}$	Instantaneous microgrid currents in phase-a, b and c respectively, A
i_{ga}, i_{gb}, i_{gc}	Instantaneous utility grid currents in phase-a, b and c respectively, A
$i_{\mu gma}, i_{\mu gmb}, i_{\mu gmc}$	Instantaneous main inverter currents in phase-a, b and c respectively, A
$i_{\mu gxa}, i_{\mu gxb}, i_{\mu gxc}$	Instantaneous auxiliary inverter currents in phase-a, b and c respectively, A
L_f	Main Inverter Interface Inductance , mH
L_x	Auxiliary Inverter Interface Inductance , mH
C_f	Filter Capacitance, mF
R_d	Interfacing Resistance for Filter Capacitance, mF
V_{dcm}	Main Inverter DC bus voltage, V
V_{dc}	Auxiliary Inverter DC bus voltage, V
p_l	Instantaneous Load Active Power, W
$P_{\mu g}$	Average Power Supplied by Microgrid, W
ω	Frequency, rad/s
ϕ	Phase angle, $degree$

CHAPTER 1

INTRODUCTION

The increase in population and automation of various industries has increased the energy demand all over the world. In addition to this, the conventional energy resources or non renewable energy sources (fossil fuel) are reducing day by day. It is very evident that the world is facing an energy crisis due to the increase in demand and reduction in the available source of energy. This has lead the power system researchers to study on the scope of extraction of energy from renewable sources such as sun, wind, hydrogen etc. The renewable sources can be considered as infinite sources of energy. The researches in extraction of power from renewable energy has lead to a solution known as microgrid systems.

1.1 Microgrid Power System

Microgrid power systems are small scale power generation solution with local generating and storage facilities. Microgrid embeds an appreciable number of Distributed Energy Resources (DER), this kind of generation is known as Distributed Generation (DG). Apart from generation microgrid comprises of energy storage devices and it may also contain local loads. DG systems are usually located at the load bus, typically ranging from 1 kW to 10 MW. DG systems may be powered by either fossil or renewable fuels, but the microgrid generating sources are usually renewable energy sources such as Photo Voltaic Systems (PVS), Wind Energy Systems (WES), Fuel Cells or other microsources [1], [2]. Photovoltaic (PV) systems convert solar energy into electricity. PV modules produce dc power. Fuel cells work by the chemical reaction of combining hydrogen and oxygen to form electricity and water. In WES, wind turbines convert wind energy into electrical energy. Microgrid mainly utilizes sustainable energy sources for its generation, thus it is very evident that microgrid promote green energy (sustainable energy resources). The use of sustainable energy can reduce the amount of harmful

emissions, when compared to the conventional coal fired generation systems and helps to keep our planet green. The harmful emissions adds on to the global warming phenomena and increasing pollution in the biosphere. Apart from the generation systems, microgrid comprises of a storage system, the storage components are usually ultra capacitors or battery banks [3]. The power generated from the DERs are not constant or controlled, therefore when more power available than the load requirement the excess power can be stored and it can be utilized based on the demand. Thus the storage system makes microgrid system very flexible. The microgrid can operate either in grid connected mode or in standalone (islanded) mode [4]. The DG systems are connected to the main grid using suitable power electronic (PE) converters. PE interfaces can improve power quality of the customer by improving harmonics and providing extremely fast switching times for sensitive loads. PE can also provide benefits to the connected electric power system by providing reactive power control and voltage regulation at the DE system connection point. A unique property of a PE interface is the ability to reduce or eliminate fault current contributions from DE system, thereby allowing negligible impacts on protection coordination [5].

1.1.1 Microgrid Architecture

Fig. 1.1 shows the architecture of a microgrid system. It can be seen that the different energy sources are first integrated on to a common DC grid with help of power electronic converters. The PV system is connected using a unidirectional DC-DC boost converter. The WE system is integrated on to the DC grid using a unidirectional phase controlled power electronic rectifier. These two converters are unidirectional as the power flow is always into the DC grid from PV system and WE system. The storage system is connected to the DC grid using a bidirectional buck boost converter as the storage system involves power flow in both directions. The buck boost converter operates in boost mode when the power flow is from storage system to DC grid and the converter operates in buck mode when the DC grid is charging the storage system. The DC grid is then further connected to the main grid at the Point of Common Coupling (PCC) with the help of a grid interactive inverter. The power flow through the grid interactive inverter is bidirectional, the storage system can get charged even from the utility

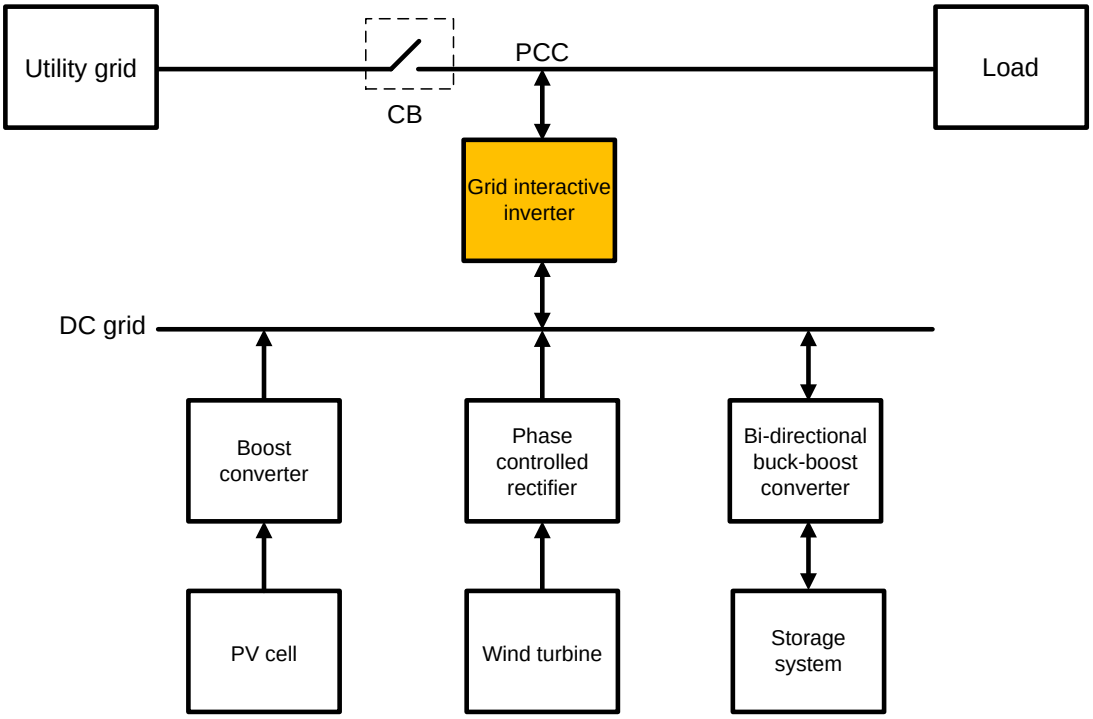

Fig. 1.1 Microgrid architecture.

grid due this arrangement. The loads are common to both the utility grid an microgrid in this architecture shown. The circuit breaker (CB) helps to either operate the system in grid connected or in islanded mode.

1.1.2 Modes of Operation of Microgrid

The operation is called grid connected, when the microgrid system is connected to the main grid(utility grid). The islanded mode of operation occurs when the microgrid is disconnected from the maingrid and supplies the local load. The islanding operation can be either intentional or unintentional. Unintentional islanding occurs due to faults in the main grid (voltage or frequency deviates from a specified band). The intentional islanding occurs due to some planned maintenance in the main grid. Since the microgrid can operate in the islanded mode even in the absence of main grid, it increases the reliability of the system. Therefore the microgrid system can be utilized for supplying critical loads. Critical loads are the loads which requires power supply for 24 hours a day. A server room consisting of servers on which important applications are hosted, operation theater of a hospital, university campus etc can be considered as critical loads.

IEEE spectrum magazine reported an article which vividly explains the reliability of microgrid. On 11 March, when the 9.0-magnitude earthquake struck off the northeast coast of Japan and triggered one of the deadliest tsunamis the world has ever seen, the bustling port city of Sendai was directly in harm's way. The port was destroyed, the airport was swamped, and waves reportedly rolled 8 kilometers inland, killing hundreds of people. While downtown Sendai escaped heavy structural damage, activity in the city ground to a halt. Every traffic light and office lamp went dark after the wall of water knocked out the electricity grid for the entire city. In some areas, the outages would last for weeks. But in one small section of the city, the lights stayed on. At Tohoku Fukushi University, in the northwest part of town, the laboratories' servers kept on humming, the clinic's MRI machines didnt lose a tesla, and the hospital's lights and equipment operated without a hitch. These facilities were the beneficiaries of an experimental microgrid project fed by three types of energy generators fuel cells, solar panels, and natural gas microturbines. Because the project also uses the thermal exhaust from the gas turbines and fuel cells to heat the buildings, the hospital's patients were kept warm through northern Japan's cold March nights.

In India, there are many remote regions which are not connected to the main grid. Extension of the main power network will obviously be time consuming and there will also be cost constraints for the expansions. Therefore, instead of extending the main transmission network, a stand alone microgrid system can act as a solution to supply electric power to the minority population in this regions. In the grid connected mode, there can be three different operation of the microgrid system, they are grid supporting mode, grid injecting mode, storage charging mode. In grid supporting mode, the microgrid and main grid together share the common load. In grid injecting mode, the microgrid generates more power than the load demand, therefore the excess power is injected into the grid. The storage charging mode happens when microgrid is not generating power, but drawing power from utility grid to charge its storage system.

1.1.3 Grid Interactive Inverter

The DC grid is integrated to the PCC, through grid interactive inverter. As the name suggests, the microgrid interact with the main grid through this inverter. Usually a voltage source inverter (VSI) is chosen for this role, different VSI topologies are chosen depending upon the requirement. This may have bidirectional operational capabilities. In grid connected mode the microgrid injects a certain amount of active power and reactive power at PCC, therefore in the grid interactive inverter will inject a certain current. In other words, the grid interactive inverter operates in current controlled mode during grid connected operations. In grid connected mode, the voltage at PCC is taken care of by the main grid. Whereas in islanding mode, the grid interactive inverter operates in voltage controlled mode and it maintains a constant voltage at the PCC. This thesis will concentrate on developing control strategies for grid interactive inverters, considering inclusion of power quality enhancements for the entire system. Power quality problems arise mainly due to non linear loads (loads including power electronic converters), as they demand harmonics and and create unbalance in the entire system. The various consequences due to harmonics are losses in ac power lines, transformers, and rotating machines. Furthermore, harmonics and unbalance cause oscillatory torque leading to mechanical stress, malfunctions in sensitive equipment, and interference with communication circuits. Therefore, if the microgrid can compensate the harmonics and unbalance demanded by the loads it will be an add on advantage of microgrid. This makes it necessary to conduct a study on various existing microgrid systems.

1.2 Microgrid Control Strategies Available in Literature

There are various microgrid systems available in literature which takes care of the power quality issues.

A single inverter system with power quality enhancement is discussed in [6]. This paper has presented in a simple way the modeling and the control strategy using *dq0* transformation of a three-phase PWM inverter to be employed in a grid-connected photo

voltaic generation system. The main focus of this work is to realize a design of a dual function system that would provide solar generation and works as an active power filter, compensating unbalances of power and the reactive power generated by other loads connected to the system. This single inverter system topology is shown in 1.2.

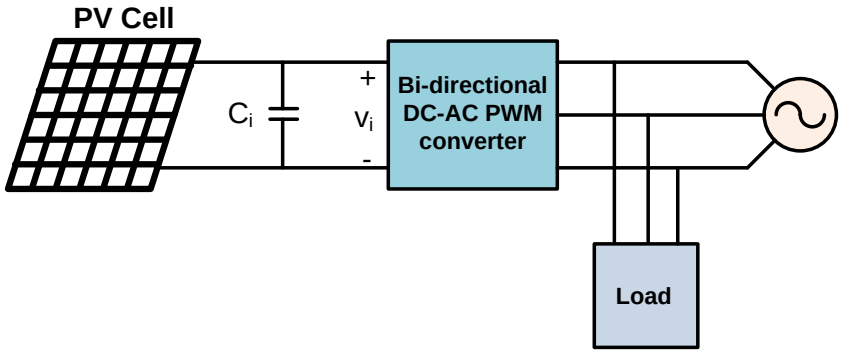

Fig. 1.2 Single inverter scheme for PV microgrid system

In [7], a voltage regulation and power flow control scheme for a WES is proposed. A DSTATCOM is utilized for voltage regulation and also for active power injection. The control scheme maintains the power balance at the grid terminal during the wind variations. It has been shown that the DSTATCOM controls the grid terminal voltage and maintain the power balance with the wind variations and the disturbances caused by either the source or the load side. This system makes use of sliding mode control algorithm.

Multi functional power electronic converter for distributed generation power system is described in [8]. In this, the grid interactive inverter captures and injects the power generated by the wind energy system and in addition to this, it also acts as a harmonic compensator. The control is applied based on instantaneous power theory. Only the average cmponents of the active($\overline{p}$) and reactive ($\overline{q}$) powers are supplied by the utility grid. The rest of the power components demanded by the load are supplied by the grid interactive inverter. One more possibility mentioned is that, only $\overline{p}$ is supplied by the utility grid. The various instantaneous power combinations studied in this paper is as shown in Fig. 1.3.

A microgrid system consisting of two inverters are demonstrated in [9]. It comprises of two inverters which shares the load equally and also the system compensates the

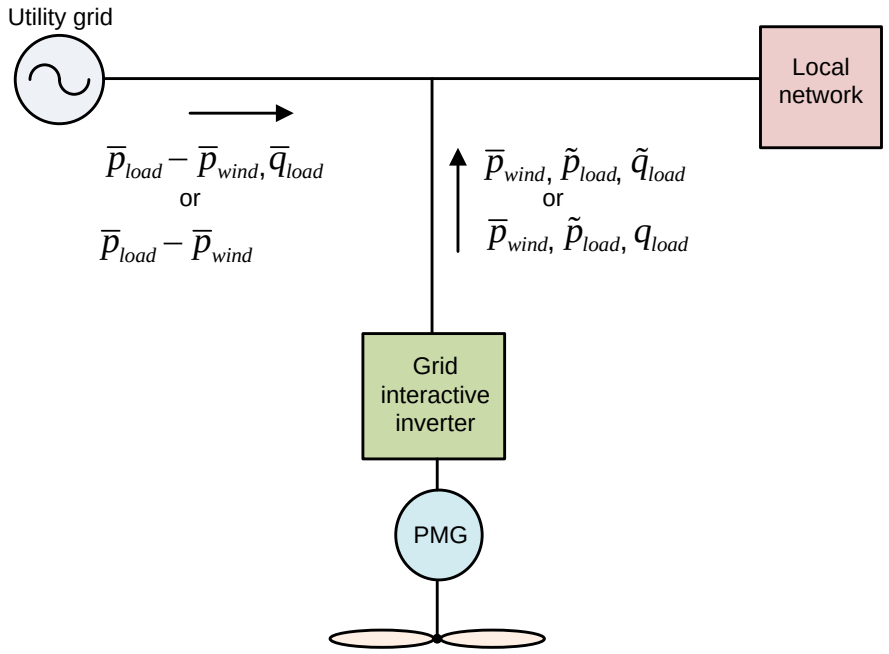

Fig. 1.3 Instantaneous power flow possibilities from the utility grid and grid interactive inverter

unbalanced and non linear load. The microgrid comprises of local and common loads. The strategy the authors have demonstrated, has succeeded in an efficient power flow control and load compensation

A power quality enhanced DG interfacing technique is discussed in [10]. The authors call the entire system as a flexible distributed generation (FDG) system as the utility can achieve the required loading level, and, at the same time, it can improve the system power factor or regulate the PCC voltage while mitigating harmonics and correcting unbalance. Therefore, FDG enhances the performance of the distribution networks. The control is developed in *dq0* reference frame.

Another power quality enhanced microgrid system is discussed in, which consists of two grid interactive inverters (two DGs) [11]. The system has local loads and common loads. The local loads is shared between the inverters and utility grid, when operated in grid connected mode.The microgrid is capable of nonlinear and unbalanced load compensation. The droop convention is used to share the common mode between the inverters in islanded mode. In islanding mode, the power sharing is proportional to the DG ratings. The system is as shown in Fig. 1.4

In [12], a two inverter system for power quality enhancement in microgrid systems

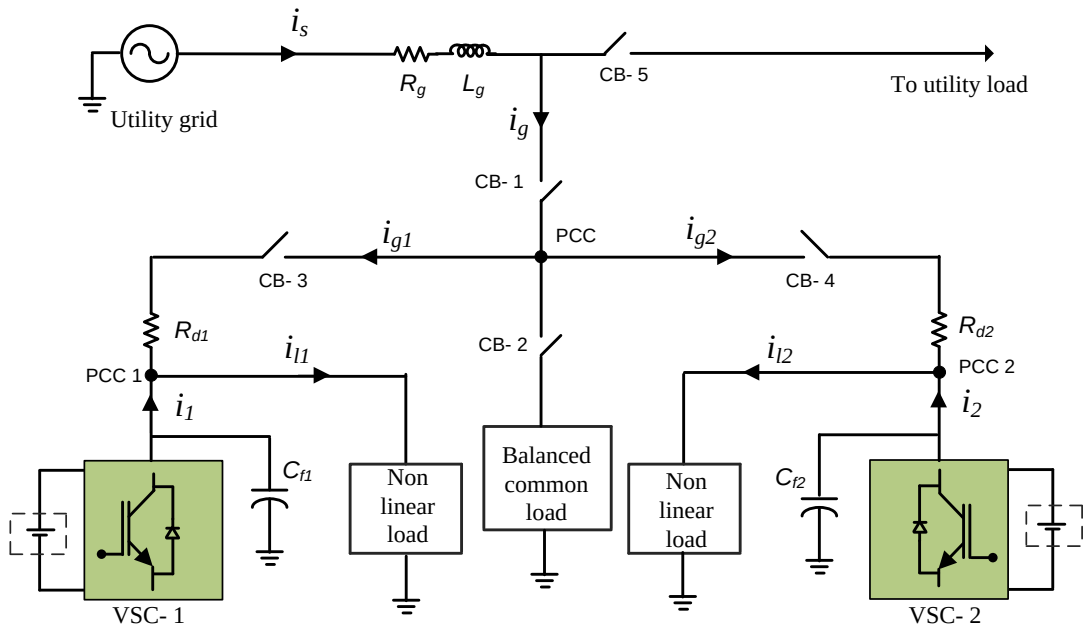

Fig. 1.4 Two inveter system, with load sharing and nonlinear load compensation capability.

has been discussed. This system comprises of two inverters arranged as shown in Fig. 1.5. This system demonstrates load sharing capabilities and in addition to this, a power quality conditioner with shunt and series inverter. The shunt inverter is responsible for keeping a set of balanced distortion-free voltages within the microgrid, while the series inverter is controlled to inject unbalanced voltages in series along the feeder to balance the line currents with no real and reactive power generated. During utility voltage sags, the series inverter can be also controlled to limit the flow of large fault currents. Collectively, the conditioner has been already shown to raise the quality of power within the microgrid and the quality of currents flowing between the microgrid and the utility.

A new technique for microgrid interfacing is discussed in [13]. A dual output four leg inverter is used for exporting the microgrid to the utility grid. This dual output inverter can act as two separate inverters, and can perform various functions including power quality enhancements. This scheme enables high utilization of the DC voltage and reduction in the mumber of power electronic switches. The control unit computations are figured out in *abc* coordinates using proportional-resonant (PR) controllers.

Another dual inverter system is discussed in [14]. This system consists of two in-

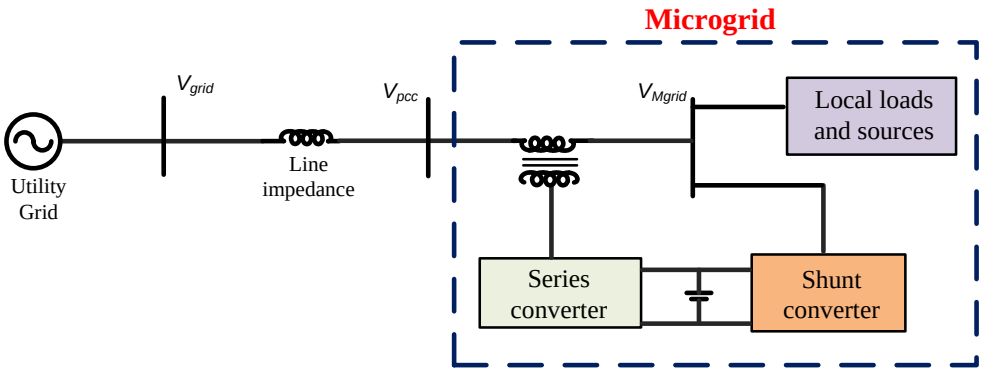

Fig. 1.5 Power quality conditioner in microgrid system.

verters supplied from the same DC link. One is called as the series inverter and other as the shunt inverter. The inverters are of 3-ϕ, 4-leg topology. The shunt inverter injects voltage accordingly, to compensate the unbalance in grid voltages. The series inverter perform the current compensation. This system has a voltage control loop and a current control loop. The controls are performed in the stationary reference frame.

These microgrid systems specified in the literature review, not only manages the power flow but focuses on power quality as well. This literature review vouches that taking power quality into consideration is of prime priority in microgrid systems. Therefore the control strategy developed for microgrid should include power quality enhancement features in addition to the power management capabilities. There has been literature with single inverters and dual inverter schemes for microgrid systems. The dual inverter systems are providing voltage and current compensations, where as the single inverter systems provide current compensations. The control strategies are found to be developed using various transformations in power engineering.

1.3 Organisation of Thesis

Chapter 2 presents a detailed study on various transformations available in power engineering. The transformations studied includes *abc* to $\alpha\beta 0$, *abc* to *dq0* and *abc* to symmetrical components. The study also comprises of the corresponding inverse transformations

In **Chapter 3**, generalized *abc* to $\alpha\beta 0$ transformation and *abc* to *dq0* transformation are developed. Using the generalized transformation, the corresponding transformation matrix can be found without performing the conventional analysis on the reference frame.

Chapter 4 describes the formulation of control algorithms for microgrid systems using various transformations. The control algorithms are developed in such a way that they all meet the same objectives. The simulation results with the algorithms are also presented. This chapter is concluded by performing a comparative study among these algorithms.

Chapter 5 proposes a dual voltage source inverter (DVSI) scheme for microgrid with enhanced power quality. Different modes of operation (grid connected and islanding) of microgrid are also explained. The simulation studies of the proposed algorithm is also performed. Towards the end this chapter lists out the advantages of the DVSI scheme.

Chapter 6 discusses the conclusions and future scope of work.

CHAPTER 2

A DETAILED STUDY ON VARIOUS TRANSFORMATIONS

2.1 Introduction

There are many transformations applied on voltages and currents in power engineering for various applications, some of them are studied in detail in this chapter. The transformations discussed in this chapter includes natural reference frame (*abc* reference frame) to $\alpha\beta 0$, *dq0* and symmetrical components. Transformations to $\alpha\beta 0$ and *dq0* were derived primarily for analyzing the dynamic models of electrical machines. *dq0* transformation was specifically derived to develop different dynamic machine models so that the parameters of the developed models are independent of the position of rotor. Hence the *dq0* reference frame was derived in such a way that it rotates at the same speed as that of the rotor and the *dq0* frame seems stationary to the rotor, hence *dq0* reference frame is also known as synchronous reference frame. Symmetrical component transformations are used to represent a set of unbalanced voltages as balanced quantities and it was applied to analyze the abnormal conditions (faults) in power system, the analysis of abnormal conditions using symmetrical components is much simpler than analysis using natural quantities. Now these transformations are extended on to many other applications in power engineering other than the specific applications for which they were developed [15]-[17]. This study concentrates on observing how exactly the quantities appear after the transformation and what is the variation happening when different voltage profiles are transformed. The different voltage profiles used in this study includes balanced voltages , unbalanced voltages, balanced voltages with harmonics and unbalanced voltages with harmonics. A simulation study is done in MATLAB to observe the transformed quantities while transforming these *abc* voltage profiles.

2.2 Transformation of Voltages in *abc* Reference Frame to $\alpha\beta 0$ Reference Frame

Transformation of *abc* voltages to $\alpha\beta 0$ frame is known as Clarke's transformation [18]. Let us consider an arbitrary set of 3-ϕ voltages v_a, v_b, v_c along the *abc* axes and define α and β axes in quadrature with each other as shown in Fig. 2.1.

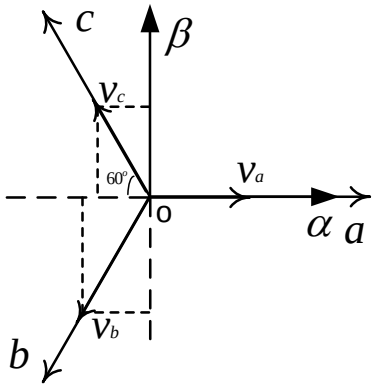

Fig. 2.1 abc to $\alpha\beta 0$ reference frame

Resolving the *abc* voltages along α and β axes we get,

$$\begin{aligned} v_\alpha &= v_a + v_b\cos 120^\circ + v_c\cos 120^\circ \\ v_\alpha &= v_a - \frac{1}{2}v_b - \frac{1}{2}v_c \\ v_\beta &= v_b\cos 150^\circ + v_c\cos 30^\circ \\ v_\beta &= -\frac{\sqrt{3}}{2}v_b + \frac{\sqrt{3}}{2}v_c \end{aligned}$$

Now we can represent the transformation in matrix form as follows,

$$\begin{bmatrix} v_\alpha \\ v_\beta \end{bmatrix} = \begin{bmatrix} 1 & -\frac{1}{2} & -\frac{1}{2} \\ 0 & -\frac{\sqrt{3}}{2} & \frac{\sqrt{3}}{2} \end{bmatrix} \begin{bmatrix} v_a \\ v_b \\ v_c \end{bmatrix} \tag{2.1}$$

Let,

$$C = \begin{bmatrix} 1 & -\frac{1}{2} & -\frac{1}{2} \\ 0 & -\frac{\sqrt{3}}{2} & \frac{\sqrt{3}}{2} \end{bmatrix}$$

While using this transformation in power system to obtain power invariance property i.e.,

$$v_a i_a + v_b i_a + v_c i_c = v_\alpha i_\alpha + v_\beta i_\beta$$

(where v and i are voltage and current respectively)
we should multiply the transformation matrix C with a constant of $\sqrt{\frac{2}{3}}$, which is not necessarily used for all applications [19]. On observing (2.1) we understand that a transformation from $\alpha\beta 0$ to *abc* frame is cumbersome as matrix 'C' is non invertible. Therefore we define zero sequence quantity in addition to the α and β voltages which makes 'C' a square matrix and let us assume all the elements of the third row is equal to K.
So now we will define the new transformation matrix A,

$$A = \sqrt{\frac{2}{3}} \begin{bmatrix} 1 & -\frac{1}{2} & -\frac{1}{2} \\ 0 & -\frac{\sqrt{3}}{2} & \frac{\sqrt{3}}{2} \\ K & K & K \end{bmatrix} \tag{2.2}$$

We have to choose the value of K in such a way that we get some advantage out of it. If we select the value of K as $\frac{1}{\sqrt{2}}$ we can see $A^{-1} = A^T$ which makes computations of inverse transform much easier. So finally the transformation matrix A turns out as follows,

$$A = \sqrt{\frac{2}{3}} \begin{bmatrix} 1 & -\frac{1}{2} & -\frac{1}{2} \\ 0 & -\frac{\sqrt{3}}{2} & \frac{\sqrt{3}}{2} \\ \frac{1}{\sqrt{2}} & \frac{1}{\sqrt{2}} & \frac{1}{\sqrt{2}} \end{bmatrix} \tag{2.3}$$

Therefore, *abc* to $\alpha\beta 0$ transformation and the inverse transformation can be concluded

as shown in (2.4) and (2.5) respectively.

$$\begin{bmatrix} v_\alpha \\ v_\beta \\ v_0 \end{bmatrix} = \sqrt{\frac{2}{3}} \begin{bmatrix} 1 & -\frac{1}{2} & -\frac{1}{2} \\ 0 & -\frac{\sqrt{3}}{2} & \frac{\sqrt{3}}{2} \\ \frac{1}{\sqrt{2}} & \frac{1}{\sqrt{2}} & \frac{1}{\sqrt{2}} \end{bmatrix} \begin{bmatrix} v_a \\ v_b \\ v_c \end{bmatrix} \tag{2.4}$$

$$\begin{bmatrix} v_a \\ v_b \\ v_c \end{bmatrix} = \sqrt{\frac{2}{3}} \begin{bmatrix} 1 & 0 & \frac{1}{\sqrt{2}} \\ -\frac{1}{2} & -\frac{\sqrt{3}}{2} & \frac{1}{\sqrt{2}} \\ -\frac{1}{2} & \frac{\sqrt{3}}{2} & \frac{1}{\sqrt{2}} \end{bmatrix} \begin{bmatrix} v_\alpha \\ v_\beta \\ v_0 \end{bmatrix} \tag{2.5}$$

2.3 Transformation of Voltages in $\alpha\beta 0$ to *dq0* Reference Frame

The *dq0* frame was first derived by R.H.Park for synchronous machine modeling known as Park's transformation [20]. To transform$\alpha\beta 0$ quantities to *dq0* Frame we need to define the *dq0* frame at an angle θ with respect to the $\alpha\beta 0$ frame as shown in the Fig. 3.7. The *dq0* frame is a rotating reference frame which rotates at the frequency of the balanced 3-ϕ quantities in natural reference frame.

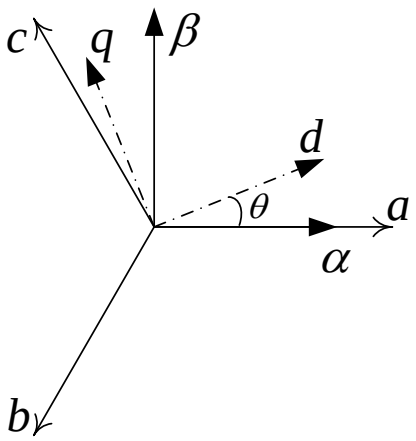

Fig. 2.2 abc, $\alpha\beta 0$ and *dq0* reference frame

Now resolving the α -β voltages along the *d-q* axes we get,

$$v_d = v_\alpha \cos\theta + v_\beta \cos(90^\circ - \theta) = v_\alpha \cos\theta + v_\beta \sin\theta$$

$$v_q = v_\alpha \cos(90^\circ + \theta) + v_\beta \cos\theta = -v_\alpha \sin(90^\circ + \theta) + v_\beta \cos\theta$$

Now we can represent the transformation in matrix form as follows,

$$\begin{bmatrix} v_d \\ v_q \\ v_0 \end{bmatrix} = \begin{bmatrix} \cos\theta & \sin\theta & 0 \\ -\sin\theta & \cos\theta & 0 \\ 0 & 0 & 1 \end{bmatrix} \begin{bmatrix} v_\alpha \\ v_\beta \\ v_0 \end{bmatrix} \tag{2.6}$$

So the whole transformation from natural reference frame to *dq0* reference frame can be obtained as shown in (2.7) by combining (2.4) and (2.6).

$$\begin{bmatrix} v_d \\ v_q \\ v_0 \end{bmatrix} = \sqrt{\frac{2}{3}} \begin{bmatrix} \cos\theta & \sin\theta & 0 \\ -\sin\theta & \cos\theta & 0 \\ 0 & 0 & 1 \end{bmatrix} \begin{bmatrix} 1 & -\frac{1}{2} & -\frac{1}{2} \\ 0 & -\frac{\sqrt{3}}{2} & \frac{\sqrt{3}}{2} \\ \frac{1}{\sqrt{2}} & \frac{1}{\sqrt{2}} & \frac{1}{\sqrt{2}} \end{bmatrix} \begin{bmatrix} v_a \\ v_b \\ v_c \end{bmatrix} \tag{2.7}$$

The transformation can be deducted as shown below using trigonometric simplification

$$\begin{bmatrix} v_d \\ v_q \\ v_0 \end{bmatrix} = \sqrt{\frac{2}{3}} \begin{bmatrix} \cos\theta & \cos(\theta + 120^\circ) & \cos(\theta - 120^\circ) \\ -\sin\theta & -\sin(\theta + 120^\circ) & -\sin(\theta - 120^\circ) \\ \frac{1}{\sqrt{2}} & \frac{1}{\sqrt{2}} & \frac{1}{\sqrt{2}} \end{bmatrix} \begin{bmatrix} v_a \\ v_b \\ v_c \end{bmatrix}. \tag{2.8}$$

Thus the transformation from natural reference frame to *dq0* reference in the chosen reference frame can be concluded as shown in (2.8).

2.4 Interpretation of Voltages in $\alpha\beta 0$ Reference Frame

We will perform an analysis on the $\alpha\beta 0$ frame when the *abc*- reference frame quantities to be transformed are a set of balanced voltages. This analysis will help us to have an idea as of how the *abc* quantities will get transformed in the $\alpha\beta 0$ frame and its trace.

Consider a set of balanced 3-ϕ sinusoidal voltages as,

$v_a = \sqrt{2}V \sin \omega t$

$v_b = \sqrt{2}V \sin(\omega t - 120^\circ)$

$v_c = \sqrt{2}V \sin(\omega t + 120^\circ)$

Where V is the rms value of phase voltage.

The $\alpha\beta 0$ reference frame consists of two axes with one in quadrature with the other, so $\alpha\beta 0$ frame will have one component along α- axis(v_α) and one component along β-axis(v_β). We will define a quantity '$\vec{v}_{\alpha\beta}$' where,

$$\vec{v}_{\alpha\beta} = v_\alpha + jv_\beta$$

$\overline{v}_{\alpha\beta}$ can be looked upon as a position vector in the $\alpha\beta 0$ frame. With the help of (2.4), v_α and v_β can be obtained as follows,

$$\begin{aligned} v_\alpha &= \sqrt{\frac{2}{3}}\left[v_a - \frac{1}{2}v_b - \frac{1}{2}v_c\right] \\ &= \sqrt{\frac{2}{3}}\left[\frac{3}{2}v_a\right] \\ &= \sqrt{\frac{2}{3}}\left[\frac{3}{2}.\sqrt{2}V \sin \omega t\right] \\ &= \sqrt{3}V \sin \omega t \end{aligned} \tag{2.9}$$

$$\begin{aligned} v_\beta &= \sqrt{\frac{2}{3}}\left[-\frac{\sqrt{3}}{2}v_b + \frac{\sqrt{3}}{2}v_c\right] \\ &= -\frac{1}{\sqrt{2}}v_{bc} \\ &= -\frac{1}{\sqrt{2}}\left[\sqrt{3}v_a \angle -\pi/2\right] \\ &= -\frac{1}{\sqrt{2}}\left[\sqrt{3}.\sqrt{2}V \sin(\omega t - \pi/2)\right] \\ &= \sqrt{3}V \sin(\pi/2 - \omega t) \\ &= \sqrt{3}V \cos \omega t \end{aligned} \tag{2.10}$$

$$
\begin{aligned}
v_\alpha + jv_\beta &= \sqrt{3}V\sin\omega t + j\sqrt{3}V\cos\omega t \\
&= \sqrt{3}Ve^{j(\pi/2-\omega t)} \\
\vec{v}_{\alpha\beta} = v_\alpha + jv_\beta &= \sqrt{3}Ve^{j(\pi/2-\omega t)}
\end{aligned} \tag{2.11}
$$

$\vec{v}_{\alpha\beta}$ is a vector in $\alpha\beta 0$ frame, hence $\overline{v}_{\alpha\beta}$ gives us an acumen about the appearance of 3-ϕ voltages in $\alpha\beta 0$ frame. From the expression of $\vec{v}_{\alpha\beta}$ in (2.11) we understand that,

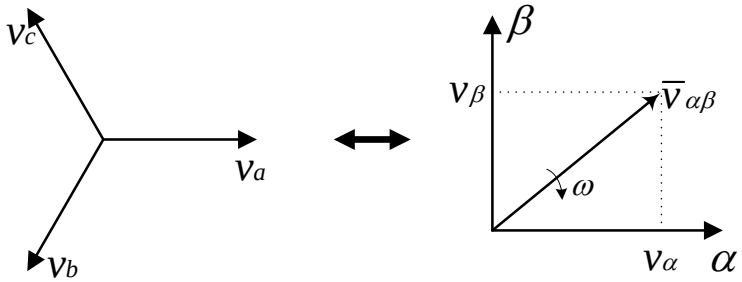

Fig. 2.3 Appearance of *abc* quantities in $\alpha\beta 0$ reference frame

1). 3-ϕ balanced quantities in *abc* reference frame gets transferred into a vector with a magnitude of '$\sqrt{3}V$' and rotates with a frequency 'ω' in $\alpha\beta 0$ reference frame .

2). The sense of rotation of $\vec{v}_{\alpha\beta}$ is clockwise, as ωt has a positive sense of rotation in clockwise direction. This can be geometrically interpreted as shown in Fig. 2.3.

2.5 Interpretation of Voltages in *dq0* Reference Frame

Now we will develop a relation between *dq0* frame and $\alpha\beta 0$ frame in such a way that we obtain a value for 'θ', which gives constant value for *d* and *q* voltages when balanced voltages in natural reference frame are transformed. From Fig. 3.7, v_d and v_q can be written as follows,

$$
\begin{aligned}
v_d &= v_\alpha\cos\theta + v_\beta\sin\theta \\
v_q &= -v_\alpha\sin\theta + v_\beta\cos\theta
\end{aligned}
$$

Therefore

$$\begin{aligned} v_d + jv_q &= v_\alpha \cos\theta + v_\beta \sin\theta + j\left(-v_\alpha \sin\theta + v_\beta \cos\theta\right) \\ &= (v_\alpha + jv_\beta)\cos\theta - j(v_\alpha + jv_\beta)\sin\theta \\ &= (v_\alpha + jv_\beta)e^{-j\theta} \end{aligned} \tag{2.12}$$

Now substituting for '$v_\alpha + jv_\beta$' from (2.11) in (3.9), we get

$$\begin{aligned} v_d + jv_q &= \sqrt{3}Ve^{j(\pi/2-\omega t)}e^{-j\theta} \\ &= \sqrt{3}Ve^{j(\frac{\pi}{2}-\omega t-\theta)} \end{aligned} \tag{2.13}$$

We will get constant values for v_d and v_q if we get rid of the exponential term in (3.10). Therefore

$$\begin{aligned} \frac{\pi}{2} - \omega t - \theta = 0 \quad &, or \\ \theta = \frac{\pi}{2} - \omega t \end{aligned} \tag{2.14}$$

Substituting the value 'θ' in (3.10) gives

$$v_d = \sqrt{3}V \tag{2.15}$$

$$v_q = 0 \tag{2.16}$$

The quantity along *0*-axis is also zero when balanced *abc* quantities are transformed.

$$v_0 = \frac{v_a + v_b + v_c}{\sqrt{3}} = 0 \tag{2.17}$$

Therefore 'θ' should be defined as $(\frac{\pi}{2} - \omega t)$ to obtain constant DC values along *d* and *q* axes when balanced abc quantities are transformed to *dq0* frame, if the reference is selected as shown in Fig. 3.7. Substituting $\theta = (\frac{\pi}{2} - \omega t)$ in (2.8) we obtain the final *abc* to *dq0* transformation as follows,

$$\begin{bmatrix} v_d \\ v_q \\ v_0 \end{bmatrix} = \sqrt{\frac{2}{3}} \begin{bmatrix} \sin\omega t & \sin(\omega t - 120^\circ) & \sin(\omega t + 120^\circ) \\ -\cos\omega t & -\cos(\omega t - 120^\circ) & -\cos(\omega t + 120^\circ) \\ \frac{1}{\sqrt{2}} & \frac{1}{\sqrt{2}} & \frac{1}{\sqrt{2}} \end{bmatrix} \begin{bmatrix} v_a \\ v_b \\ v_c \end{bmatrix} \tag{2.18}$$

2.6 Analysis of *dq0* transformation with a Different Reference Frame

It has been seen that different reference frames have been used in various studies, so we will look at a different reference frame and perform the analysis.Consider the reference frame shown in the Fig. 2.4. On performing similar analysis shown in section 4 we get,

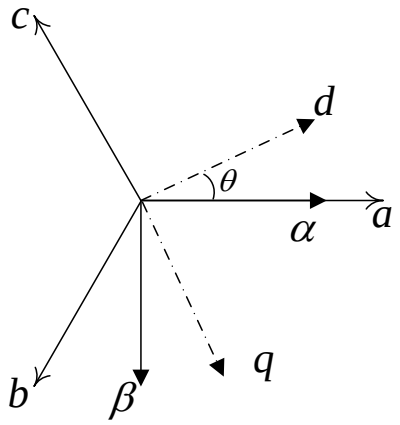

Fig. 2.4 abc to $\alpha\beta 0$ reference frame

$$\vec{v}_{\alpha\beta} = v_\alpha + jv_\beta = \sqrt{3}Ve^{j(\omega t - \pi/2)}$$

On observivg $\vec{v}_{\alpha\beta}$ we understand that this is vector rotating in anticlockwise direction, and now the positive sense of rotation of 'ωt' is clockwise. So there is shift in the rotation of $\vec{v}_{\alpha\beta}$ and positive sense of rotation of ωt in the two reference frames considered in Fig. 3.7 and Fig. 2.4.

Now on performing similar analysis shown in section 5 we get,

$$\begin{aligned} v_d + jv_q &= (v_\alpha + jv_\beta)e^{j\theta} \\ &= \sqrt{3}Ve^{j(\omega t - \pi/2)}e^{j\theta} \\ &= \sqrt{3}Ve^{-j(\frac{\pi}{2} - \omega t - \theta)} \end{aligned}$$

Now in this reference frame also we find that on selecting θ=$(\frac{\pi}{2} - \omega t)$ we obtain con-

stant DC values along *d* and *q* axes when balanced abc quantities are transformed to d-q frame i.e.,
$v_d = \sqrt{3}V$, $v_q = 0$.

This makes it clear that we can define the reference frame by changing the alignment of α-β and *d*-*q* axis in many ways. But we should make sure that we define the value of 'θ' in such a way that we obtain constant DC quantities along d and q axes. In the both the reference frames considered in this study it happened that $\theta = (\frac{\pi}{2} - \omega t)$ gives us constant DC quantities along *d* and *q* axes but it not necessary that θ is always equal to $(\frac{\pi}{2} - \omega t)$.

2.7 Transformation to Symmetrical Components

The electrical power system operates as balanced 3-ϕ system but during abnormal condition(faults), this balance is broken and the result is an unbalanced system. Symmetrical components, which was first suggested by Dr. C.L Fortescue can transform the unbalanced quantities to symmetrical set of balanced phasors known as positive, negative and zero sequence components [21]. Symmetrical components reduces the complexity in solving for the electrical quantities during disturbances.

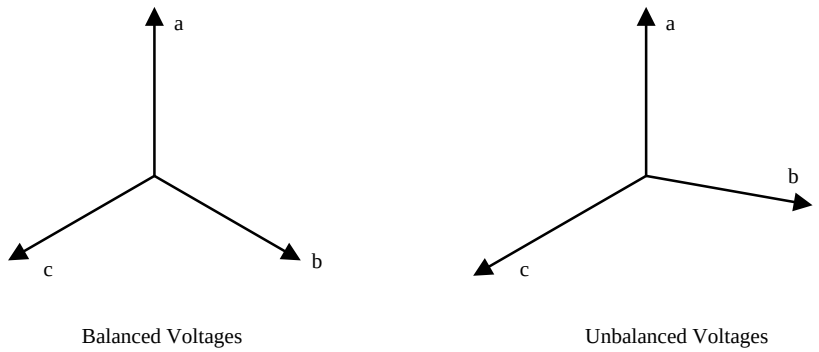

Fig. 2.5 Balanced and unbalanced voltages

The positive sequence components can be notated as v_{a1}, v_{b1}, v_{c1}, the negative sequence components are v_{a2}, v_{b2}, v_{c2}. By the definition of symmetrical components v_{b1} always lags v_{a1} by 120° and v_{b2} leads v_{a2} by 120°. Since the direction of rotation of

v_{a1}, v_{b1}, v_{c1} is same as that of the actual *abc* quantities they are known as positive sequence components and the direction of rotation of v_{a2}, v_{b2}, v_{c2} is opposite to that of *abc* hence they are known as negative sequence components. The rotation sequence is shown in the Fig. 2.6. For analysis we will use the voltages v_1, v_2 and v_0 as positve, negative and zero sequence respectively, these are components not specific to any phase but represents all the phases. The transformation is defined as shown in (2.19).

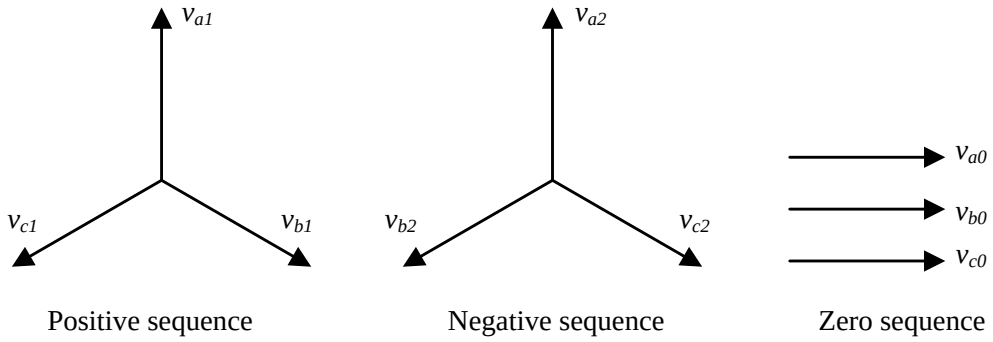

Fig. 2.6 Symmetrical components

operator 'a'= $1\angle 120° = -\frac{1}{2} + j\frac{\sqrt{3}}{2}$

$$\begin{bmatrix} v_0 \\ v_1 \\ v_2 \end{bmatrix} = \frac{1}{\sqrt{3}} \begin{bmatrix} 1 & 1 & 1 \\ 1 & a & a^2 \\ 1 & a^2 & a \end{bmatrix} \begin{bmatrix} v_a \\ v_b \\ v_c \end{bmatrix} \tag{2.19}$$

From the transformation,

$$v_0 = \frac{v_a + v_b + v_c}{\sqrt{3}} \tag{2.20}$$

and

$$\begin{aligned} v_1 &= \frac{1}{\sqrt{3}} \left(v_a + a v_b + a^2 v_c\right) \\ v_1 &= \frac{1}{\sqrt{3}} \left(v_a + \left(-\frac{1}{2} + j\frac{\sqrt{3}}{2}\right) v_b + \left(-\frac{1}{2} - j\frac{\sqrt{3}}{2}\right) v_c\right) \\ v_1 &= \frac{1}{\sqrt{3}} \left(v_a - \frac{1}{2} v_b - \frac{1}{2} v_b\right) + j\frac{1}{\sqrt{3}} \left(\frac{\sqrt{3}}{2} v_b - \frac{\sqrt{3}}{2} v_c\right) \end{aligned}$$

From the definition of α-β transformation explained in (2.1)

$$\begin{aligned} v_1 &= \frac{1}{\sqrt{2}}[v_\alpha - jv_\beta] \\ v_1 &= \sqrt{\frac{3}{2}}Vsin\omega t - j\sqrt{\frac{3}{2}}Vcos\omega t \end{aligned} \tag{2.21}$$

On performing similar analysis on v_2 we get,

$$v_2 = \sqrt{\frac{3}{2}}Vsin(\omega t) + j\sqrt{\frac{3}{2}}Vcos(\omega t) \tag{2.22}$$

Voltages in *abc* reference frame when subjected to symmetrical component transformation gets transformed into complex time varying quantities as shown in (2.21) and (2.22). We can plot the imaginary part Vs the real part of the symmetrical components, in this case $\sqrt{\frac{3}{2}}Vsin(\omega t)$ along x-axis and $\sqrt{\frac{3}{2}}Vcos(\omega t)$ along y-axis

$$x^2 + y^2 = \left(\sqrt{\frac{3}{2}}Vsin(\omega t)\right)^2 + \left(\sqrt{\frac{3}{2}}Vcos(\omega t)\right)^2 = \left(\sqrt{\frac{3}{2}}V\right)^2. \tag{2.23}$$

From equation(2.23) we can understand that the plot will be a circle with centre at origin and radius $\sqrt{\frac{3}{2}}V$.

2.8 Simulation Studies

Simulations of these transformations are done in MATLAB. Simulations are done using various voltage profiles and the corresponding transformed voltages are observed. The various voltage profiles considered in this study includes balanced, unbalanced, balanced with harmonics, unbalanced with harmonics. The transformation used in (2.4) is uded for *abc* to $alphabeta0$ transformation and the transformation shown in (2.18) is made used for *abc dq0* transformation.

2.8.1 Transformed Voltages, when Transformations are Applied to Balanced *abc* Voltages

In this section the the transformed voltages are observed when a set of balanced voltages in *abc* reference frame are transformed. The balanced voltages selected are as shown

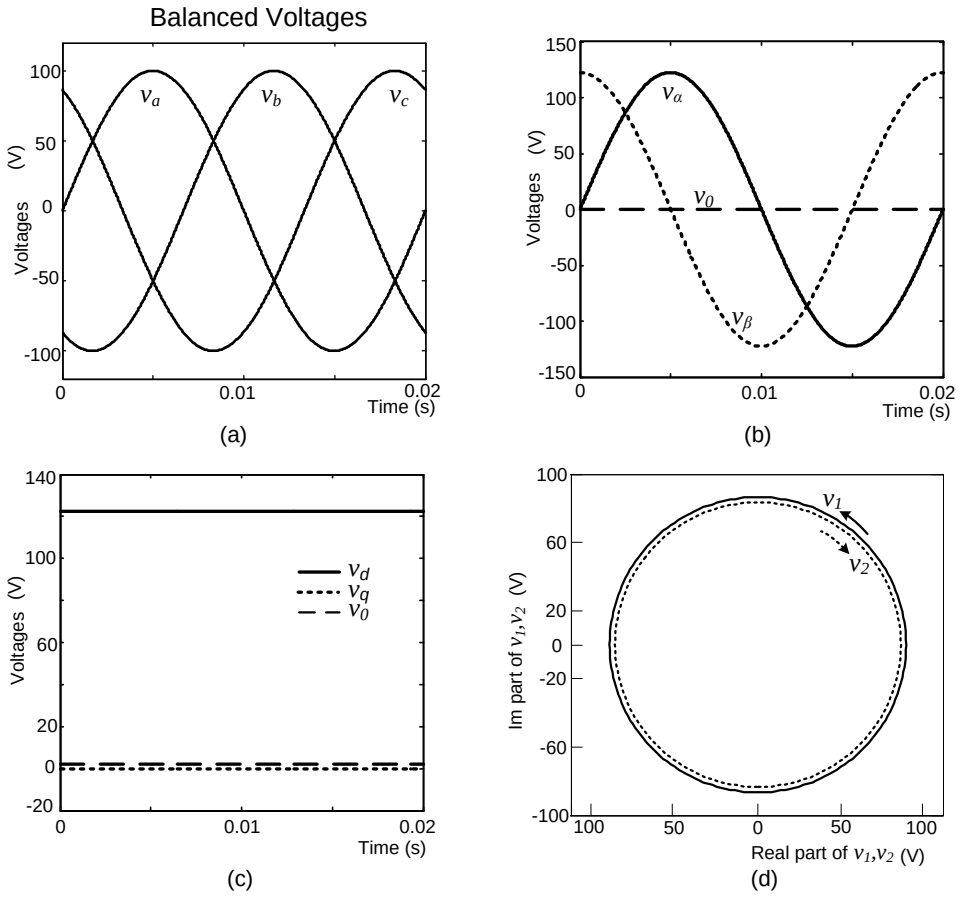

Fig. 2.7 (a) Balanced voltages (b) $\alpha\beta 0$ voltages (c) *dq0* voltages (d) loci of symmetrical components

below and Fig. 2.7(a) shows its plot, frequency is chosen as 50Hz.

$v_a = 100 \sin \omega t$

$v_b = 100 \sin(\omega t - \frac{2\pi}{3})$

$v_c = 100 \sin(\omega t + \frac{2\pi}{3})$

Fig. 2.7(b), 2.7(c)and 2.7(d) shows the $\alpha\beta 0$ quantities, *dqo* quantities and loci of symmetrical components respectively, for selected voltages $v_\alpha = 122.47\text{sin}\omega\text{t}$ and $v_\beta = 122.47\text{cos}\omega t$ as per (2.11) and $v_d = 122.47V, v_q = 0, v_0 = 0$ as per (3.12).

It can be observed that the calculated values of the transformed quantities are matching with values obtained by performing the simulation. The loci of the symmetrical components turn out to be a circle when a set of balanced voltages are used for transformation. The loci of symmetrical components v_1 and v_2 has overlapped in this case but the direction is opposite to each other i.e, v_1 traces in the clockwise direction and v_2 traces in anti- clockwise direction.

2.8.2 Transformed Voltages, when Transformation is Applied to Unbalanced *abc* quantities

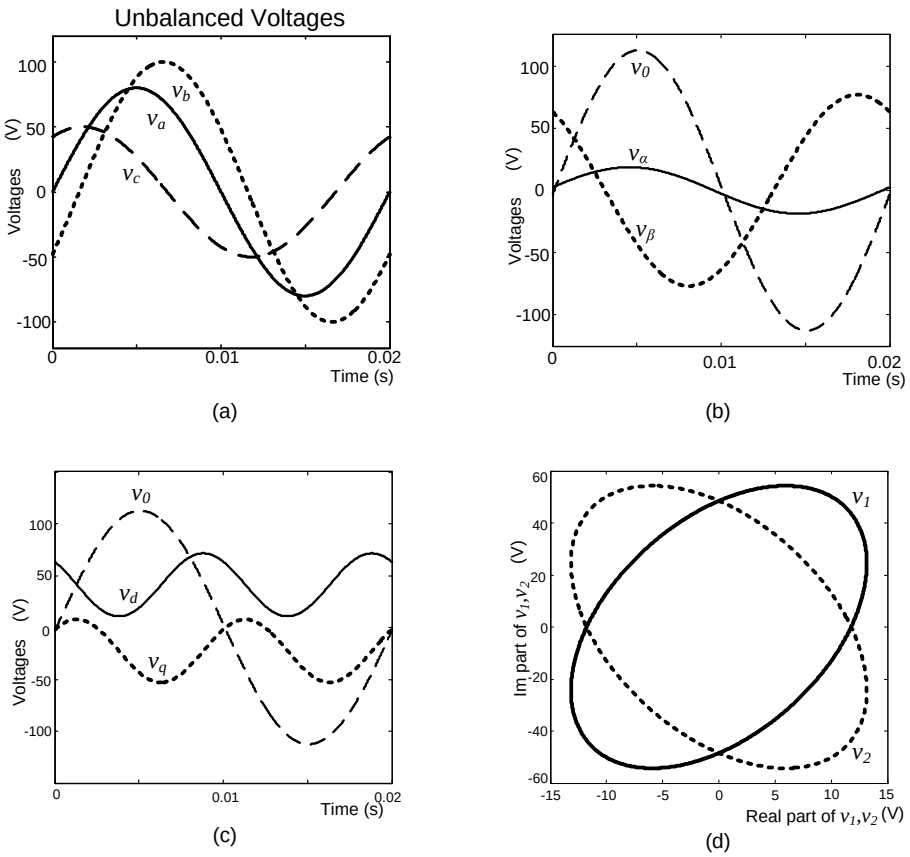

Fig. 2.8 (a) Unbalanced voltages (b) $\alpha\beta 0$ voltages (c) *dqo* voltages (d) loci of symmetrical components

In this section the the transformed quantities are observed when a set of unbalanced voltages in *abc* reference frame are transformed. The unbalanced voltages selected are as shown below and Fig. 2.8(a) shows its plot. $v_a = 80\sin\omega t$, $v_b = 100\sin(\omega t - 0.5)$, $v_c = 50\sin(\omega t + 1)$

(The phase shifts are shown in radians, frequency is selected as 50Hz). Fig. 2.8(b), 2.8(c)and 2.8(d) shows the $\alpha\beta 0$ quantities, *dq0* quantities and loci of symmetrical components respectively. It can be observed that the α-β voltages now has different magnitudes and *dq* voltages oscillates at double the frequency of the *abc* quantities, with a non zero average.

Average value of v_d = 41.05 V, Average value of v_q= -22.67 V

The *0*-quantity oscillates with the same frequency as that of *abc* quantities with a zero average. The loci of symmetrical components forms two ellipses but does not overlap which reflects the unbalance.

2.8.3 Transformed Quantities, when Transformation is Applied to Balanced *abc* voltages with Harmonics

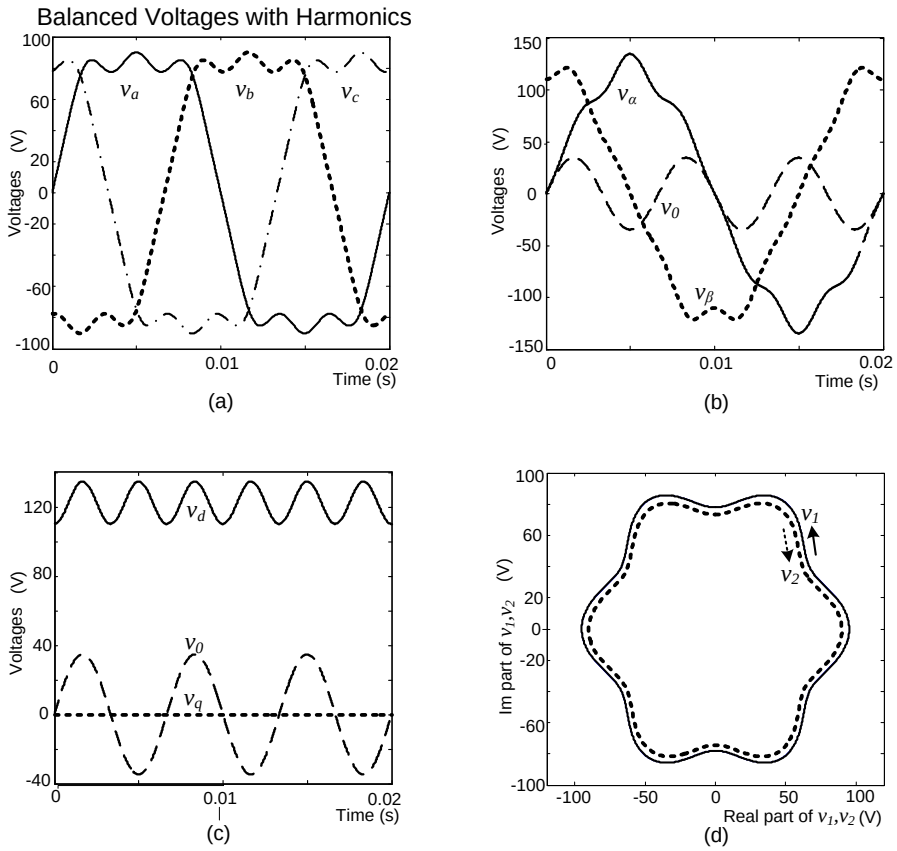

Fig. 2.9 (a) Balanced voltage with harmonics (b) $\alpha\beta 0$ voltages (c) *dq0* voltages (d) loci of symmetrical components

This section observes the different transformed quantities when transformations are

applied to a set of balanced voltages with harmonics. The voltage profile in Fig. 2.9(a) is being transformed and the Fig. 2.9(b), 2.9(c)and 2.9(d) shows the $\alpha\beta 0$ quantities, *dq0* quantities and loci of symmetrical components respectively, It is observed that the *dq0* voltages has now become oscillatory but when the system is balanced the *q*- voltage has a zero average. Harmonics are introduced into α-β voltages. Loci of symmetrical components is no more a circle but the loci of positive and negative sequence overlaps each other eventhough they trace in opposite directions.

2.8.4 Transformed Quantities, when Transformation is Applied to Unbalanced *abc* voltages with Harmonics

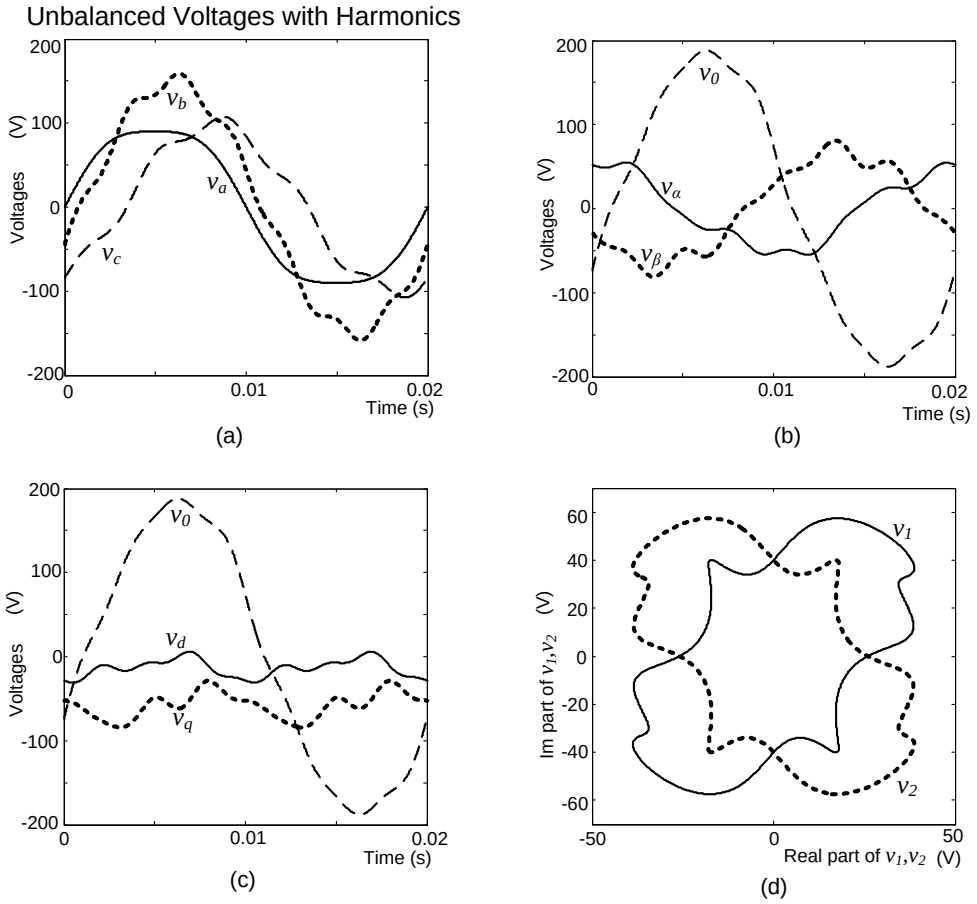

Fig. 2.10 (a) Unbalanced voltages with harmonics (b) $\alpha\beta 0$ voltages (c) *dq0* voltages (d) loci of symmetrical components

This section observes the different transformed quantities when transformations are applied to a set of unbalanced voltages with harmonics. The voltage profile in Fig.

2.10(a) has been transformed and the Fig. 2.10(b), 2.10(c)and 2.10(d) shows the $\alpha\beta 0$ quantities, *dqo* quantities and loci of symmetrical components respectively, it is observed that harmonics are introduced into all the transformed voltages.

2.9 Summary

This study concentrated on the the profiles of transformed voltages when $\alpha\beta 0$, *dq0* and symmetrical component transformations are applied on *abc* voltages with various profiles. With $\alpha\beta 0$ transformation the balanced 3-ϕ *abc* voltages get transformed on to a rotating position vector $v_{\alpha\beta}$ consisting of real and imaginary part. The real part corresponds to voltage along α-axis and imaginary part corresponds to voltage along β-axis. The voltages v_α and v_β turns out to be sinusoidal quantities when balanced voltages are transformed. With the help of simulation the transformation is extended to other voltage profiles. Then from $\alpha\beta 0$ frame, *dq0* reference frame is derived and the corresponding *dq0* voltages are obtained. It is observed that the balanced sinusoidal quantities reforms to DC voltages in *dq0* reference frame. There can be different reference frame depending upon the alignment of *d-q* and α-β axes. But by defining proper value for 'θ' we can end up getting DC along along d and q axes which is the ultimate goal of *dq0* transformation. Frame chosen in this study has been subjected to simulations and it is observed that the values obtained with simulation matches with the calculated values. Towards the end of the chapter an investigation on the loci of symmetrical components is done and the loci is obtained for various voltage profiles. If the loci of positive and negative sequence components overlaps it indicates a balance in the system and if it does'nt overlap then its symbol of unbalance. If the system is devoid of harmonics then the loci will either be an ellipse or a circle but if harmonics is present then the loci will be distorted.

CHAPTER 3

GENARALIZED $\alpha\beta 0$ and *dq0* TRANSFORMATIONS

3.1 Introduction

It has been observed that different reference frames are chosen while transforming *abc* quantities to $\alpha\beta 0$ and *dq0* reference frames. There happens to be different reference frames existing, depending upon the orientation of the axes. There will be a change in the transformation matrix depending upon how you choose your axes orientation, that makes it necessary to perform an analysis on the reference frame and find out the transformation matrix corresponding to the selected reference frame. In this chapter efforts have been put on to develop a generalized transformation for transforming *abc* quantities to $\alpha\beta 0$ and *dq0* frames.

3.2 Different Reference Frames for *abc* to $\alpha\beta 0$ Transformation

In this section we will consider different $\alpha\beta 0$ reference frames and derive the corresponding transformation matrices. From these matrices we can obtain a generalized matrix which can generate transformation corresponding to all these reference frames. Let us assume that the quantity being transformed is voltage.

3.2.1 $\alpha\beta 0$ Reference Frame -1

$\alpha\beta 0$ reference frame-1 is shown in Fig. 3.1(a). Reference frame shown in Fig. 3.1(b) is a mirror image of frame shown in Fig. 3.1(a), when the mirror is aligned along the α-axis. Resolving the *abc* voltages along the $\alpha\beta 0$ axes will result in the transformation matrix is shown in (3.1).

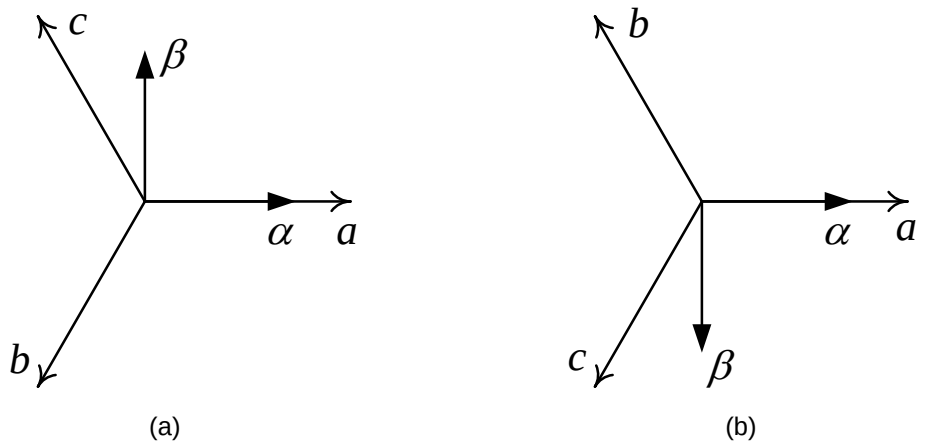

Fig. 3.1 (a) $\alpha\beta 0$ reference frame -1 (b) Mirror of $\alpha\beta 0$ reference frame -1.

$$\begin{aligned} v_\alpha &= v_a + v_b\cos 120^\circ + v_c\cos 120^\circ \\ v_\alpha &= v_a - \frac{1}{2}v_b - \frac{1}{2}v_c \\ v_\beta &= v_b\cos 150^\circ + v_c\cos 30^\circ \\ v_\beta &= -\frac{\sqrt{3}}{2}v_b + \frac{\sqrt{3}}{2}v_c \end{aligned}$$

$$\begin{bmatrix} v_\alpha \\ v_\beta \\ v_0 \end{bmatrix} = \sqrt{\frac{2}{3}} \begin{bmatrix} 1 & -\frac{1}{2} & -\frac{1}{2} \\ 0 & -\frac{\sqrt{3}}{2} & \frac{\sqrt{3}}{2} \\ \frac{1}{\sqrt{2}} & \frac{1}{\sqrt{2}} & \frac{1}{\sqrt{2}} \end{bmatrix} \begin{bmatrix} v_a \\ v_b \\ v_c \end{bmatrix} \tag{3.1}$$

With the help of (3.1), v_α and v_β can be obtained as follows,

$$\begin{aligned} v_\alpha &= \sqrt{\frac{2}{3}}\left[v_a - \frac{1}{2}v_b - \frac{1}{2}v_c\right] \\ &= \sqrt{\frac{2}{3}}\left[\frac{3}{2}v_a\right] \\ &= \sqrt{\frac{2}{3}}\left[\frac{3}{2}.\sqrt{2}V\sin\omega t\right] \\ &= \sqrt{3}V\sin\omega t \end{aligned} \tag{3.2}$$

$$v_\beta = \sqrt{\frac{2}{3}}\left[-\frac{\sqrt{3}}{2}v_b + \frac{\sqrt{3}}{2}v_c\right]$$

$$
\begin{aligned}
v_\beta &= -\frac{1}{\sqrt{2}} v_{bc} && (3.3)\\
&= -\frac{1}{\sqrt{2}} \left[\sqrt{3} v_a \angle -\pi/2\right] \\
&= -\frac{1}{\sqrt{2}} \left[\sqrt{3}.\sqrt{2} V \sin(\omega t - \pi/2)\right] \\
&= \sqrt{3} V \sin(\pi/2 - \omega t) \\
&= \sqrt{3} V \cos \omega t && (3.4)
\end{aligned}
$$

While transforming the *abc* voltages to $\alpha\beta 0$ voltages considering reference frame shown in Fig. 3.1(b), it can be observed that it will result in same transformation shown in (3.1). These reference frames which are mirror images of each other will result in same transformations and they are termed as mirrors of each other in this study. Hence we will term the reference frame shown in Fig. 3.1(b) as the mirror of Fig. 3.1(a).

3.2.2 $\alpha\beta 0$ Reference Frame -2

$\alpha\beta 0$ Reference Frame-2 is shown in Fig. 3.2(a) and its mirror is shown in Fig. 3.2(b). The transformation matrix for these reference frames can be can be obtained by resolv-

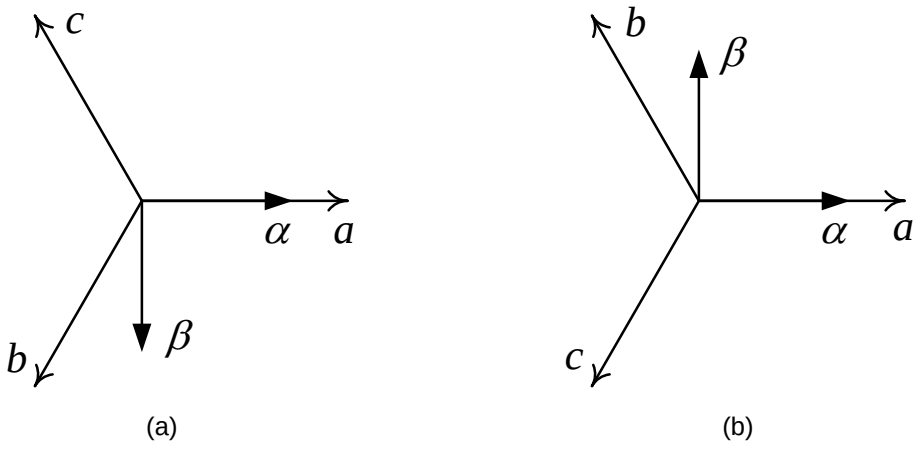

Fig. 3.2 (a) $\alpha\beta 0$ reference frame-2 (b) Mirror of $\alpha\beta 0$ reference frame-2.

ing the *abc* along α-β axes as shown in (3.5).

$$\begin{bmatrix} v_\alpha \\ v_\beta \\ v_0 \end{bmatrix} = \sqrt{\frac{2}{3}} \begin{bmatrix} 1 & -\frac{1}{2} & -\frac{1}{2} \\ 0 & \frac{\sqrt{3}}{2} & -\frac{\sqrt{3}}{2} \\ \frac{1}{\sqrt{2}} & \frac{1}{\sqrt{2}} & \frac{1}{\sqrt{2}} \end{bmatrix} \begin{bmatrix} v_a \\ v_b \\ v_c \end{bmatrix} \tag{3.5}$$

3.3 Different Reference Frames for *abc* to *dq0* Transformation

We have different *dq0* reference frames available depending on the orientation of *dq0* axes with respect to the *abc* and α-β axes. We will consider four different reference frames and derive a generalized transformation matrix for the all the frames.

3.3.1 *dq0* Reference Frame - 1

dq0 reference frame -1 is shown in Fig. 3.3(a). The *abc* to $\alpha\beta 0$ transformation is same

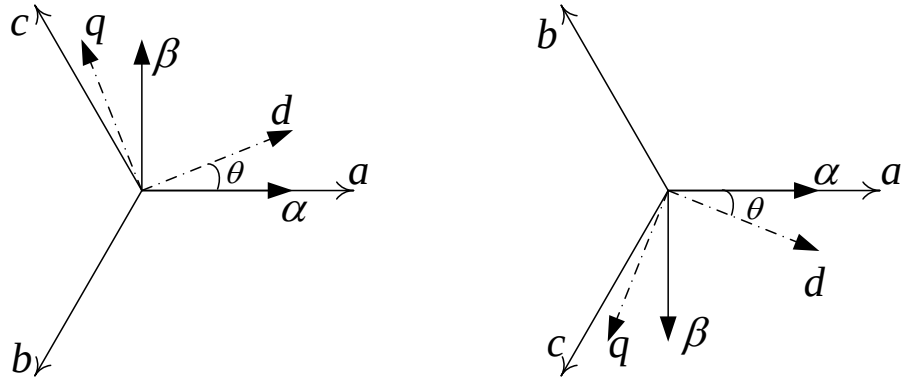

Fig. 3.3 (a) *dq0* reference frame -1 (b) Mirror of *dq0* reference frame -1

as what is shown in (3.1). The transformation from $\alpha\beta 0$ frame to *dq0* can be found out as follows.

$$v_d = v_\alpha \cos\theta + v_\beta \cos(90^\circ - \theta) = v_\alpha \cos\theta + v_\beta \sin\theta$$

$$v_q = v_\alpha \cos(90^\circ + \theta) + v_\beta \cos\theta = -v_\alpha \sin\theta + v_\beta \cos\theta$$

Now we can represent the $\alpha\beta 0$ to *dq0* transformation in matrix form as follows,

$$\begin{bmatrix} v_d \\ v_q \\ v_0 \end{bmatrix} = \begin{bmatrix} \cos\theta & \sin\theta & 0 \\ -\sin\theta & \cos\theta & 0 \\ 0 & 0 & 1 \end{bmatrix} \begin{bmatrix} v_\alpha \\ v_\beta \\ v_0 \end{bmatrix} \tag{3.6}$$

So the whole transformation from natural reference frame to *dq0* reference frame can be obtained as shown in (3.7) by combining (3.1) and (3.6).

$$\begin{bmatrix} v_d \\ v_q \\ v_0 \end{bmatrix} = \sqrt{\frac{2}{3}} \begin{bmatrix} \cos\theta & \sin\theta & 0 \\ -\sin\theta & \cos\theta & 0 \\ 0 & 0 & 1 \end{bmatrix} \begin{bmatrix} 1 & -\frac{1}{2} & -\frac{1}{2} \\ 0 & -\frac{\sqrt{3}}{2} & \frac{\sqrt{3}}{2} \\ \frac{1}{\sqrt{2}} & \frac{1}{\sqrt{2}} & \frac{1}{\sqrt{2}} \end{bmatrix} \begin{bmatrix} v_a \\ v_b \\ v_c \end{bmatrix} \tag{3.7}$$

The transformation can be deducted as shown below using trigonometric simplification.

$$\begin{bmatrix} v_d \\ v_q \\ v_0 \end{bmatrix} = \sqrt{\frac{2}{3}} \begin{bmatrix} \cos\theta & \cos(\theta + \frac{2\pi}{3}) & \cos(\theta - \frac{2\pi}{3}) \\ -\sin\theta & -\sin(\theta + \frac{2\pi}{3}) & -\sin(\theta - \frac{2\pi}{3}) \\ \frac{1}{\sqrt{2}} & \frac{1}{\sqrt{2}} & \frac{1}{\sqrt{2}} \end{bmatrix} \begin{bmatrix} v_a \\ v_b \\ v_c \end{bmatrix} \tag{3.8}$$

We have to obtain a value for θ, which gives constant value for *d* and *q* voltages when balanced voltages in natural reference frame are transformed in these reference frames. The value of θ can be derived as follows,

$$\begin{aligned} v_d &= v_\alpha \cos\theta + v_\beta \sin\theta \\ v_q &= -v_\alpha \sin\theta + v_\beta \cos\theta \end{aligned}$$

Therefore

$$\begin{aligned} v_d + jv_q &= v_\alpha \cos\theta + v_\beta \sin\theta + j\left(-v_\alpha \sin\theta + v_\beta \cos\theta\right) \\ &= (v_\alpha + jv_\beta)\cos\theta - j(v_\alpha + jv_\beta)\sin\theta \\ &= (v_\alpha + jv_\beta)e^{-j\theta} \end{aligned} \tag{3.9}$$

Now substituting for v_α and v_β from (3.2) and (3.3) in (3.9), we get

$$\begin{aligned} v_d + jv_q &= \sqrt{3}Ve^{j(\pi/2-\omega t)}e^{-j\theta} \\ &= \sqrt{3}Ve^{j(\frac{\pi}{2}-\omega t-\theta)} \end{aligned} \tag{3.10}$$

We will get constant values for v_d and v_q if we get rid of the exponential term in (3.10). Therefore,

$$\begin{aligned} \frac{\pi}{2} - \omega t - \theta = 0 \quad &, or \\ \theta = \frac{\pi}{2} - \omega t \end{aligned} \tag{3.11}$$

Assume v_a, v_b, v_c to be balanced voltages i.e,

$v_a = \sqrt{2}Vsin(\omega t)$, $v_b = \sqrt{2}Vsin(\omega t - 120^\circ)$, $v_c = \sqrt{2}Vsin(\omega t + 120^\circ)$
and substituting the value θ in (3.8) gives

$$v_d = \sqrt{3}V \tag{3.12}$$

$$v_q = 0 \tag{3.13}$$

The frame shown in Fig. 3.3(b) the mirror of frame shown in Fig. 3.3(a) in terms of *dq0* transformation. By performing similar analysis on the reference frame shown Fig. 3.3(b), it is understood that the transformation is same as that shown in (3.8). The final transformation matrix for both the frames can be obtained by substituting $\theta = \frac{\pi}{2} - \omega t$ in (3.8) and it is as shown below,

$$\begin{bmatrix} v_d \\ v_q \\ v_0 \end{bmatrix} = \sqrt{\frac{2}{3}} \begin{bmatrix} \sin\omega t & \sin\left(\omega t - \frac{2\pi}{3}\right) & \sin\left(\omega t + \frac{2\pi}{3}\right) \\ -\cos\omega t & -\cos\left(\omega t - \frac{2\pi}{3}\right) & -\cos\left(\omega t + \frac{2\pi}{3}\right) \\ \frac{1}{\sqrt{2}} & \frac{1}{\sqrt{2}} & \frac{1}{\sqrt{2}} \end{bmatrix} \begin{bmatrix} v_a \\ v_b \\ v_c \end{bmatrix} \tag{3.14}$$

3.3.2 *dq0* Reference Frame -2

Now we will consider another reference frame and we will name it as *dq0* reference frame - 2, the reference frame and its mirror are shown in Fig. 3.4(a) and Fig. 3.4(b)

respectively. In these frames, the *abc* to $\alpha\beta 0$ transformation is exactly same as (3.5)

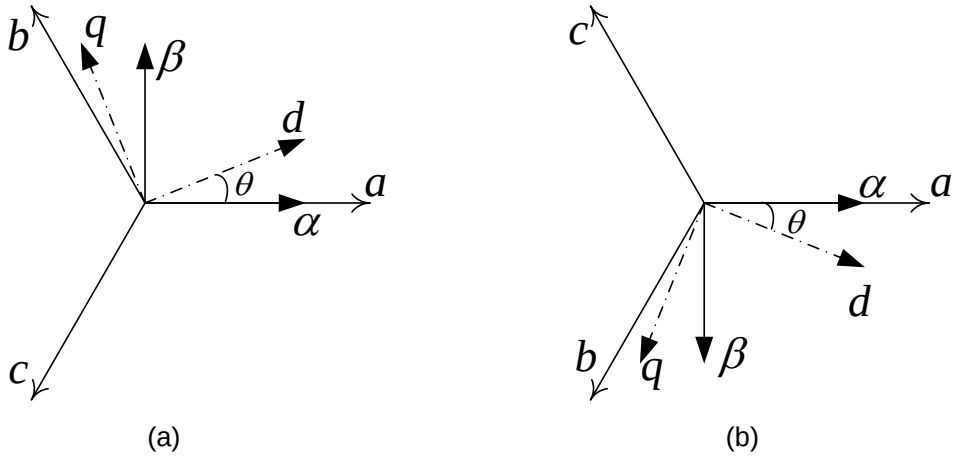

Fig. 3.4 (a) *dq0* reference frame -2 (b) Mirror of *dq0* reference frame -2

and the $\alpha\beta 0$ to *dq0* transformation is a replica of (3.6). Combining (3.5) and (3.6) we obtain the *abc* to *dq0* transformation as shown in (3.16).

$$\begin{bmatrix} v_d \\ v_q \\ v_0 \end{bmatrix} = \sqrt{\frac{2}{3}} \begin{bmatrix} \cos\theta & \sin\theta & 0 \\ -\sin\theta & \cos\theta & 0 \\ 0 & 0 & 1 \end{bmatrix} \begin{bmatrix} 1 & -\frac{1}{2} & -\frac{1}{2} \\ 0 & \frac{\sqrt{3}}{2} & -\frac{\sqrt{3}}{2} \\ \frac{1}{\sqrt{2}} & \frac{1}{\sqrt{2}} & \frac{1}{\sqrt{2}} \end{bmatrix} \begin{bmatrix} v_a \\ v_b \\ v_c \end{bmatrix} \tag{3.15}$$

$$\begin{bmatrix} v_d \\ v_q \\ v_0 \end{bmatrix} = \sqrt{\frac{2}{3}} \begin{bmatrix} \cos\theta & \cos(\theta - \frac{2\pi}{3}) & \cos(\theta + \frac{2\pi}{3}) \\ -\sin\theta & -\sin(\theta - \frac{2\pi}{3}) & -\sin(\theta + \frac{2\pi}{3}) \\ \frac{1}{\sqrt{2}} & \frac{1}{\sqrt{2}} & \frac{1}{\sqrt{2}} \end{bmatrix} \begin{bmatrix} v_a \\ v_b \\ v_c \end{bmatrix} \tag{3.16}$$

Choosing θ as $(\omega t - \frac{\pi}{2})$ gives DC quantities along d and q axis in these reference frames. The final transformation matrix can be obtained by substituting $\theta = \omega t - \frac{\pi}{2}$ in (3.16) and it is shown in (3.17).

$$\begin{bmatrix} v_d \\ v_q \\ v_0 \end{bmatrix} = \sqrt{\frac{2}{3}} \begin{bmatrix} \sin\omega t & \sin\left(\omega t - \frac{2\pi}{3}\right) & \sin\left(\omega t + \frac{2\pi}{3}\right) \\ \cos\omega t & \cos\left(\omega t - \frac{2\pi}{3}\right) & \cos\left(\omega t + \frac{2\pi}{3}\right) \\ \frac{1}{\sqrt{2}} & \frac{1}{\sqrt{2}} & \frac{1}{\sqrt{2}} \end{bmatrix} \begin{bmatrix} v_a \\ v_b \\ v_c \end{bmatrix} \tag{3.17}$$

3.3.3 *dq0* Reference Frame - 3

We will analyze another possible reference frame(*dq0* reference frame - 3) shown in Fig. 3.5(a) and its mirror is shown in Fig. 3.5(b). *abc* to $\alpha\beta 0$ transformation is same

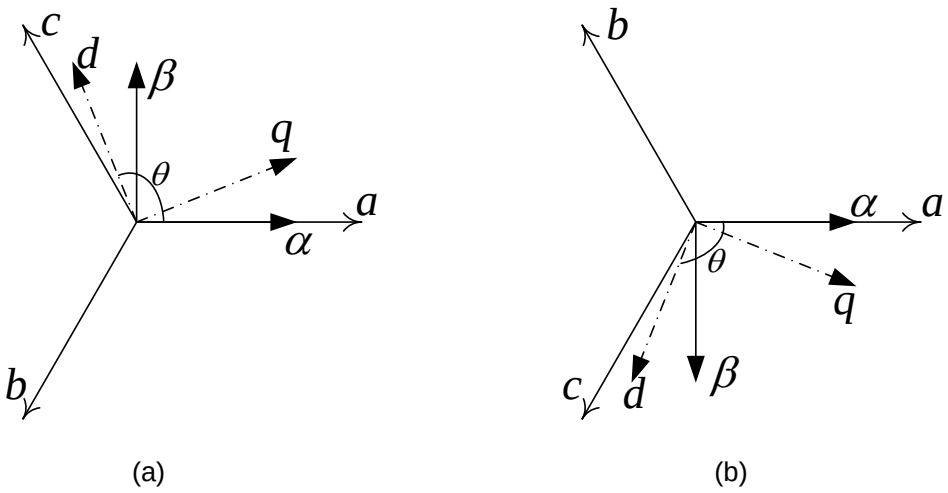

Fig. 3.5 (a) *dq0* reference frame -3 (b) Mirror of *dq0* reference frame -3

as (3.1). The $\alpha\beta 0$ to *dq0* transformation can be found by resolving $\alpha - \beta$ components along *dq0* axes as follows,

$$v_d = v_\alpha \cos\theta + v_\beta \cos(\theta - 90^\circ) = v_\alpha \cos\theta + v_\beta \sin\theta$$

$$v_q = v_\alpha \cos(\theta - 90^\circ) + v_\beta \cos(\theta - 2(\theta - 90^\circ)) = v_\alpha \sin\theta - v_\beta \cos\theta$$

We can define the $\alpha\beta 0$ to *dq0* transformation as shown in (3.18).

$$\begin{bmatrix} v_d \\ v_q \\ v_0 \end{bmatrix} = \begin{bmatrix} \cos\theta & \sin\theta & 0 \\ \sin\theta & -\cos\theta & 0 \\ 0 & 0 & 1 \end{bmatrix} \begin{bmatrix} v_\alpha \\ v_\beta \\ v_0 \end{bmatrix} \tag{3.18}$$

$$\begin{bmatrix} v_d \\ v_q \\ v_0 \end{bmatrix} = \sqrt{\frac{2}{3}} \begin{bmatrix} \cos\theta & \sin\theta & 0 \\ \sin\theta & -\cos\theta & 0 \\ 0 & 0 & 1 \end{bmatrix} \begin{bmatrix} 1 & -\frac{1}{2} & -\frac{1}{2} \\ 0 & -\frac{\sqrt{3}}{2} & \frac{\sqrt{3}}{2} \\ \frac{1}{\sqrt{2}} & \frac{1}{\sqrt{2}} & \frac{1}{\sqrt{2}} \end{bmatrix} \begin{bmatrix} v_a \\ v_b \\ v_c \end{bmatrix} \tag{3.19}$$

On simplification,

$$\begin{bmatrix} v_d \\ v_q \\ v_0 \end{bmatrix} = \sqrt{\frac{2}{3}} \begin{bmatrix} \cos\theta & \cos(\theta + \frac{2\pi}{3}) & \cos(\theta - \frac{2\pi}{3}) \\ \sin\theta & \sin(\theta + \frac{2\pi}{3}) & \sin(\theta - \frac{2\pi}{3}) \\ \frac{1}{\sqrt{2}} & \frac{1}{\sqrt{2}} & \frac{1}{\sqrt{2}} \end{bmatrix} \begin{bmatrix} v_a \\ v_b \\ v_c \end{bmatrix} \tag{3.20}$$

A choice of θ = ($\frac{\pi}{2} - \omega t$) gives DC quantities along *d* and *q* axis in these reference frames.The final transformation matrix can be obtained by substituting $\theta = \frac{\pi}{2} - \omega t$ in (3.20) and it is shown in (3.21).

$$\begin{bmatrix} v_d \\ v_q \\ v_0 \end{bmatrix} = \sqrt{\frac{2}{3}} \begin{bmatrix} \sin\omega t & \sin\left(\omega t - \frac{2\pi}{3}\right) & \sin\left(\omega t + \frac{2\pi}{3}\right) \\ \cos\omega t & \cos\left(\omega t - \frac{2\pi}{3}\right) & \cos\left(\omega t + \frac{2\pi}{3}\right) \\ \frac{1}{\sqrt{2}} & \frac{1}{\sqrt{2}} & \frac{1}{\sqrt{2}} \end{bmatrix} \begin{bmatrix} v_a \\ v_b \\ v_c \end{bmatrix} \tag{3.21}$$

3.3.4 *dq0* Reference Frame -4

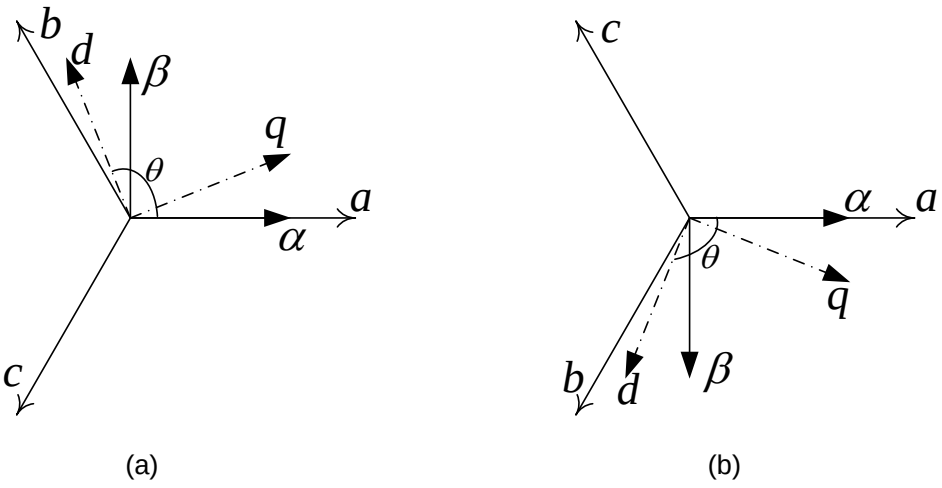

Fig. 3.6 (a) *dq0* reference frame -4 (b) Mirror of *dq0* reference frame -4

The last reference frame considered is shown in Fig. 3.6(a)(*dq0* reference frame -4) and its mirror is shown in Fig. 3.6(b). The *abc* to $\alpha\beta 0$ transformation is same as (3.5), the $\alpha\beta 0$ to *dq0* transformation follows (3.18). The complete *abc* to *dq0* transformation

can be obtained as follows by clubbing these equations,

$$\begin{bmatrix} v_d \\ v_q \\ v_0 \end{bmatrix} = \sqrt{\frac{2}{3}} \begin{bmatrix} \cos\theta & \sin\theta & 0 \\ \sin\theta & -\cos\theta & 0 \\ 0 & 0 & 1 \end{bmatrix} \begin{bmatrix} 1 & -\frac{1}{2} & -\frac{1}{2} \\ 0 & \frac{\sqrt{3}}{2} & -\frac{\sqrt{3}}{2} \\ \frac{1}{\sqrt{2}} & \frac{1}{\sqrt{2}} & \frac{1}{\sqrt{2}} \end{bmatrix} \begin{bmatrix} v_a \\ v_b \\ v_c \end{bmatrix} \tag{3.22}$$

$$\begin{bmatrix} v_d \\ v_q \\ v_0 \end{bmatrix} = \sqrt{\frac{2}{3}} \begin{bmatrix} \cos\theta & \cos(\theta - \frac{2\pi}{3}) & \cos(\theta + \frac{2\pi}{3}) \\ \sin\theta & \sin(\theta - \frac{2\pi}{3}) & \sin(\theta + \frac{2\pi}{3}) \\ \frac{1}{\sqrt{2}} & \frac{1}{\sqrt{2}} & \frac{1}{\sqrt{2}} \end{bmatrix} \begin{bmatrix} v_a \\ v_b \\ v_c \end{bmatrix} \tag{3.23}$$

Selecting $\theta = (\omega t - \frac{\pi}{2})$ gives DC quantities along *d* and *q* axis in these reference frames. The final transformation matrix for both the frames can be obtained by substituting $\theta = \omega t - \frac{\pi}{2}$ in (3.23) and it is as given below,

$$\begin{bmatrix} v_d \\ v_q \\ v_0 \end{bmatrix} = \sqrt{\frac{2}{3}} \begin{bmatrix} \sin\omega t & \sin\left(\omega t - \frac{2\pi}{3}\right) & \sin\left(\omega t + \frac{2\pi}{3}\right) \\ -\cos\omega t & -\cos\left(\omega t - \frac{2\pi}{3}\right) & -\cos\left(\omega t + \frac{2\pi}{3}\right) \\ \frac{1}{\sqrt{2}} & \frac{1}{\sqrt{2}} & \frac{1}{\sqrt{2}} \end{bmatrix} \begin{bmatrix} v_a \\ v_b \\ v_c \end{bmatrix} \tag{3.24}$$

3.4 Generalized $\alpha\beta 0$ and *dq0* Transformations

3.4.1 Generalized *abc* to $\alpha\beta 0$ Transformation

There are four different reference frames defined and the corresponding two transformations also have been derived. α-axis is always aligned along the *a*-axis of *abc* reference frame. Now we require a single transformation matrix to swap between the two transformations (3.1) and (3.5), depending upon the reference frame we choose. To achieve this objective, we will introduce two indices *m* and *n*, *m* represents the alignment of *abc* axes and *n* points at the orientation of $\alpha\beta 0$ axes.

m= 1, when the sequence is *a-b-c* anticlockwise.
m= -1, when the sequence is *a-c-b* anticlockwise.

n= 1, when β-axis makes a quadrature with α-axis, in anticlockwise direction.

n= -1, when β-axis makes a quadrature with α-axis, in clockwise direction.

$$l = m\,n \tag{3.25}$$

Let us define the generalized transformation matrix as,

$$\begin{bmatrix} v_\alpha \\ v_\beta \\ v_0 \end{bmatrix} = \sqrt{\frac{2}{3}} \begin{bmatrix} 1 & -\frac{1}{2} & -\frac{1}{2} \\ 0 & -l\frac{\sqrt{3}}{2} & l\frac{\sqrt{3}}{2} \\ \frac{1}{\sqrt{2}} & \frac{1}{\sqrt{2}} & \frac{1}{\sqrt{2}} \end{bmatrix} \begin{bmatrix} v_a \\ v_b \\ v_c \end{bmatrix} \tag{3.26}$$

It can be observed that now depending upon the values of *m* and *n* we choose, the corresponding transform for all the four reference frames can be directly obtained from the generalized transformation given in (3.26).

The inverse transformation can be generalized as shown in (3.27).

$$\begin{bmatrix} v_a \\ v_b \\ v_c \end{bmatrix} = \sqrt{\frac{2}{3}} \begin{bmatrix} 1 & 0 & \frac{1}{\sqrt{2}} \\ -\frac{1}{2} & -l\frac{\sqrt{3}}{2} & \frac{1}{\sqrt{2}} \\ -\frac{1}{2} & l\frac{\sqrt{3}}{2} & \frac{1}{\sqrt{2}} \end{bmatrix} \begin{bmatrix} v_\alpha \\ v_\beta \\ v_0 \end{bmatrix} \tag{3.27}$$

3.4.2 Verification of Generalized *abc* to $\alpha\beta$*0* Transformation

We will verify the generalized transformation with various values of *m* and *n*.

Case 1: *m*=1, *n*=1

Here *m*=1 corresponds to a reference frame where *abc* axes orients with *a-b-c* sequence in anticlockwise and *n*=1 indicates β-axis makes a quadrature with α-axis in anticlockwise direction. This forms the reference frame shown in Fig. 3.1(a).Here,

$$l = m\,n = 1$$

With the help of (3.26) the transformation can be directly formed as shown below.

$$\begin{bmatrix} v_\alpha \\ v_\beta \\ v_0 \end{bmatrix} = \sqrt{\frac{2}{3}} \begin{bmatrix} 1 & -\frac{1}{2} & -\frac{1}{2} \\ 0 & -\frac{\sqrt{3}}{2} & \frac{\sqrt{3}}{2} \\ \frac{1}{\sqrt{2}} & \frac{1}{\sqrt{2}} & \frac{1}{\sqrt{2}} \end{bmatrix} \begin{bmatrix} v_a \\ v_b \\ v_c \end{bmatrix} \tag{3.28}$$

We can observe that the transformation obtained from generalized matrix i.e, (3.28), exactly matches with transformation formed by conventional analysis which is (3.1).

Case 2: *m*= -1, *n*= -1

In this case *m*= -1 corresponds to a reference frame where *abc* axes orients with *a-c-b* sequence in anticlockwise and *n*= -1 indicates β-axis makes a quadrature with α-axis in clockwise direction. This gives rise to a reference frame shown in Fig. 3.1(b) which is the mirror of frame explained in *case1*. In this case

$$l = m\,n = 1$$

Since *l* =1, the transformation is same as (3.28) according to generalized transformation and it is identical to the transformation obtained by conventional analysis i.e, (3.1).

Case 3: *m*=1, *n*= -1 The index *m*=1 produces a reference frame where *abc* axes orients with *a-b-c* anticlockwise and *n*= -1 indicates β-axis makes a quadrature with α-axis in clockwise direction. This is identical to the reference frame shown in Fig. 3.2(a).

$$l = m\,n = -1$$

With the help of (3.26) the transformation can be directly formed as shown below.

$$\begin{bmatrix} v_\alpha \\ v_\beta \\ v_0 \end{bmatrix} = \sqrt{\frac{2}{3}} \begin{bmatrix} 1 & -\frac{1}{2} & -\frac{1}{2} \\ 0 & \frac{\sqrt{3}}{2} & -\frac{\sqrt{3}}{2} \\ \frac{1}{\sqrt{2}} & \frac{1}{\sqrt{2}} & \frac{1}{\sqrt{2}} \end{bmatrix} \begin{bmatrix} v_a \\ v_b \\ v_c \end{bmatrix} \tag{3.29}$$

We can observe that the transformation obtained from generalized matrix i.e, (3.29), exactly matches with transformation formed by conventional analysis which is (3.5).

Case 4: *m*= -1, *n*= 1

In this case *m*= -1 corresponds to a reference frame where *abc* axes orients with *a-c-b* sequence in anticlockwise and *n*=1 indicates β-axis makes a quadrature with α-axis in anticlockwise direction, the indices chosen in this case gives rise to frame shown in Fig.

3.2(b) which is the mirror of frame explained in case3. Since,

$$l = m\,n = -1$$

The transformation is same as (3.29) according to generalized transformation and it is identical to the transformation obtained by conventional analysis i.e, (3.5).

The indices for various α-β frames are shown in Table 3.1. We have tried all the four

Table 3.1 Indices corresponding to various *dq0* frames

$\alpha\beta 0$ Frame	m	n	l
Frame -1	1	1	1
Mirror of Frame -1	-1	-1	1
Frame -2	-1	1	-1
Mirror of Frame -2	1	-1	-1

possible cases and found that the transformation matrices obatined using the generalized transformation and using conventional analysis is one and the same, this proves the novelty of generalized $\alpha\beta 0$ to *abc* transformation.

3.5 Generalized *abc* to *dq0* Transformation

We have considered a total of 8 different reference frames and corresponding to this there are 4 different transformation matrices. We require an additional index *q* to represent the orientation of *dq0* axes, in addition to indices m and n to derive a generalized transformation for all these 8 reference frames. Always measure θ as the angle between α-axis and *d*-axis. *l* is the same variable used in generalizing $\alpha\beta 0$ transformation.

q=1, when *q*-axis leads *d*-axis.

q= -1, when *q*-axis lags *d*-axis.

$$\begin{bmatrix} v_d \\ v_q \\ v_0 \end{bmatrix} = \sqrt{\frac{2}{3}} \begin{bmatrix} \cos\theta & \cos(\theta + \frac{2\pi}{3}l) & \cos(\theta - \frac{2\pi}{3}l) \\ -q\sin\theta & -q\sin(\theta + \frac{2\pi}{3}l) & -q\sin(\theta - \frac{2\pi}{3}l) \\ \frac{1}{\sqrt{2}} & \frac{1}{\sqrt{2}} & \frac{1}{\sqrt{2}} \end{bmatrix} \begin{bmatrix} v_a \\ v_b \\ v_c \end{bmatrix} \tag{3.30}$$

For obtaining DC quantities along *dq0* axes we need to define the value of θ. The value of θ can be generalized as follows,

$$\theta = l\left(\frac{\pi}{2} - \omega t\right) \tag{3.31}$$

3.5.1 Verification of Generalized *abc* to *dq0* Transformation

The generalized transformation needs to be verified by choosing various values for the indices and whether it matches with the results obtained by conventional analysis. The novelty of the generalized transform can be verified by comparing the transformations obtained out of the generalized transform and the transformation deducted using the conventional analysis for all the 8 reference frames.

Case 1: *m*=1, *n*=1, *q*=1

m=1 corresponds to a frame where *abc* frame orients with *a-b-c* anticlockwise, *n*=1 indicates that β-axis makes a quadrature with α-axis in anticlockwise direction and *q*=1 specifies that *q*-axis leads *d*-axis. This is analogous to reference frame shown in Fig. 3.3(a).

$$l = m\,n = 1$$

The transformation matrix for this reference frame is obtained by substituting *l* and *q* in (3.30) and it is as shown below,

$$\begin{bmatrix} v_d \\ v_q \\ v_0 \end{bmatrix} = \sqrt{\frac{2}{3}} \begin{bmatrix} \cos\theta & \cos(\theta + \frac{2\pi}{3}) & \cos(\theta - \frac{2\pi}{3}) \\ -\sin\theta & -\sin(\theta + \frac{2\pi}{3}) & -\sin(\theta - \frac{2\pi}{3}) \\ \frac{1}{\sqrt{2}} & \frac{1}{\sqrt{2}} & \frac{1}{\sqrt{2}} \end{bmatrix} \begin{bmatrix} v_a \\ v_b \\ v_c \end{bmatrix} \tag{3.32}$$

It is observed that the transformation obtained using generalized transform which is (3.32), is identical to the transformation deducted using conventional analysis i.e, (3.8). The value of θ as per generalization is obtained as $\frac{\pi}{2} - \omega t$ by substituting the value of *l* in (3.31).

Case 2: *m*= -1, *n*= -1, *q*=1

m= -1 reflects a reference frame where *abc* frame orients with *a-c-b* anticlockwise, *n*= -1 specifies that β-axis makes a quadrature with α-axis in clockwise direction and *q*=1 specifies that *q*-axis leads *d*-axis. These orientations of various axes gives rise to reference frame shown in Fig. 3.3(b), which is the mirror of Fig. 3.3(a).

$$l = m\,n = 1$$

Since *l*=*q*=1, the transformation is same as in (3.32). This is identical to transformation obtained for this frame using conventional analysis i.e,(3.8).

Case 3: *m*= -1, *n*= 1, *q*=1

m= -1 reflects a reference frame where *abc* frame orients with *a-c-b* anticlockwise, *n*=1 points out that β-axis makes a quadrature with α-axis in anticlockwise direction and *q*=1 specifies that *q*-axis leads *d*-axis. This reference frame is identical to frame shown in Fig. 3.4(a).

$$l = m\,n = -1$$

The *abc* to *dq0* can be obtained by substituting the values of *l* and *q* in (3.30) and it is as shown below,

$$\begin{bmatrix} v_d \\ v_q \\ v_0 \end{bmatrix} = \sqrt{\frac{2}{3}} \begin{bmatrix} \cos\theta & \cos(\theta - \frac{2\pi}{3}) & \cos(\theta + \frac{2\pi}{3}) \\ -\sin\theta & -\sin(\theta - \frac{2\pi}{3}) & -\sin(\theta + \frac{2\pi}{3}) \\ \frac{1}{\sqrt{2}} & \frac{1}{\sqrt{2}} & \frac{1}{\sqrt{2}} \end{bmatrix} \begin{bmatrix} v_a \\ v_b \\ v_c \end{bmatrix} \tag{3.33}$$

The transformation obtained using generalized transform which is (3.33), is identical to the transformation found out using conventional analysis i.e, (3.16). The value of θ as per generalization is obtained as $\omega t - \frac{\pi}{2}$ by substituting the value of *l* in (3.31).

Case 4: *m*= 1, *n*= -1, *q*=1

m= 1 reflects a reference frame where *abc* frame orients with *a-b-c* anticlockwise, *n*= -1 shows that β-axis makes a quadrature with α-axis in clockwise direction and *q*=1 specifies that *q*-axis leads *d*-axis. These orientations of various axes gives rise to reference

frame shown in Fig. 3.4(b), which turns out to be the mirror of Fig. 3.4(a).

$$l = m\,n = -1$$

Since *l*= -1 and *q*=1, the transformation is same as in (3.33) and it is same as the transformation obtained for this frame using conventional analysis i.e,(3.16).

Case 5: *m*= 1, *n*= 1, *q*= -1

m= -1 reflects a reference frame where *abc* frame orients with *a-b-c* anticlockwise, *n*=1 points out that β-axis makes a quadrature with α-axis in anticlockwise direction and *q*= -1 specifies that *q*-axis lags *d*-axis. This reference frame is identical to frame shown in Fig. 3.5(a).

$$l = m\,n = 1$$

The *abc* to *dq0* transformation can be obtained by substituting the values of *l* and *q* in (3.30) and it is as shown below,

$$\begin{bmatrix} v_d \\ v_q \\ v_0 \end{bmatrix} = \sqrt{\frac{2}{3}} \begin{bmatrix} \cos\theta & \cos(\theta + \frac{2\pi}{3}) & \cos(\theta - \frac{2\pi}{3}) \\ \sin\theta & \sin(\theta + \frac{2\pi}{3}) & \sin(\theta - \frac{2\pi}{3}) \\ \frac{1}{\sqrt{2}} & \frac{1}{\sqrt{2}} & \frac{1}{\sqrt{2}} \end{bmatrix} \begin{bmatrix} v_a \\ v_b \\ v_c \end{bmatrix} \tag{3.34}$$

The transformation obtained using generalized transform which is (3.34), is identical to the transformation found out using conventional analysis i.e, (3.20). The value of θ as per generalization is obtained as $\frac{\pi}{2} - \omega t$ by substituting the value of *l* in (3.31).

Case 6: *m*= -1, *n*= -1, *q*=1

m= -1 reflects a reference frame where *abc* frame orients with *a-c-b* anticlockwise, *n*= -1 β-axis makes a quadrature with α-axis in clockwise direction and *q*= -1 specifies that *q*-axis lags *d*-axis. These orientations of various axes gives rise to reference frame shown in Fig. 3.5(b), which turns out to be the mirror of Fig. 3.5(a).

$$l = m\,n = 1$$

Since *l*=1 and *q*=1, the transformation is same as in (3.34) and it is same as the transformation obtained for this frame using conventional analysis i.e,(3.20).

Case 7: *m*= -1, *n*= 1, *q*= -1

m= -1 reflects a reference frame where *abc* frame orients with *a-c-b* anticlockwise, *n*=1 points out that β-axis makes a quadrature with α-axis in anticlockwise direction and *q*= -1 specifies that *q*-axis lags *d*-axis. This reference frame is identical to frame shown in Fig. 3.6(a).

$$l = m\,n = -1$$

The *abc* to *dq0* can be obtained by substituting the values of *l* and *q* in (3.30) and it is as shown below,

$$\begin{bmatrix} v_d \\ v_q \\ v_0 \end{bmatrix} = \sqrt{\frac{2}{3}} \begin{bmatrix} \cos\theta & \cos(\theta - \frac{2\pi}{3}) & \cos(\theta + \frac{2\pi}{3}) \\ \sin\theta & \sin(\theta - \frac{2\pi}{3}) & \sin(\theta + \frac{2\pi}{3}) \\ \frac{1}{\sqrt{2}} & \frac{1}{\sqrt{2}} & \frac{1}{\sqrt{2}} \end{bmatrix} \begin{bmatrix} v_a \\ v_b \\ v_c \end{bmatrix} \tag{3.35}$$

The transformation obtained using generalized transform which is (3.35), is identical to the transformation found out using conventional analysis i.e, (3.23). The value of θ as per generalization is obtained as $\omega t - \frac{\pi}{2}$ by substituting the value of *l* in (3.31).

Case 8: *m*= 1, *n*= -1, *q*= -1

m=1 reflects a reference frame where *abc* frame orients with *a-b-c* anticlockwise, *n*= -1 β-axis makes a quadrature with α-axis in clockwise direction and *q*= -1 specifies that *q*-axis lags *d*-axis. These orientations of various axes gives rise to reference frame shown in Fig. 3.6(b), which turns out to be the mirror of Fig. 3.6(a).

$$l = m\,n = -1$$

Since *l*= -1 and *q*=1, the transformation is same as in (3.35) and it is same as the transformation obtained for this frame using conventional analysis i.e,(3.23).

Table. 3.2, shows the indices for various *dq0* frames. We have used 3 different indices (*m,n,q*) in this *abc* to *dq0* generalization, there are 8 different possible reference frame with different combination of these three indices. The transformation for all the 8 possibilities has been found from generalized transformation and also through con-

Table 3.2 Indices Corresponding to Various *dq0* Frames

dq0 Frame	m	n	l	q
Frame -1	1	1	1	1
Mirror of Frame -1	-1	-1	1	1
Frame -2	-1	1	-1	1
Mirror of Frame -2	1	-1	-1	1
Frame -3	1	1	1	-1
Mirror of Frame -3	-1	-1	1	-1
Frame -4	-1	1	-1	-1
Mirror of Frame -4	1	-1	-1	-1

ventional analysis. Transformations deducted through both the methods are identical.

3.6 Deduction of a Modified Generalized Transformation for *abc* to *dq0* Conversion

Even after the generalization of *abc* to *dq0* transformation we have to substitute the value of θ accordingly, so that we obtain DC quantities along *d* and *q* axes. We will make further analysis and try to integrate the generalized transformation matrix and the generalized value of θ, so that we have to look at only one single transformation matrix which takes care of θ and the axes orientation in different reference frames.

Name the generalized transformation matrix shown in (3.30) as $T^{'}$

$$T^{'} = \sqrt{\frac{2}{3}} \begin{bmatrix} \cos\theta & \cos(\theta + \frac{2\pi}{3}l) & \cos(\theta - \frac{2\pi}{3}l) \\ -q\sin\theta & -q\sin(\theta + \frac{2\pi}{3}l) & -q\sin(\theta - \frac{2\pi}{3}l) \\ \frac{1}{\sqrt{2}} & \frac{1}{\sqrt{2}} & \frac{1}{\sqrt{2}} \end{bmatrix} \tag{3.36}$$

Substitute the generalized value of θ i.e, (3.31) in (3.36) and call the resultant matrix as *T*.

$$T = \sqrt{\frac{2}{3}} \begin{bmatrix} \cos\left(l\left(\frac{\pi}{2} - \omega t\right)\right) & \cos(l\left(\frac{\pi}{2} - \omega t\right) + \frac{2\pi}{3}l) & \cos(l\left(\frac{\pi}{2} - \omega t\right) - \frac{2\pi}{3}l) \\ -q\sin\left(l\left(\frac{\pi}{2} - \omega t\right)\right) & -q\sin(l\left(\frac{\pi}{2} - \omega t\right) + \frac{2\pi}{3}l) & -q\sin(l\left(\frac{\pi}{2} - \omega t\right) - \frac{2\pi}{3}l) \\ \frac{1}{\sqrt{2}} & \frac{1}{\sqrt{2}} & \frac{1}{\sqrt{2}} \end{bmatrix} \tag{3.37}$$

Now we will simplify each element of the matrix *T*,

$$T_{11} = \cos\left(l\left(\frac{\pi}{2} - \omega t\right)\right)$$

l can be +1 or -1, but it is immaterial with cosine terms because $\cos(-\theta) = \cos\theta$. Therefore,

$$T_{11} = \sin\omega t$$

$$T_{12} = \cos(l\left(\frac{\pi}{2} - \omega t\right) + \frac{2\pi}{3}l) = \cos\left(\frac{\pi}{2} - \left(\omega t - \frac{2\pi}{3}\right)\right) = \sin\left(\omega t - \frac{2\pi}{3}\right)$$

Similarly

$$T_{13} = \sin\left(\omega t + \frac{2\pi}{3}\right)$$

$$T_{21} = -q\sin\left(l\left(\frac{\pi}{2} - \omega t\right)\right)$$

when *l*= 1

$$T_{21} = -q\cos\omega t$$

when *l*= -1

$$T_{21} = q\cos\omega t$$

It is as good as saying,

$$T_{21} = -ql\cos\omega t$$

$$T_{22} = -q\sin\left(l\left(\frac{\pi}{2} - \omega t\right) + \frac{2\pi}{3}l\right) = -q\sin\left(l\left(\frac{\pi}{2} - \left(\omega t - \frac{2\pi}{3}\right)\right)\right)$$

when *l*= 1

$$T_{22} = -q\cos\left(\omega t - \frac{2\pi}{3}\right)$$

when *l*= -1

$$T_{22} = q\cos\left(\omega t - \frac{2\pi}{3}\right)$$

Or,

$$T_{22} = -ql\cos\left(\omega t - \frac{2\pi}{3}\right)$$

Similarly

$$T_{23} = -ql\cos\left(\omega t + \frac{2\pi}{3}\right)$$

The elements of *T* are as follows,

$$\begin{aligned} T_{11} &= \sin\omega t \\ T_{12} &= \sin\left(\omega t - \frac{2\pi}{3}\right) \\ T_{13} &= \sin\left(\omega t + \frac{2\pi}{3}\right) \\ T_{21} &= -ql\cos\omega t \\ T_{22} &= -ql\cos\left(\omega t - \frac{2\pi}{3}\right) \\ T_{23} &= -ql\cos\left(\omega t + \frac{2\pi}{3}\right) \end{aligned}$$

Let,

$$k = -q\,l$$

Now *T* can be reformed after simplification as shown in (3.38)

$$T = \sqrt{\frac{2}{3}}\begin{bmatrix} \sin\omega t & \sin\left(\omega t - \frac{2\pi}{3}\right) & \sin\left(\omega t + \frac{2\pi}{3}\right) \\ k\cos\omega t & k\cos\left(\omega t - \frac{2\pi}{3}\right) & k\cos\left(\omega t + \frac{2\pi}{3}\right) \\ \frac{1}{\sqrt{2}} & \frac{1}{\sqrt{2}} & \frac{1}{\sqrt{2}} \end{bmatrix} \tag{3.38}$$

Now we can modify the generalized transformation as follows,

$$\begin{bmatrix} v_d \\ v_q \\ v_0 \end{bmatrix} = \sqrt{\frac{2}{3}}\begin{bmatrix} \sin\omega t & \sin\left(\omega t - \frac{2\pi}{3}\right) & \sin\left(\omega t + \frac{2\pi}{3}\right) \\ k\cos\omega t & k\cos\left(\omega t - \frac{2\pi}{3}\right) & k\cos\left(\omega t + \frac{2\pi}{3}\right) \\ \frac{1}{\sqrt{2}} & \frac{1}{\sqrt{2}} & \frac{1}{\sqrt{2}} \end{bmatrix}\begin{bmatrix} v_a \\ v_b \\ v_c \end{bmatrix} \tag{3.39}$$

We can directly obtain the transformation matrix for any of the 8 reference frames from (3.38), by finding out the value of *k* using the various indices depending upon the orientaion of the axes. The different possible indices and the corresponding *k* values are shown in Table 3.3. Since *k* can take only 2 values +1 or -1, there are only two transformation matrices possible and they are as shown below,

$$\begin{bmatrix} v_d \\ v_q \\ v_0 \end{bmatrix} = \sqrt{\frac{2}{3}}\begin{bmatrix} \sin\omega t & \sin\left(\omega t - \frac{2\pi}{3}\right) & \sin\left(\omega t + \frac{2\pi}{3}\right) \\ \cos\omega t & \cos\left(\omega t - \frac{2\pi}{3}\right) & \cos\left(\omega t + \frac{2\pi}{3}\right) \\ \frac{1}{\sqrt{2}} & \frac{1}{\sqrt{2}} & \frac{1}{\sqrt{2}} \end{bmatrix}\begin{bmatrix} v_a \\ v_b \\ v_c \end{bmatrix} \tag{3.40}$$

Table 3.3 Indices corresponding to various *dq0* frames and corresponding *k* values

dq0 Frame	m	n	l	q	k
Frame -1	1	1	1	1	-1
Mirror of Frame -1	-1	-1	1	1	-1
Frame -2	-1	1	-1	1	1
Mirror of Frame -2	1	-1	-1	1	1
Frame -3	1	1	1	-1	1
Mirror of Frame -3	-1	-1	1	-1	1
Frame -4	-1	1	-1	-1	-1
Mirror of Frame -4	1	-1	-1	-1	-1

and

$$\begin{bmatrix} v_d \\ v_q \\ v_0 \end{bmatrix} = \sqrt{\frac{2}{3}} \begin{bmatrix} \sin\omega t & \sin\left(\omega t - \frac{2\pi}{3}\right) & \sin\left(\omega t + \frac{2\pi}{3}\right) \\ -\cos\omega t & -\cos\left(\omega t - \frac{2\pi}{3}\right) & -\cos\left(\omega t + \frac{2\pi}{3}\right) \\ \frac{1}{\sqrt{2}} & \frac{1}{\sqrt{2}} & \frac{1}{\sqrt{2}} \end{bmatrix} \begin{bmatrix} v_a \\ v_b \\ v_c \end{bmatrix} \tag{3.41}$$

On finding out the inverse of the above two matrices, the inverse transform of the modified generalized transform can be generalized as shown below,

$$\begin{bmatrix} v_a \\ v_b \\ v_c \end{bmatrix} = \sqrt{\frac{2}{3}} \begin{bmatrix} \sin\omega t & k\cos\omega t & \frac{1}{\sqrt{2}} \\ \sin\left(\omega t - \frac{2\pi}{3}\right) & k\cos\left(\omega t - \frac{2\pi}{3}\right) & \frac{1}{\sqrt{2}} \\ \sin\left(\omega t + \frac{2\pi}{3}\right) & k\cos\left(\omega t + \frac{2\pi}{3}\right) & \frac{1}{\sqrt{2}} \end{bmatrix} \begin{bmatrix} v_d \\ v_q \\ v_0 \end{bmatrix} \tag{3.42}$$

3.6.1 Illustration:

Find the *abc* to $\alpha\beta 0$ transformation using generalized transform and *abc* to *dq0* transformations using the Modified Generalized Transform for an arbitrarily chosen frame.

Discussion: Consider an arbitrary reference frame given in Fig. 3.7. In this reference frame *abc* orientation is in counter clockwise direction (*m*=1), β-axis makes a quadrature with α-axis in anticlockwise direction (*n*=1), *q*- axis leads *d*- axis(*q*=1). To find out *abc* to $\alpha\beta 0$ transformation and its inverse transformation we require the index *l*, which can be found out as shown in (3.43).

$$l = mn = 1 \tag{3.43}$$

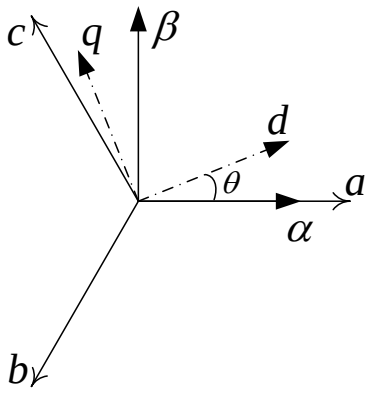

Fig. 3.7 Arbitrary reference frame- 1

By substituting *l*=1 in generalized transform in (3.26) gives us the *abc* to $\alpha\beta 0$ transformation in this chosen reference frame as shown in (3.44).

$$\begin{bmatrix} v_\alpha \\ v_\beta \\ v_0 \end{bmatrix} = \sqrt{\frac{2}{3}} \begin{bmatrix} 1 & -\frac{1}{2} & -\frac{1}{2} \\ 0 & -\frac{\sqrt{3}}{2} & \frac{\sqrt{3}}{2} \\ \frac{1}{\sqrt{2}} & \frac{1}{\sqrt{2}} & \frac{1}{\sqrt{2}} \end{bmatrix} \begin{bmatrix} v_a \\ v_b \\ v_c \end{bmatrix} \tag{3.44}$$

$\alpha\beta 0$ to *abc* transformation can be obtained by substituting *l* in the generalized $\alpha\beta 0$ to *abc* transformation (3.27) and the inverse transformation for this chosen reference frame is obtained as shown in (3.45).

$$\begin{bmatrix} v_a \\ v_b \\ v_c \end{bmatrix} = \sqrt{\frac{2}{3}} \begin{bmatrix} 1 & 0 & \frac{1}{\sqrt{2}} \\ -\frac{1}{2} & -\frac{\sqrt{3}}{2} & \frac{1}{\sqrt{2}} \\ -\frac{1}{2} & \frac{\sqrt{3}}{2} & \frac{1}{\sqrt{2}} \end{bmatrix} \begin{bmatrix} v_\alpha \\ v_\beta \\ v_0 \end{bmatrix} \tag{3.45}$$

To find out the *abc* to *dq0* we have to find the index *k* as shown below,

$$k = -ql = -1$$

$$\begin{bmatrix} v_d \\ v_q \\ v_0 \end{bmatrix} = \sqrt{\frac{2}{3}} \begin{bmatrix} \sin\omega t & \sin\left(\omega t - \frac{2\pi}{3}\right) & \sin\left(\omega t + \frac{2\pi}{3}\right) \\ -\cos\omega t & -\cos\left(\omega t - \frac{2\pi}{3}\right) & -\cos\left(\omega t + \frac{2\pi}{3}\right) \\ \frac{1}{\sqrt{2}} & \frac{1}{\sqrt{2}} & \frac{1}{\sqrt{2}} \end{bmatrix} \begin{bmatrix} v_a \\ v_b \\ v_c \end{bmatrix} \tag{3.46}$$

By substituting *k*=-1 in the modified generalized transformation in (3.39) we obtain the *abc* to *dq0* transformation matrix for this reference frame as shown in (3.46).

dq0 to *abc* transformation for this chosen frame can be found out as shown in (3.47) by substituting *k* in the inverse transformation in (3.42).

$$\begin{bmatrix} v_a \\ v_b \\ v_c \end{bmatrix} = \sqrt{\frac{2}{3}} \begin{bmatrix} \sin\omega t & -\cos\omega t & \frac{1}{\sqrt{2}} \\ \sin\left(\omega t - \frac{2\pi}{3}\right) & -\cos\left(\omega t - \frac{2\pi}{3}\right) & \frac{1}{\sqrt{2}} \\ \sin\left(\omega t + \frac{2\pi}{3}\right) & -\cos\left(\omega t + \frac{2\pi}{3}\right) & \frac{1}{\sqrt{2}} \end{bmatrix} \begin{bmatrix} v_d \\ v_q \\ v_0 \end{bmatrix} \tag{3.47}$$

We will consider one more reference frame and try and deduct the transformations. Consider the reference frame shown in Fig. 3.8. *abc* orientation is in clockwise direction (*m*=-1), β-axis makes a quadrature with α-axis in anticlockwise direction (*n*=1), *q*-axis lags *d*- axis(*q*=-1). First finding out index *l*,

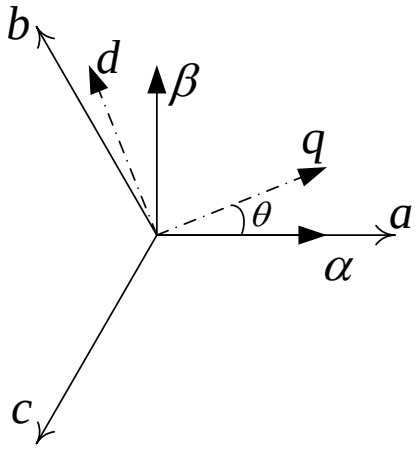

Fig. 3.8 Arbitrary reference frame- 2

$$l = mn = -1$$

By substituting *l*=-1 in generalized transform (3.26) gives us the *abc* to $\alpha\beta 0$ transformation in this reference frame as shown in (3.48).

$$\begin{bmatrix} v_\alpha \\ v_\beta \\ v_0 \end{bmatrix} = \sqrt{\frac{2}{3}} \begin{bmatrix} 1 & -\frac{1}{2} & -\frac{1}{2} \\ 0 & \frac{\sqrt{3}}{2} & -\frac{\sqrt{3}}{2} \\ \frac{1}{\sqrt{2}} & \frac{1}{\sqrt{2}} & \frac{1}{\sqrt{2}} \end{bmatrix} \begin{bmatrix} v_a \\ v_b \\ v_c \end{bmatrix} \tag{3.48}$$

$\alpha\beta 0$ to *abc* transformation can be obtained by substituting *l* in the generalized $\alpha\beta 0$ to *abc* transformation (3.27) and the inverse transformation for this chosen reference frame is obtained as shown in (3.49).

$$\begin{bmatrix} v_a \\ v_b \\ v_c \end{bmatrix} = \sqrt{\frac{2}{3}} \begin{bmatrix} 1 & 0 & \frac{1}{\sqrt{2}} \\ -\frac{1}{2} & -\frac{\sqrt{3}}{2} & \frac{1}{\sqrt{2}} \\ -\frac{1}{2} & \frac{\sqrt{3}}{2} & \frac{1}{\sqrt{2}} \end{bmatrix} \begin{bmatrix} v_\alpha \\ v_\beta \\ v_0 \end{bmatrix} \tag{3.49}$$

To find out the *abc* to *dq0* we have to find the index *k* as shown below,

$$k = -ql = -1$$

By substituting *k*=-1 in the modified generalized transformation in (3.39) we obtain the transformation matrix for this reference frame as shown in (3.50).

$$\begin{bmatrix} v_d \\ v_q \\ v_0 \end{bmatrix} = \sqrt{\frac{2}{3}} \begin{bmatrix} \sin\omega t & \sin\left(\omega t - \frac{2\pi}{3}\right) & \sin\left(\omega t + \frac{2\pi}{3}\right) \\ -\cos\omega t & -\cos\left(\omega t - \frac{2\pi}{3}\right) & -\cos\left(\omega t + \frac{2\pi}{3}\right) \\ \frac{1}{\sqrt{2}} & \frac{1}{\sqrt{2}} & \frac{1}{\sqrt{2}} \end{bmatrix} \begin{bmatrix} v_a \\ v_b \\ v_c \end{bmatrix} \tag{3.50}$$

dq0 to *abc* transformation can be found out as shown in (3.51) by substituting *k* in the inverse transformation in (3.42).

$$\begin{bmatrix} v_a \\ v_b \\ v_c \end{bmatrix} = \sqrt{\frac{2}{3}} \begin{bmatrix} \sin\omega t & -\cos\omega t & \frac{1}{\sqrt{2}} \\ \sin\left(\omega t - \frac{2\pi}{3}\right) & -\cos\left(\omega t - \frac{2\pi}{3}\right) & \frac{1}{\sqrt{2}} \\ \sin\left(\omega t + \frac{2\pi}{3}\right) & -\cos\left(\omega t + \frac{2\pi}{3}\right) & \frac{1}{\sqrt{2}} \end{bmatrix} \begin{bmatrix} v_d \\ v_q \\ v_0 \end{bmatrix} \tag{3.51}$$

3.7 Summary

Various possible reference frames in $\alpha\beta 0$ and *dq0* transformations are analyzed. It was observed that, depending upon the frame chosen there is a variation in the transforma-

tion matrix. Therefore generalized $\alpha\beta 0$ and *dq0* transformation matrices are derived, which directly gives the transformation matrix without performing conventional analysis on the selected reference frame.

CHAPTER 4

FORMULATION AND COMPARISON OF CONTROL ALGORITHMS FOR GRID INTERACTIVE INVERTER

In this chapter, control strategies used for microgrid applications are discussed. It has been observed that control algorithms for the grid interactive inverters can be developed using the application of the transformations in power engineering. Here control algorithms are formulated using the transformations studied in the previous chapters. They are *abc* to $\alpha\beta 0$, *abc* to *dq0* and symmetrical components. The control algorithms will be formulated in such a way that the microgrid will supply a specified amount of average active power, entire oscillatory active power and reactive power. This strategy will help in drawing only sinusoidal current from the utility grid. If the utility is to supply only balanced sinusoidal current, then only average active power($\overline{p}_l$) demanded by the load should be drawn from the source. The microgrid should supply $\widetilde{p}_l$ and q_l, which are the oscillatory active power and instantaneous reactive power demanded by the load. Since the microgrid can also generate active power, a specified amount load active power demand can be met by the microgrid. Let the fraction of load active power demand met by the microgrid be *x*. So the objectives to be met by this microgrid system is,

- Generate a fraction (x) of the active power demand by the load($\overline{p}_l$).
- Generate oscillatory power $\widetilde{p}_l$, of the load.
- Generate the reactive power demand by the load.
- Compensate the zero sequence currents.

The conditions mentioned above will be obtained through different strategies. DC grid is integrated onto the utility grid using a grid interactive inverter as shown in Fig.

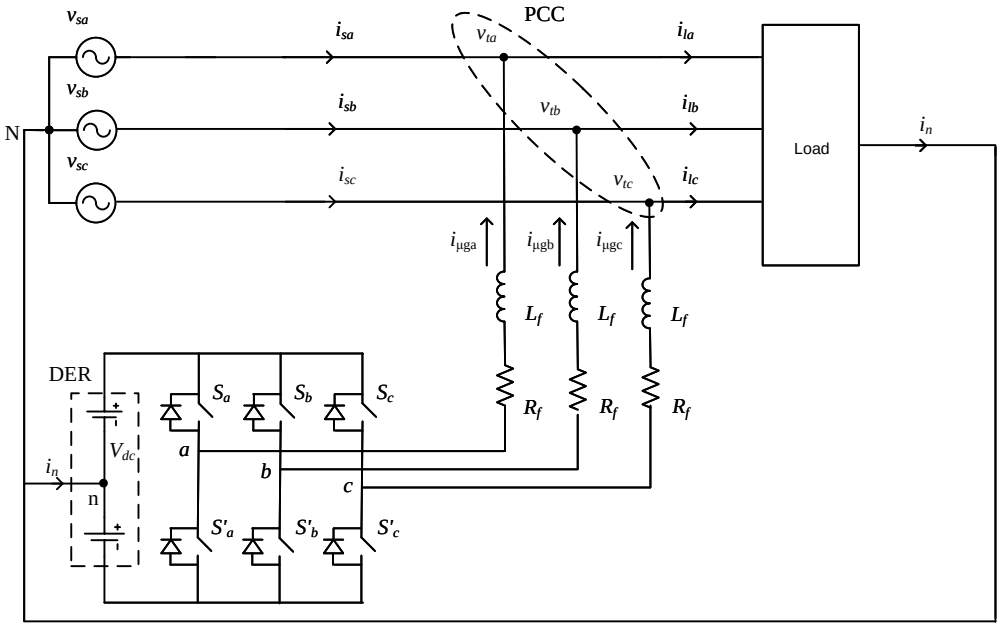

Fig. 4.1 System topology

4.1. Control strategies are developed for this system topology.

v_{sa}, v_{sb}, v_{sc} are the utility grid voltages; v_{ta}, v_{tb}, v_{tc} are the PCC voltages; i_{sa}, i_{sb}, i_{sc} are the currents drawn from utility; $i_{\mu ga}, i_{\mu gb}, i_{\mu gc}$ are the currents injected by microgrid. V_{dc} is the DC grid voltage. A 3-ϕ, 3-leg, 2-level, neutral clamped topology is considered for the grid interactive inverter as it has to supply the zero sequence currents.

4.1 Control Strategy Using *abc* to $\alpha\beta 0$ Transformation

This control strategy will be formulated out of *p-q* theory by H. Akagi [22]. This concept is applied onto microgrid which also include active power injection. A 3-ϕ, 4-wire system with a stiff utility grid is considered, let v_a, v_b, v_c be utility grid voltages, since utility is assumed to be stiff the PCC (Point of Common Coupling) voltage will be same as that of the utility grid voltage. The PCC voltages and the load currents are transformed into the $\alpha\beta 0$ reference frame using (4.1) and (4.2)

$$\begin{bmatrix} v_{t\alpha} \\ v_{t\beta} \\ v_{t0} \end{bmatrix} = \sqrt{\frac{2}{3}} \begin{bmatrix} 1 & -\frac{1}{2} & -\frac{1}{2} \\ 0 & -\frac{\sqrt{3}}{2} & \frac{\sqrt{3}}{2} \\ \frac{1}{\sqrt{2}} & \frac{1}{\sqrt{2}} & \frac{1}{\sqrt{2}} \end{bmatrix} \begin{bmatrix} v_{ta} \\ v_{tb} \\ v_{tc} \end{bmatrix} \tag{4.1}$$

$$\begin{bmatrix} i_{l\alpha} \\ i_{l\beta} \\ i_{l0} \end{bmatrix} = \sqrt{\frac{2}{3}} \begin{bmatrix} 1 & -\frac{1}{2} & -\frac{1}{2} \\ 0 & -\frac{\sqrt{3}}{2} & \frac{\sqrt{3}}{2} \\ \frac{1}{\sqrt{2}} & \frac{1}{\sqrt{2}} & \frac{1}{\sqrt{2}} \end{bmatrix} \begin{bmatrix} i_{la} \\ i_{lb} \\ i_{lc} \end{bmatrix}. \tag{4.2}$$

According to *p-q* theory, instantaneous active power and reactive power are calculated using (4.3)

$$\begin{bmatrix} p_l \\ q_l \end{bmatrix} = \begin{bmatrix} v_{t\alpha} & v_{t\beta} \\ -v_{t\beta} & v_{t\alpha} \end{bmatrix} \begin{bmatrix} i_{l\alpha} \\ i_{l\beta} \end{bmatrix}. \tag{4.3}$$

Where p_l is the instantaneous active power and q_l is the instantaneous reactive power, demanded by the load. The instantaneous active power thus found can be split into *ac* and *dc* components. These components can be separated using a moving average filter as shown in (4.4)

$$p_l = \overline{p}_l + \widetilde{p}_l. \tag{4.4}$$

For obtaining non linear load compensation $\widetilde{p}_l$ and q_l should be supplied by microgrid. For specified load, a fraction of average active power ($x\,\overline{p}_l$) should also be supplied by the microgrid. Therefore the reference microgrid currents in $\alpha\beta 0$ frame can be generated using (4.5)

$$\begin{bmatrix} i^*_{\mu g\alpha} \\ i^*_{\mu g\beta} \end{bmatrix} = \begin{bmatrix} v_{t\alpha} & v_{t\beta} \\ -v_{t\beta} & v_{t\alpha} \end{bmatrix}^{-1} \begin{bmatrix} x\,\overline{p_l} + \widetilde{p}_l \\ q_l \end{bmatrix} \tag{4.5}$$

$$\begin{bmatrix} i^*_{\mu g\alpha} \\ i^*_{\mu g\beta} \end{bmatrix} = \frac{1}{{v_{t\alpha}}^2 + {v_{t\beta}}^2} \begin{bmatrix} v_{t\alpha} & -v_{t\beta} \\ v_{t\beta} & v_{t\alpha} \end{bmatrix} \begin{bmatrix} x\,\overline{p}_l + \widetilde{p}_l \\ q_l \end{bmatrix}. \tag{4.6}$$

Since zero sequence current compensation is also required,

$$i^*_{\mu g0} = i_{l0} \tag{4.7}$$

$$\begin{bmatrix} i^*_{\mu ga} \\ i^*_{\mu gb} \\ i^*_{\mu gc} \end{bmatrix} = \sqrt{\frac{2}{3}} \begin{bmatrix} 1 & 0 & \frac{1}{\sqrt{2}} \\ -\frac{1}{2} & -\frac{\sqrt{3}}{2} & \frac{1}{\sqrt{2}} \\ -\frac{1}{2} & \frac{\sqrt{3}}{2} & \frac{1}{\sqrt{2}} \end{bmatrix} \begin{bmatrix} i^*_{\mu g\alpha} \\ i^*_{\mu g\beta} \\ i^*_{\mu g0} \end{bmatrix}. \tag{4.8}$$

Now these currents in $\alpha\beta 0$ frame can be transferred to the natural reference frame using inverse $\alpha\beta 0$ transformation as shown in (4.8). If we succeed in injecting these reference currents from the microgrid then we will achieve our objectives. Now we have to generate switching pulses to the grid interactive inverter to track these currents. We make use of a hysteresis band controller to obtain the switching pulses which will be explained in the next section. The entire control strategy can be represented as a block diagram shown in Fig. 4.2.

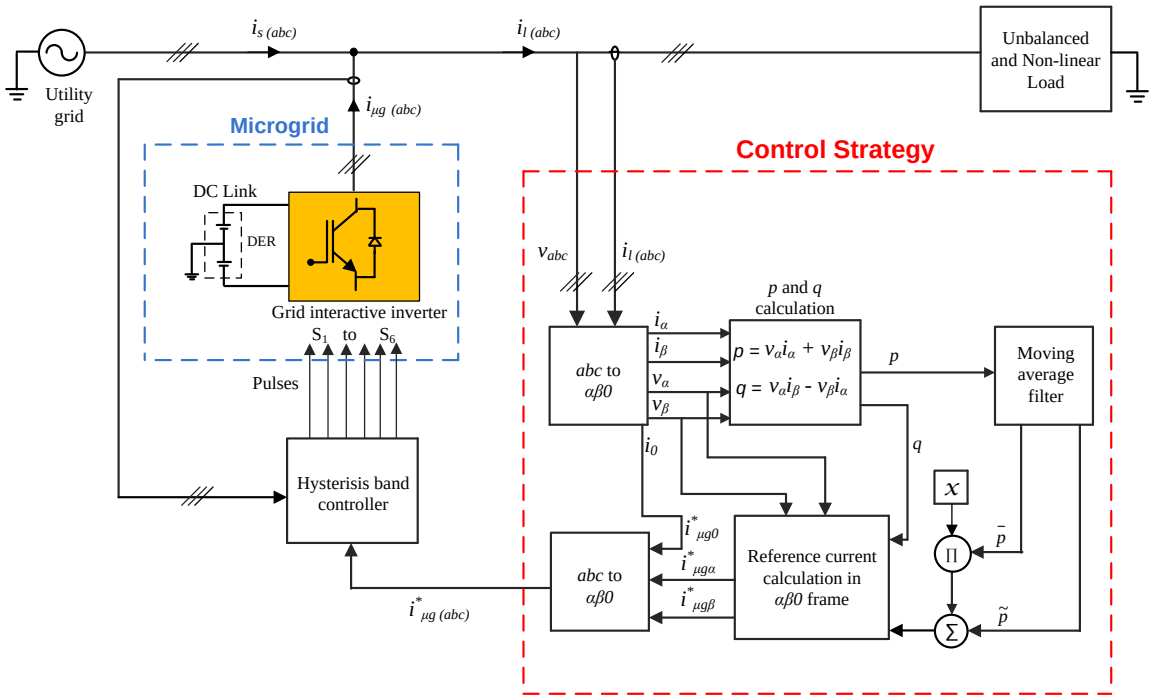

Fig. 4.2 Control strategy using $\alpha\beta 0$ transformation

4.1.1 Hysteresis Based PWM Controller

The hysteresis band control is used to generate the switching pattern of the inverter. Hysteresis controller is chosen ahead of various other controllers because of its fast dynamics, robust control and ease of implementation. The operation can be understood by observing Fig. 4.3. An upper band and a lower band are defined (+h and -h), whenever the error goes above +h, the upper switch should be turned OFF and the lower switch should be turned ON. Whenever the error goes below -h, complement to the previous operation should take place.

If $error \geq h$ then $u = 1$

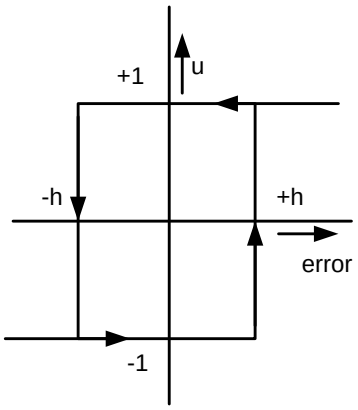

Fig. 4.3 Two-level hysteresis scheme

If $error \leq -h$ then $u = -1$

Error will be generated by calculating the difference in reference quantity and actual quantity.

4.2 Control Strategy Using *abc* to *dq0* Transformation

This algorithm involves transformation of natural reference frame quantities into *dq0* frame and then obtain the desired objectives. Here only load currents need to be transferred for the development of control strategy.

$$\begin{bmatrix} i_d \\ i_q \\ i_0 \end{bmatrix} = \sqrt{\frac{2}{3}} \begin{bmatrix} \cos\theta & \cos(\theta + \frac{2\pi}{3}) & \cos(\theta - \frac{2\pi}{3}) \\ -\sin\theta & -\sin(\theta + \frac{2\pi}{3}) & -\sin(\theta - \frac{2\pi}{3}) \\ \frac{1}{\sqrt{2}} & \frac{1}{\sqrt{2}} & \frac{1}{\sqrt{2}} \end{bmatrix} \begin{bmatrix} i_{la} \\ i_{lb} \\ i_{lc} \end{bmatrix} \tag{4.9}$$

where,

$$\theta = \frac{\pi}{2} - \omega t \tag{4.10}$$

It has shown in the previous study that if balanced quantities in natural reference frame are transformed into *dq0* frame, a constant *dc* quantity is obtained along the *d*-axis and *q, 0* quantities are zero. Hence i_q, i_0 and oscillatory component of i_d will be supplied by the microgrid to draw balanced sinusoidal current from utility. Therefore i_d can be split into two components

$$i_d = \overline{i_d} + \widetilde{i_d} \tag{4.11}$$

$\overline{i_d}$ is responsible meeting the average active power demand by the load $\overline{p}$. For specifying

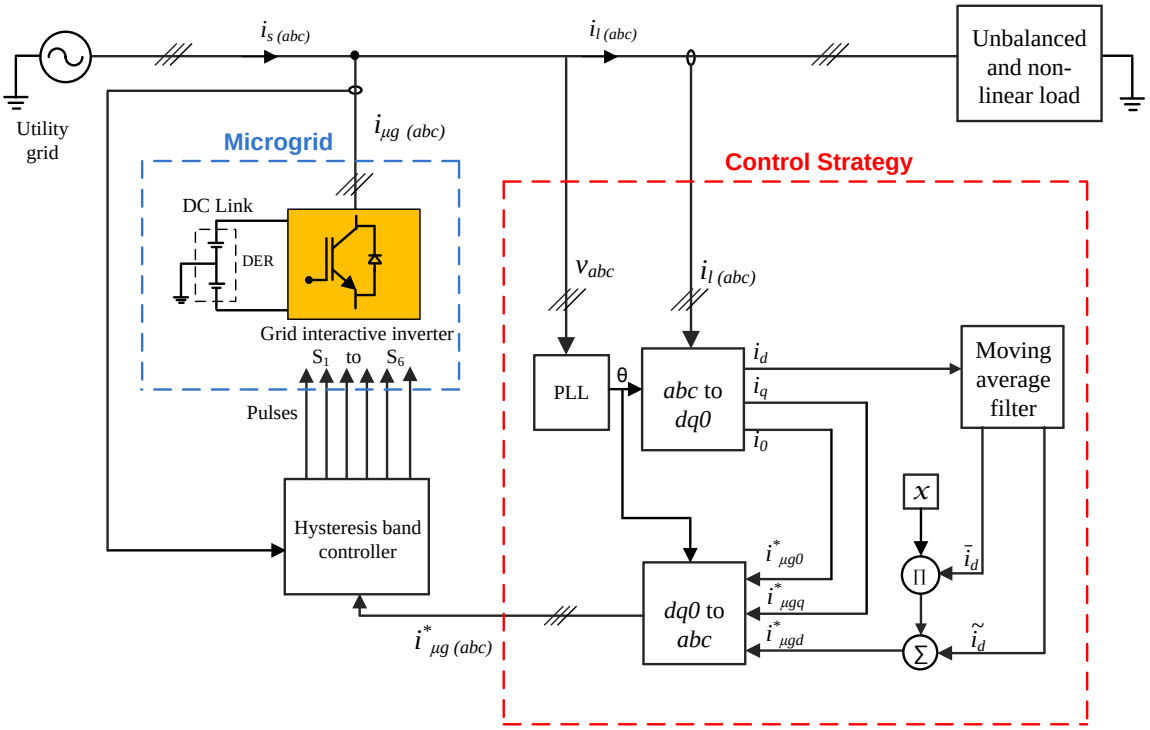

Fig. 4.4 Control strategy using *dq0* transformation

the active power we can make use of $\overline{i_d}$, a fraction *(x)* of $\overline{i_d}$ will also be supplied by the microgrid. Which indirectly says fraction (x) of average active power demand by load is supplied by microgrid. So the reference currents for the microgrid in *dq0* reference frame can be obtained as follows.

$$\begin{bmatrix} i^*_{\mu gd} \\ i^*_{\mu gq} \\ i^*_{\mu g0} \end{bmatrix} = \begin{bmatrix} x\,\bar{i}_d + \tilde{i}_d \\ i_q \\ i_0 \end{bmatrix} \tag{4.12}$$

Now the reference current in *abc* reference frame can be obtained using inverse *dq0* transformation as given below

$$\begin{bmatrix} i^*_{\mu ga} \\ i^*_{\mu gb} \\ i^*_{\mu gc} \end{bmatrix} = \sqrt{\frac{2}{3}} \begin{bmatrix} \cos\theta & -\sin\theta & \frac{1}{\sqrt{2}} \\ \cos(\theta + \frac{2\pi}{3}) & -\sin(\theta + \frac{2\pi}{3}) & \frac{1}{\sqrt{2}} \\ \cos(\theta - \frac{2\pi}{3}) & -\sin(\theta - \frac{2\pi}{3}) & \frac{1}{\sqrt{2}} \end{bmatrix} \begin{bmatrix} i^*_{\mu gd} \\ i^*_{\mu gq} \\ i^*_{\mu g0} \end{bmatrix}. \tag{4.13}$$

Once the reference current is generated, we track it using hysteresis band controller. The entire control strategy can be summarized as shown in Fig. 4.4.

4.2.1 PLL Structure

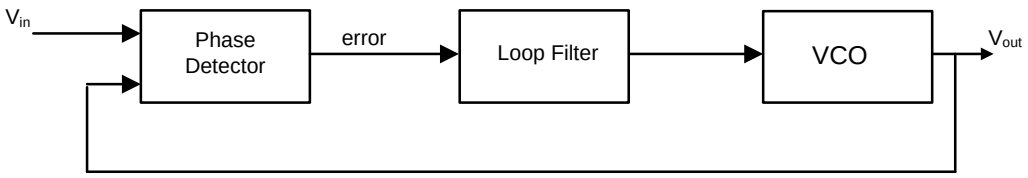

Fig. 4.5 PLL structure

θ can extracted from the PCC voltages using a phase locked loop (PLL). Main components of PLL include a phase detector, loop filter and a voltage controlled oscillator (VCO). PLL locks the phase of the output of the oscillator to the phase of the reference input, thus deriving the phase of the input reference. Phase detector generates an error proportional to the phase difference between the input reference quantity and the VCO output. Loop filter reduces the input phase error and generates a signal which drives the VCO. VCO generates the phase and frequency output.

4.3 Control Strategy Using Instantaneous Symmetrical Component Theory

This control algorithm is developed based on instantaneous symmetrical component theory which is primarily used for load compensations [23], [17]. Instantaneous values of symmetrical components can be found out as follows

$$\begin{bmatrix} v_{a0} \\ v_{a1} \\ v_{a2} \end{bmatrix} = \frac{1}{3} \begin{bmatrix} 1 & 1 & 1 \\ 1 & a & a^2 \\ 1 & a^2 & a \end{bmatrix} \begin{bmatrix} v_{sa} \\ v_{sb} \\ v_{sc} \end{bmatrix}. \tag{4.14}$$

This theory for load compensation is derived out of three conditions they are,

1). The neutral current must be zero. Therefore,

$$i_{sa} + i_{sb} + i_{sc} = 0. \tag{4.15}$$

2). The phase angle between the fundamental positive sequence of voltage and current is ϕ.

$$\angle v_{sa1} = \angle i_{sa1} + \phi \tag{4.16}$$

3). The average real power demand by the load should be met by the utility grid. This can be put across as,

$$v_{sa}i_{sa} + v_{sb}i_{sb} + v_{sc}i_{sc} = \overline{p}_l = \frac{1}{T}\int_{t_1}^{t_1+T}(v_{sa}i_{la} + v_{sb}i_{lb} + v_{sc}i_{lc})dt \tag{4.17}$$

Now we have to get an expression for the micrigrid reference curents $i^*_{\mu ga}, i^*_{\mu gb}, i^*_{\mu gc}$. Let i^*_{sa}, i^*_{sb}, i^*_{sc} be the desired source currents. Then we can formulate as,

$$\begin{aligned} i^*_{sa} &= i_{la} - i^*_{\mu ga} \\ i^*_{sb} &= i_{lb} - i^*_{\mu gb} \\ i^*_{sb} &= i_{lc} - i^*_{\mu gc} \end{aligned} \tag{4.18}$$

The second condition can be rewritten as (4.19),

$$\angle\frac{1}{3}(v_{sa} + av_{sb} + a^2v_{sc}) = \angle\frac{1}{3}(i_{sa} + ai_{sb} + a^2i_{sc}) + \phi \tag{4.19}$$

Substituting the value of *a* and rearranging,

$$\angle\frac{1}{3}\left(v_{sa} - \frac{v_{sb}}{2} - \frac{v_{sc}}{2} + \frac{j\sqrt{3}}{2}(v_{sb} - v_{sc})\right) = \angle\frac{1}{3}\left(i_{sa} - \frac{i_{sb}}{2} - \frac{i_{sc}}{2} + \frac{j\sqrt{3}}{2}(i_{sb} - i_{sc})\right) + \phi$$

Taking tan of the equation on both sides and rearranging we get,

$$\begin{aligned} &\frac{\sqrt{3}}{2}(v_{sb} - v_{sc}) + \frac{\tan\phi}{2}[v_{sb} + v_{sc} - 2v_{sa}]i_{sa} + \\ &\frac{\sqrt{3}}{2}(v_{sc} - v_{sa}) + \frac{\tan\phi}{2}[v_{sa} + v_{sc} - 2v_{sb}]i_{sb} + \\ &\frac{\sqrt{3}}{2}(v_{sa} - v_{sb}) + \frac{\tan\phi}{2}[v_{sa} + v_{sb} - 2v_{sc}]i_{sc} = 0 \end{aligned} \tag{4.20}$$

On substituting $\frac{tan\phi}{\sqrt{3}} = \beta$ we obtain,

$$\begin{aligned}
&[(v_{sb} - v_{sc}) + \beta(v_{sb} + v_{sc} - 2v_{sa})]\, i_{sa} + \\
&[(v_{sc} - v_{sa}) + \beta(v_{sa} + v_{sc} - 2v_{sb})]\, i_{sb} + \\
&[(v_{sa} - v_{sb}) + \beta(v_{sa} + v_{sb} - 2v_{sc})]\, i_{sc} = 0.
\end{aligned} \tag{4.21}$$

Using the equation $v_{sa} + v_{sb} + v_{sc} = 3v_{s0}$, where v_{s0} is the zero sequence component of the source voltage. The above equation becomes,

$$\begin{aligned}
&[(v_{sb} - v_{sc}) + \beta(3v_{s0} - 3v_{sa})]\, i_{sa} + \\
&[(v_{sc} - v_{sa}) + \beta(3v_{s0} - 3v_{sb})]\, i_{sb} + \\
&[(v_{sa} - v_{sb}) + \beta(3v_{s0} - 3v_{sc})]\, i_{sc} = 0
\end{aligned} \tag{4.22}$$

Now the three conditions can be rewritten in the form of equations as following,

$$i^*_{sa} + i^*_{sb} + i^*_{sc} = 0 \tag{4.23}$$

$$\begin{aligned}
&[(v_{sb} - v_{sc}) + \beta(3v_{s0} - 3v_{sa})]\, i^*_{sa} + \\
&[(v_{sc} - v_{sa}) + \beta(3v_{s0} - 3v_{sb})]\, i^*_{sb} + \\
&[(v_{sa} - v_{sb}) + \beta(3v_{s0} - 3v_{sc})]\, i^*_{sc} = 0
\end{aligned} \tag{4.24}$$

$$v_{sa} i^*_{sa} + v_{sb} i^*_{sb} + v_{sc} i^*_{sc} = \overline{p}_l \tag{4.25}$$

Solving the above three equations the desired source current can be obtained as,

$$\begin{aligned}
i^*_{sa} &= \left[\frac{(v_{sa} - v_{s0}) + \beta(v_{sb} - v_{sc})}{\sum_{j=a,b,c} v^2_{sj} - 3v^2_{s0}}\right] \overline{p}_l \\
i^*_{sb} &= \left[\frac{(v_{sb} - v_{s0}) + \beta(v_{sc} - v_{sa})}{\sum_{j=a,b,c} v^2_{sj} - 3v^2_{s0}}\right] \overline{p}_l \\
i^*_{sc} &= \left[\frac{(v_{sc} - v_{s0}) + \beta(v_{sa} - v_{sb})}{\sum_{j=a,b,c} v^2_{sj} - 3v^2_{s0}}\right] \overline{p}_l.
\end{aligned} \tag{4.26}$$

$v_{s0} = 0$ for balanced voltages, $\beta = tan\phi/\sqrt{3}$ and since the source power factor should be unity , $\beta = 0$. $\beta = 0$ implies that the reactive power required by the load is entirely supplied by the VSI.

$$\begin{aligned} v_{s0} &= 0 \\ \beta &= 0 \end{aligned} \tag{4.27}$$

By substituting (4.27) in (4.26) we get (4.28)

$$\begin{aligned} i^*_{sa} &= \left(\frac{v_{sa}}{\sum_{j=a,b,c} v^2_{sj}} \right) \overline{p}_l \\ i^*_{sb} &= \left(\frac{v_{sb}}{\sum_{j=a,b,c} v^2_{sj}} \right) \overline{p}_l \\ i^*_{sc} &= \left(\frac{v_{sc}}{\sum_{j=a,b,c} v^2_{sj}} \right) \overline{p}_l. \end{aligned} \tag{4.28}$$

These equations are true when entire $\overline{p}$ is supplied by utility. Some modifications are required to this equations when we use it for microgrid application. Let *x* be the fraction of load active power ($\overline{p}$) supplied by the microgrid.

$$P_{\mu g} = x\,\overline{p}_l$$

Then the average active power demand from utility is $\overline{p}_l - P_{\mu g}$. The equations for the reference source currents can be modified as shown in (4.29)

$$\begin{aligned} i^*_{sa} &= \frac{v_{sa}(\overline{p}_l - P_{\mu g})}{\sum_{j=a,b,c} v^2_{sj}} \\ i^*_{sb} &= \frac{v_{sb}(\overline{p}_l - P_{\mu g})}{\sum_{j=a,b,c} v^2_{sj}} \\ i^*_{sc} &= \frac{v_{sc}(\overline{p}_l - P_{\mu g})}{\sum_{j=a,b,c} v^2_{sj}}. \end{aligned} \tag{4.29}$$

It can be observed that using instantaneous symmetrical component theory we are deriving reference source currents, but in *dq0* and $\alpha\beta 0$ the formulation made will directly give the reference microgrid currents. Now the reference current for microgrid can be

formulated by substituting (4.29) in (4.18) as shown in (4.30)

$$
\begin{aligned}
i^{*}_{\mu ga} &= i_{la} - \frac{v_{sa}(\overline{p}_l - P_{\mu g})}{\sum_{j=a,b,c} v^2_{sj}} \\
i^{*}_{\mu gb} &= i_{lb} - \frac{v_{sb}(\overline{p}_l - P_{\mu g})}{\sum_{j=a,b,c} v^2_{sj}} \\
i^{*}_{\mu gc} &= i_{lc} - \frac{v_{sc}(\overline{p}_l - P_{\mu g})}{\sum_{j=a,b,c} v^2_{sj}}.
\end{aligned}
\tag{4.30}
$$

The power drawn from utility can also be derived as follows,

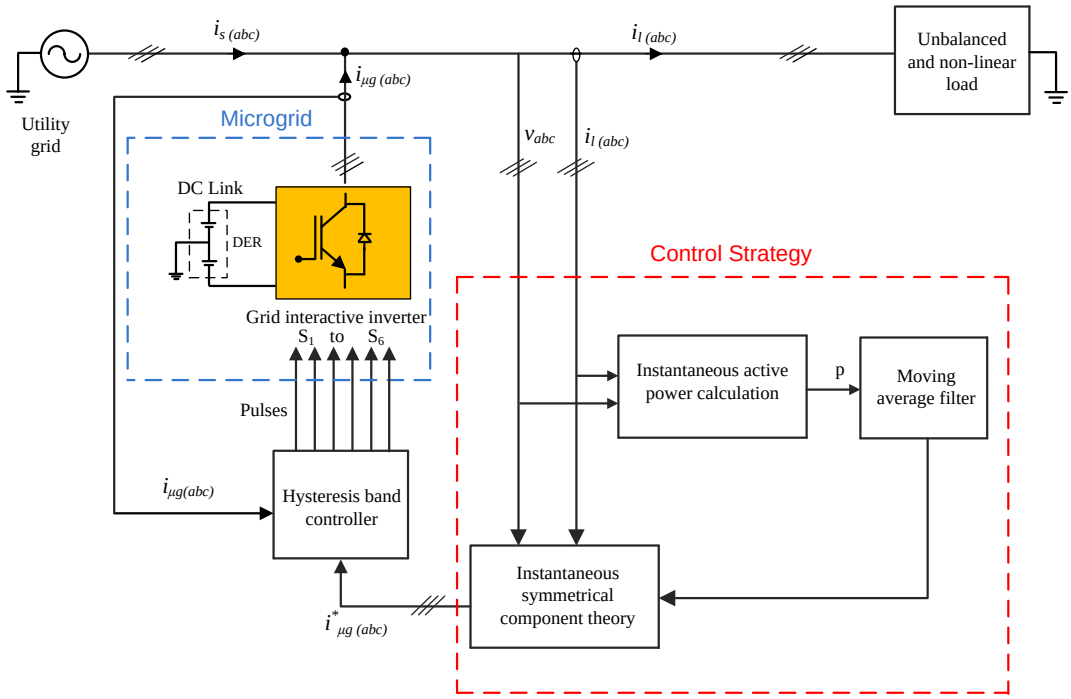

Fig. 4.6 Control strategy using instantaneous symmetrical component theory

$$
\overline{p}_l - P_{\mu g} = (1 - x)\overline{p}_l \tag{4.31}
$$

The reference microgrid currents can be finally obtained as,

$$
\begin{aligned}
i^{*}_{\mu ga} &= i_{la} - \frac{v_{sa}(1 - x)\,\overline{p}_l}{\sum_{j=a,b,c} v^2_{sj}} \\
i^{*}_{\mu gb} &= i_{lb} - \frac{v_{sb}(1 - x)\,\overline{p}_l}{\sum_{j=a,b,c} v^2_{sj}} \\
i^{*}_{\mu gc} &= i_{lc} - \frac{v_{sc}(1 - x)\,\overline{p}_l}{\sum_{j=a,b,c} v^2_{sj}}.
\end{aligned}
\tag{4.32}
$$

Thus the reference microgrid current using instantaneous symmetrical component theory can be obtained as shown in (4.32). These currents generated from the grid interactive inverter and the pulses for the the invereter is generated using a hysteresis band controller.

4.4 Comparison of Formulated Control Strategies

This section will give the comparison of the control strategies developed using various transformations. Simulations are carried out in PSCAD with the parameters shown in Table 4.1. Now that we have developed control strategies using $\alpha\beta 0$ transformation,

Table 4.1 Parameter values for simulation study

Parameter	Value
Output Power	4 kW
DC link Voltage ($V_{dc}/2$)	600 V
Fundamental frequency	50 Hz
Inductor(L_f)	20 mH
Inductor Resistance(R_f)	0.5 Ω
Hysteresis band ($\pm h$)	0.1
Unbalanced R-L Loads	Z_a= 40+j 31.41 Ω Z_b=50+j 62.82 Ω Z_c=30+j 94.27 Ω
Non-Linear Load	Three-phase full bridge diode rectifier supplying an R-L load (250Ω, 0.3 mH)

dq0 transformation and instantaneous symmetrical component theory where they meet the same objectives using same system parameters and topology, we will make a comparative study. The system topology considered for this study is shown in Fig. 4.1. The system parameters considered for this study is shown in Table 4.1. Simulations were carried out with all the discussed strategies, in PSCAD 4.2.1. All the strategies gave the desired results. The simulation results using instantaneous symmetrical component theory as the control strategy is shown in Fig. 4.7. Microgrid is injecting 20% of the active power demand by the load. The simulations using $\alpha\beta 0$ control and *dq0* control also gave the same results with slight variation in THDs.

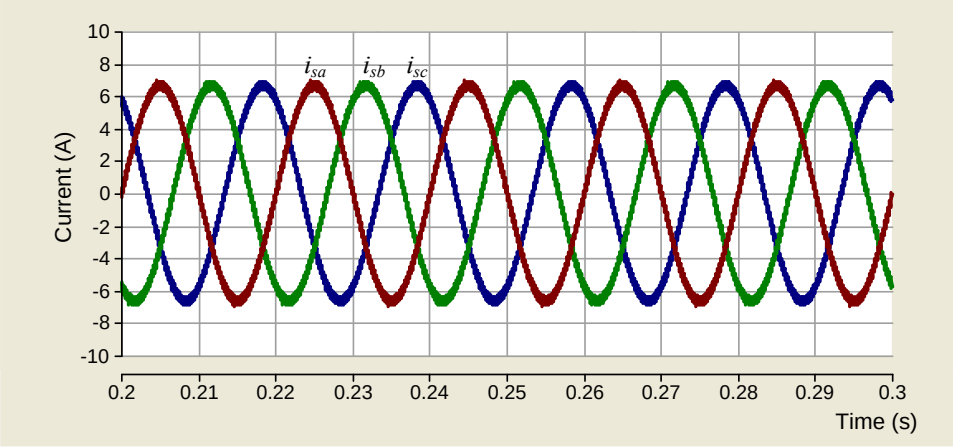

(a)

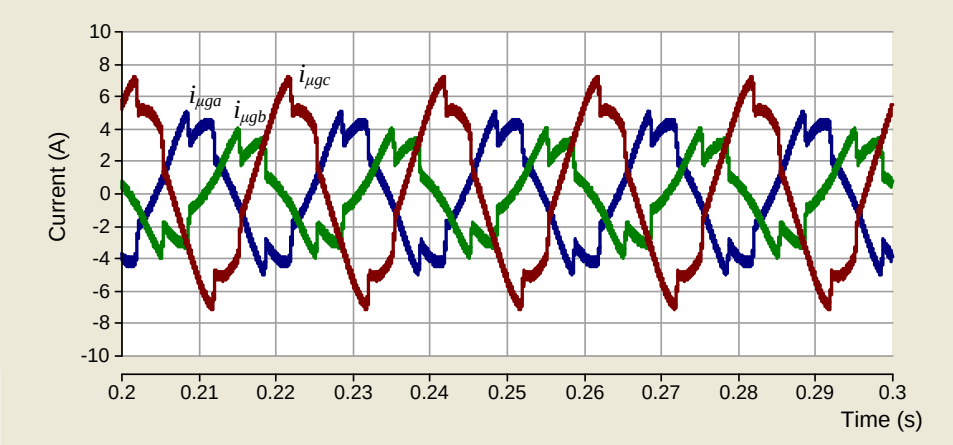

(b)

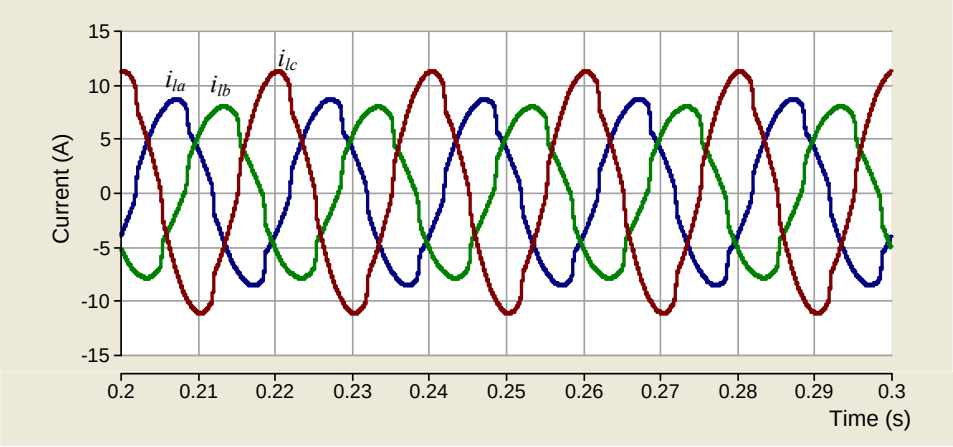

(c)

Fig. 4.7 (a) Utility grid currents (b) Microgrid currents (c) Load currents, when microgrid is injecting 20% of load active power with instantaneous symmetrical component theory as the control strategy

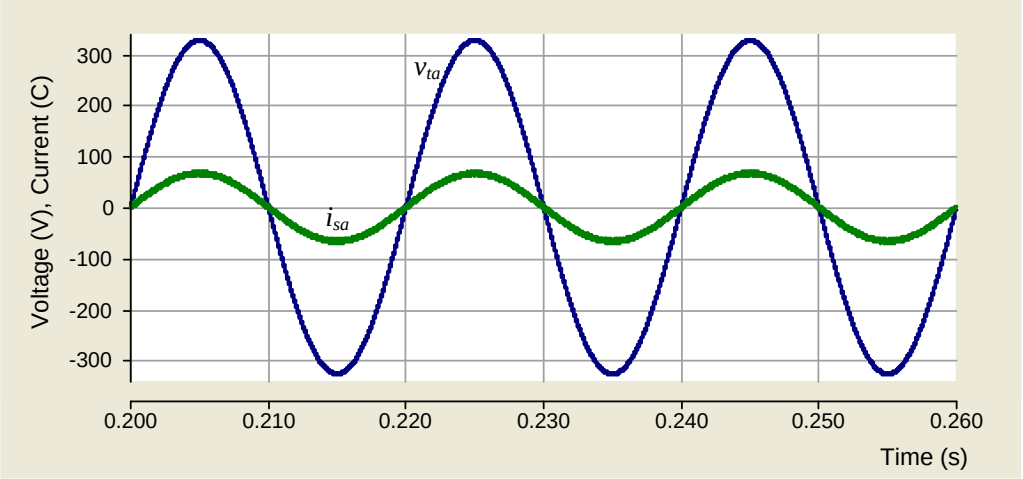

Fig. 4.8 Phase-*a* PCC voltage and utility grid current

Fig. 4.7(a) shows the plot of the utility grid currents, and it can be observed that it is perfectly balanced and sinusoidal as desired. Fig. 4.7(b) shows the microgrid current, this current is responsible for suppling 20 % of the fundamental current demanded by the load. These currents also compenstes the unbalance and harmonics in the load current. The plot of the unbalanced and harmonic load currents are shown in Fig. 4.7(c). The phase-*a* PCC voltage and current drawn from utility grid are shown in Fig. 4.8. The current magnitude has been multiplied by a factor of 10 for proper visibility. It can be seen that the current and voltage are exactly in phase, this makes it evident that the utility grid is operating in unity power factor (UPF) and it is sharing only the average active power demmanded by the load.

A comparative study based on some parameters chosen are shown in Table 4.2. This comparison shows that the instantaneous symmetrical component theory requires less time to simulate the system when compared to control strategies developed using $\alpha\beta 0$ and *dq0* transformation. Instantaneous symmetrical component theory doesn't demand a transformation even though it is derived out of symmetrical component transformation, the calculations are done in natural reference frame. Since it requires less calculations it is easier to implement.

Table 4.2 Comparative study of the control strategies

Parameters	*dq0* control	$\alpha\beta 0$ control	Instantaneous symmetrical component theory
THD of source currents	2.8%	2.2%	2.2%
Time required to simulate 25 cycles in PSCAD	18.1 s	17.2 s	14.3 s
Transformation to another reference frame	required	required	not required
Calculation of $\overline{p}$	not required	required	required
Calculation of q	not required	required	not required
Phase measurement (PLL)	required	not required	not required
Number of sensors required	9	9	9
Refererence current expression formulated gives	$i^*_{\mu g(abc)}$	$i^*_{\mu g(abc)}$	$i^*_{s(abc)}$
Non linear load compensation	possible	possible	possible
Moving average filter	required	required	required

4.5 Summary

Control algorithms are formulated using $\alpha\beta 0$ transformation, *dq0* transformation and instantaneous symmetrical component theory. All the algorithms were subjected to simulation studies and found that they all gave similar results apart from slight variation in THDs. Conducted a comparison study among various algorithms and found out that control strategy using instantaneous symmetrical component theory had an edge over other algorithms as it does not involve any transformation and have a reduced simulation time.

CHAPTER 5

DUAL VOLTAGE SOURCE INVERTER SCHEME FOR MICROGRID SYSTEMS

5.1 Introduction

A Dual Voltage Source Inverter (DVSI) scheme is proposed. This scheme is shown in Fig. 5.20. It comprises of two grid interactive inverters called as main inverter and auxiliary inverter in the microgrid connected to the utility. The task of the main inverter is to supply fundamental average real power demanded by the load connected to the utility grid. The auxiliary inverter supplies the rest of power components such as unbalance, reactive and harmonics. This scheme thus will have an advantage of using the main inverter to its highest rating. This is because the main inverter is not supplying any unbalance, reactive and harmonic components. This way the reliability and utilization of the main VSI is much more than those schemes which embed power quality aspects in the main inverter.

As mentioned, the auxiliary inverter will meet the reactive power, oscillatory active power and other unbalance demanded by the load. While the average active power demanded by the load will be shared by both main inverter and the utility grid. Therefore, the currents drawn from the main inverter and utility grid will be balanced and sinusoidal. In this scheme it is advantageous to have separate DC links for the two inverters. This is due to the fact that the requirements for the operation of the main and auxiliary inverters are different. The main inverter is supplied by a DC link which is charged by Distributed Energy Source (DER) such as photo voltaic systems. The auxiliary inverter makes use of DC storage capacitors as it does not inject real power. The main and auxiliary inverters may have different inverter topologies. In this scheme the main inverter topology taken is 3-ϕ, 3-wire, 2 -level VSI as it supplies only balanced sinusoidal currents. The auxiliary inverter topology is 3-ϕ, 4-wire, 2 -level neutral clamped VSI as

it has to supply the zero sequence currents due to the unbalance and non linearity of the load. The main inverter should supply the average active power depending upon the available power from the DER and rest of the average active power should be drawn from the utility grid. If the power generated by the DER is more than the load requirement then the remaining power will be delivered into the utility grid.

$i_{g\,(abc)} \Rightarrow$ Utility grid currents

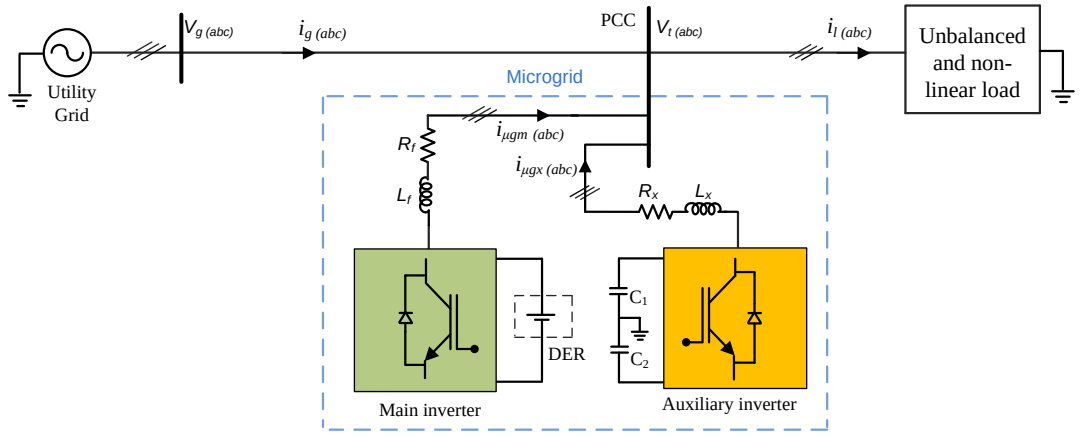

Fig. 5.1 Dual voltage source inverter topology

$i_{l\,(abc)} \Rightarrow$ Load currents

$i_{\mu gm\,(abc)} \Rightarrow$ Main inverter currents

$i_{\mu gx\,(abc)} \Rightarrow$ Auxiliary inverter currents

$v_{t(abc)} \Rightarrow$ PCC voltages

$v_{g(abc)} \Rightarrow$ Utility grid voltages

L_f , $L_x \Rightarrow$ Filter inductances

R_f , $R_x \Rightarrow$ Filter resistances

$C_1, C_2 \Rightarrow$ DC Link capacitors of auxiliary inverter.

Here we have three sources (utility grid, main inverter and auxiliary inverter) and a set of load connected at the PCC. We can equate the currents as shown in (5.1)

$$i_{l\,(abc)} = i_{g\,(abc)} + i_{\mu gm\,(abc)} + i_{\mu gx\,(abc)}\,. \tag{5.1}$$

A control strategy should be developed to generate reference currents for both inverters in grid connected mode. Both the inverters will be working in current controlled mode when the system is connected to utility grid.

5.2 Control Strategy

Control strategy should be developed in such a way that the the utility grid and main inverter together share the average active power demand, and auxiliary inverter supplies rest of the power demand by the load. Instantaneous symmetrical component theory can be made used for the control of both the inverters. Instantaneous symmetrical component theory is primarily developed for unbalanced and non linear load compensation. This theory can be directly applied to generate the reference currents for the auxiliary inverter as the role of the auxiliary inverter is load current compensation. Instantaneous symmetrical component theory can be extended to generate reference currents for main inverter.

5.2.1 Reference Current Generation for Auxiliary Inverter

In this microgrid system, the role of auxiliary inverter is to supply reactive power (q_l), oscillatory active power ($\tilde{p}_l$) demanded by the load. In other words, to compensate the harmonics in the load currents. The expressions for the source current references using instantaneous symmetrical component theory [17] is given below

$$\begin{aligned} i^*_{sa} &= \left(\frac{v_{ta}}{\sum_{j=a,b,c} v^2_{tj}}\right)\overline{p}_l \\ i^*_{sb} &= \left(\frac{v_{tb}}{\sum_{j=a,b,c} v^2_{tj}}\right)\overline{p}_l \\ i^*_{sc} &= \left(\frac{v_{tc}}{\sum_{j=a,b,c} v^2_{tj}}\right)\overline{p}_l. \end{aligned} \tag{5.2}$$

In the above equation i^*_{sa}, i^*_{sb} and i^*_{sc} refer to ideal source currents which are balanced and sinusoidal, consequently the source delivers only average active power ($\overline{p}_l$). In the system considered there are two sources of average active power, utility grid and

main inverter. Thus, the source current (i_s^*) can be split into two components, the main inverter current ($i_{\mu gm}^*$) and the utility grid current (i_g^*) as given in the following equation.

$$\begin{aligned} i_{sa}^* &= i_{\mu gma}^* + i_{ga}^* \\ i_{sb}^* &= i_{\mu gmb}^* + i_{gb}^* \\ i_{sc}^* &= i_{\mu gmc}^* + i_{gb}^* \end{aligned} \tag{5.3}$$

In the light of (5.3) we can modify (5.2) as shown in (5.4)

$$\begin{aligned} i_{\mu gma}^* + i_{ga}^* &= \left(\frac{v_{ta}}{\sum_{j=a,b,c} v_{tj}^2} \right) \overline{p}_l \\ i_{\mu gmb}^* + i_{gb}^* &= \left(\frac{v_{tb}}{\sum_{j=a,b,c} v_{tj}^2} \right) \overline{p}_l \\ i_{\mu gmc}^* + i_{gc}^* &= \left(\frac{v_{tc}}{\sum_{j=a,b,c} v_{tj}^2} \right) \overline{p}_l. \end{aligned} \tag{5.4}$$

The above expression makes it clear that $\overline{p}_l$ will be shared by main inverter and utility grid. The reference currents for the auxiliary inverter can be derived by substituting (5.4) in (5.1) and rearranging we get (5.5)

$$\begin{aligned} i_{\mu gxa}^* &= i_{la} - \left(\frac{v_{ta}}{\sum_{j=a,b,c} v_{tj}^2} \right) \overline{p}_l \\ i_{\mu gxb}^* &= i_{lb} - \left(\frac{v_{tb}}{\sum_{j=a,b,c} v_{tj}^2} \right) \overline{p}_l \\ i_{\mu gxc}^* &= i_{lc} - \left(\frac{v_{tc}}{\sum_{j=a,b,c} v_{tj}^2} \right) \overline{p}_l. \end{aligned} \tag{5.5}$$

If we generate these currents from the auxiliary inverter it will compensate the unbalanced and non linear load. The DC link voltage of the auxiliary inverter should be maintained constant for proper operation of the auxiliary inverter. DC link voltage variation occurs due the inverter loss (P_{loss}), this quantity should also be supplied by the utility grid. First we have to generate an expression for (P_{loss}) [17].

The average DC capacitor voltage can be kept constant if the average of DC capacitor current is zero over a cycle as $V_{dc} = \frac{1}{c} \int i_{dc} dt$. The deviation of V_{dc} from a reference

value at the end of a cycle shows the deviation of average value of i_{dc} from zero. A Proportional Integral (PI) controller is made used to generate P_{loss} term as given below

$$P_{loss} = K_p\, e_{vdc} + K_i \int e_{vdc} dt \tag{5.6}$$

where $e_{vdc} = V_{dcref} - V_{dc}^{cyl}$ and V_{dc}^{cyl}, is the value of V_{dc} at the end of a cycle.

P_{loss} thus obtained should be supplied by the utility grid, so now (5.5) can be modified by adding P_{loss} to $\overline{p}$ as shown in (5.7)

$$\begin{aligned}
i^*_{\mu gxa} &= i_{la} - \left(\frac{v_{ta}}{\sum_{j=a,b,c} v_{tj}^2}\right)(\overline{p}_l + P_{loss}) \\
i^*_{\mu gxb} &= i_{lb} - \left(\frac{v_{tb}}{\sum_{j=a,b,c} v_{tj}^2}\right)(\overline{p}_l + P_{loss}) \\
i^*_{\mu gxc} &= i_{lc} - \left(\frac{v_{tc}}{\sum_{j=a,b,c} v_{tj}^2}\right)(\overline{p}_l + P_{loss}).
\end{aligned} \tag{5.7}$$

The reference currents for the auxiliary inverters thus obtained will be tracked by a hysteresis band controller.

5.2.2 Reference Current Generation for Main Inverter

The main inverter is acting as a source of balanced sinusoidal currents. Therefore, the reference currents for the main inverter can be generated using the instantaneous symmetrical component theory (reference source current generation in (5.2)). The equations given below, which are derived out of instantaneous symmetrical component theory can be used to generate the main inverter reference currents if we know the available microgrid average active power ($P_{\mu g}$).

$$\begin{aligned}
i^*_{\mu gma} &= \left(\frac{v_{ta}}{\sum_{j=a,b,c} v_{tj}^2}\right) P_{\mu g} \\
i^*_{\mu gmb} &= \left(\frac{v_{tb}}{\sum_{j=a,b,c} v_{tj}^2}\right) P_{\mu g}
\end{aligned} \tag{5.8}$$

$$i^*_{\mu gmc} = \left(\frac{v_{tc}}{\sum_{j=a,b,c} v^2_{tj}} \right) P_{\mu g}.$$

If the main inverter delivers $i^*_{\mu gma}$, $i^*_{\mu gma}$, $i^*_{\mu gma}$, that implies the inverter is delivering $P_{\mu g}$. The reference currents are tracked using hysteresis band controller.

5.2.3 Utility Grid Currents

Since the main microgrid inverter is generating $P_{\mu g}$, remaining average active power demanded by the load will be met by the utility grid,

$$P_g = \overline{p}_l + P_{loss} - P_{\mu g}$$

Where P_g is the corresponding power drawn out of the utility grid. Thus, the total average active power demand by the load is shared between the main inverter and utility grid. For this case, the current drawn out of the utility can be expressed as,

$$\begin{aligned} i^*_{ga} &= \left(\frac{v_{ta}}{\sum_{j=a,b,c} v^2_{tj}} \right) P_g \\ i^*_{gb} &= \left(\frac{v_{tb}}{\sum_{j=a,b,c} v^2_{tj}} \right) P_g \\ i^*_{gc} &= \left(\frac{v_{tc}}{\sum_{j=a,b,c} v^2_{tj}} \right) P_g. \end{aligned} \tag{5.9}$$

The current drawn from utility grid will be perfectly balanced and sinusoidal as the auxiliary inverter is acting as a compensator. But, the utility grid currents can be either in phase or in phase-opposition (out of pase by 180°) with the PCC voltages depending upon the load power demand ($\overline{p}_l$) and available microgrid power ($P_{\mu g}$). This can be explained with the help of instantaneous symmetrical component theory. From (5.9) it is evident that i^*_{ga} is in phase with v_{ta}, if P_g is positive. From (5.9) we can find the condition in which P_g will become negative. Consider the expression for i^*_{ga},

$$i^*_{ga} = \left(\frac{v_{ta}}{\sum_{j=a,b,c} v^2_{tj}} \right) ((\overline{p}_l + P_{loss}) - P_{\mu g}) \tag{5.10}$$

It can be observed that if the quantity $(\overline{p}_l + P_{loss})$ is greater than $P_{\mu g}$ then P_g will become negative, consequently i^*_{ga} gets a negative sign which specifies that i^*_{ga} is in phase opposition with v_{ta}. Similarly, i^*_{gb} and i^*_{gc} will be in phase opposition with the respective PCC voltage under this condition. The entire control strategy can be schematically

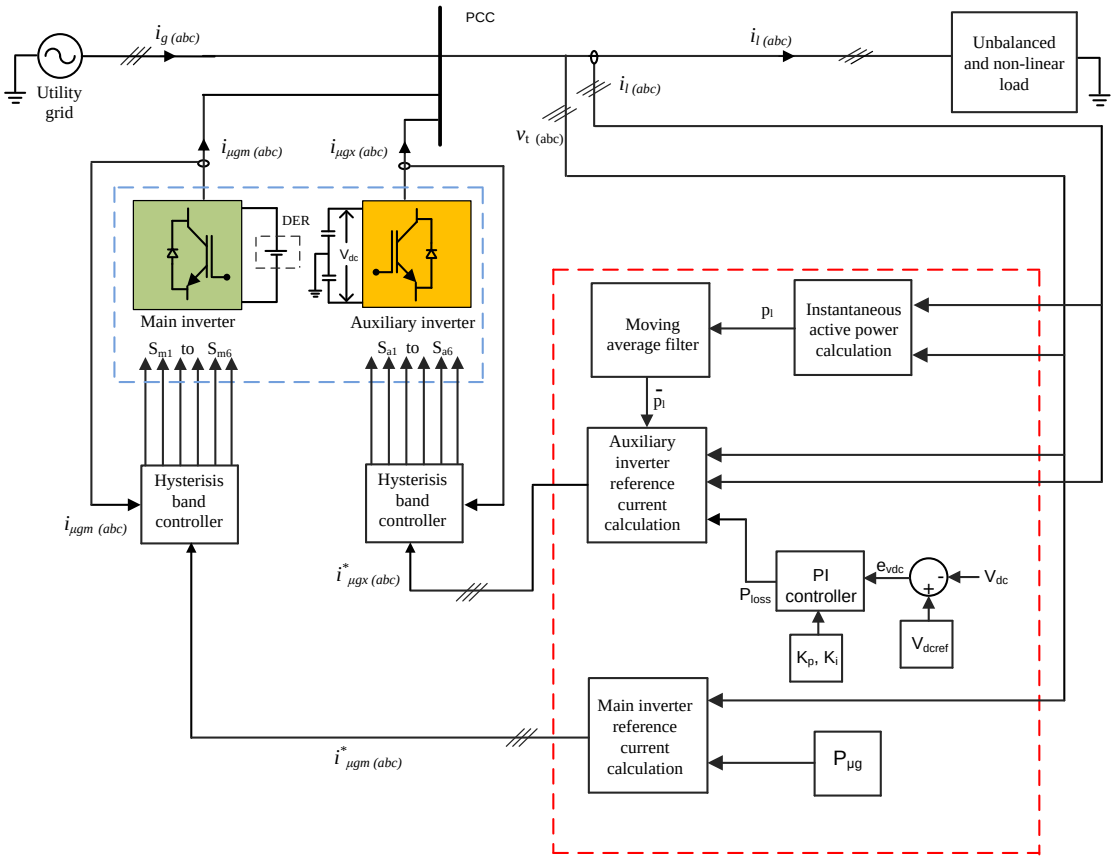

Fig. 5.2 Control strategy for DVSI scheme

represented as shown in Fig. 5.2.

5.3 Simulation Studies

5.3.1 System Details

It is important to look upon the response of the control strategy developed to variations in the power profiles. In this section we will look upon the profiles of load power, microgrid power and utility grid power profiles chosen for this study.

Load Variations

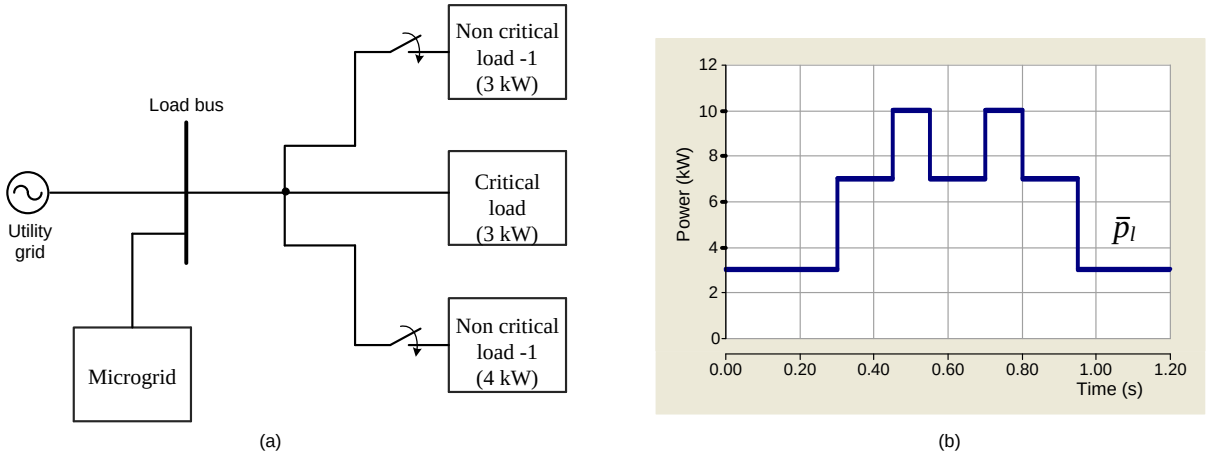

Fig. 5.3 (a) Loads connected to the system (b) Load power profile

In this study we will consider three sets of load. They are Critical load (CL), non critical load -1 (L_1) and non critical load -2 (L_2). These loads are connected to the load bus or PCC as shown in Fig. 5.3(a). This study will consider 24 hours of day and the corresponding load variations. The critical loads are loads which are always connected

Table 5.1 Daily load pattern

Time(hours)	Loads present	Load (kW)
0 - 6	CL	3
6 - 9	CL+L_1	7
9 - 11	CL+L_1+L_2	10
11 - 14	CL+L_1	7
14 - 16	CL+L_1+L_2	10
16 - 19	CL+L_1	7
19 - 24	CL	3

to load bus. The other two sets of load will be connected or disconnected depending upon the requirement. The variation of loads are done in steps with respect to time and it is as shown in Table 5.1. The maximum load demand is 10 kW. It can be noted that the non critical loads are connected to the load bus for a certain period of time. In this study 24 hours of a day will be scaled down to 1.2 seconds of simulation, 1 hour corresponds to 0.05 seconds in simulation.The reference load active power variation can be graphically represented as shown Fig. 5.3(b). Now we have defined a load profile which will be shared by both the main inverter and utility grid. The utility share is dependent on the available power from the microgrid.

Microgrid Power Variation

In this study the DER is assumed to be solar energy. A power profile is defined for the microgrid, where it is assumed that this microgrid has a storage system that can support the 3 kW critical load even in the absence of solar energy. The power profile is defined in step variations as shown in Table 5.2. The microgrid reference power variation can be graphically represented as shown in Fig. 5.4. It can be observed that microgrid

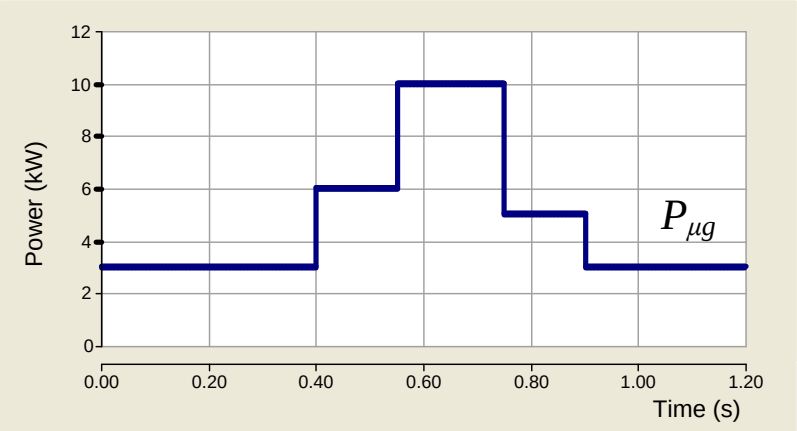

Fig. 5.4 Available microgrid power

Table 5.2 Microgrid power variation

Time(hours)	Microgrid Power (kW)
0 - 8	3
8 - 11	6
11 - 15	10
15 - 17	5
17 - 24	3

is delivering maximum power between 11 - 15 hrs, as the irradiance is assumed to be maximum during noontime. The utility grid will deliver the power difference between the load average active power demand and the microgrid power.

5.3.2 Simulation Parameters

The various parameters of the system under study are given in Table. 5.3. The system should be verified for its effectivness. Therefore, this dual inverter system for microgrid is simulated using PSCAD 4.2.1. The simulation parameters chosen for the study is

Table 5.3 Parameter values for simulation study

Parameter	Value
Maximum microgrid power	10 kW
Auxiliary inverter DC link Voltage ($V_{dc}/2$)	600 V
Main inverter DC link Voltage (V_{dcm})	700 V
Utility grid voltage	400 V
Fundamental frequency	50 Hz
Inductor(L_f)	20 mH
Inductor Resistance(R_f)	0.5 Ω
k_p, k_i for PI controller	5, 0.0025
Hysteresis band ($\pm h$)	0.3 A
Critical load (CL)	Z_a= 70+j 43.98 Ω Z_b=60+j 31.41 Ω Z_c=45+j 26.70 Ω 3-ϕ full bridge diode rectifier supplying an R-L (320 Ω - 300 mH) load
Non critical load -1 (L_1)	Z_a= 40+j 31.41 Ω Z_b=50+j 26.70 Ω Z_c=30+j 20.42 Ω 3-ϕ full bridge diode rectifier supplying an R-L (250 Ω - 300 mH) load
Non critical load -2 (L_2)	Z_a= 70+j 43.98 Ω Z_b=60+j 31.41 Ω Z_c=45+j 26.70 Ω 3-ϕ full bridge diode rectifier supplying an R-L (320 Ω - 300 mH) load

shown in Table. 5.3. In the simulation study, as mentioned previously 24 hours is scaled down to 1.2 seconds and the load, main inverter, grid, auxiliary inverter powers and currents are plotted. The load variations and microgrid available power variations are predefined as given in Table 5.1 and 5.2 . When voltages and currents are shown together, currents are multiplied by a factor of 10 for proper resolution of the plots.

5.3.3 Simulation Results

The instantaneous active power demanded by the load is shon in Fig. 5.5. The average component of this active power is shared by the utility grid and the main inverter. The active power of the load, main inverter, utility grid, and auxiliary inverter are shown in Fig. 5.6. Fig. 5.6(a) shows the load average active power, Fig. 5.6(a) plots the active power delivered by main inverter. It can be observed that the power profiles of

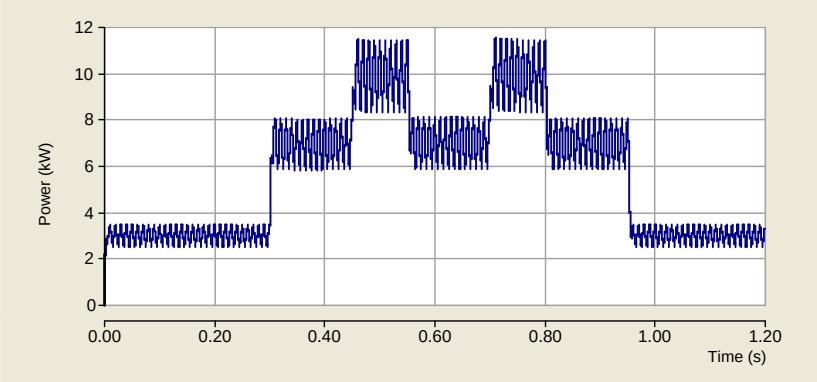

Fig. 5.5 Instsntaneous active power demanded by the load

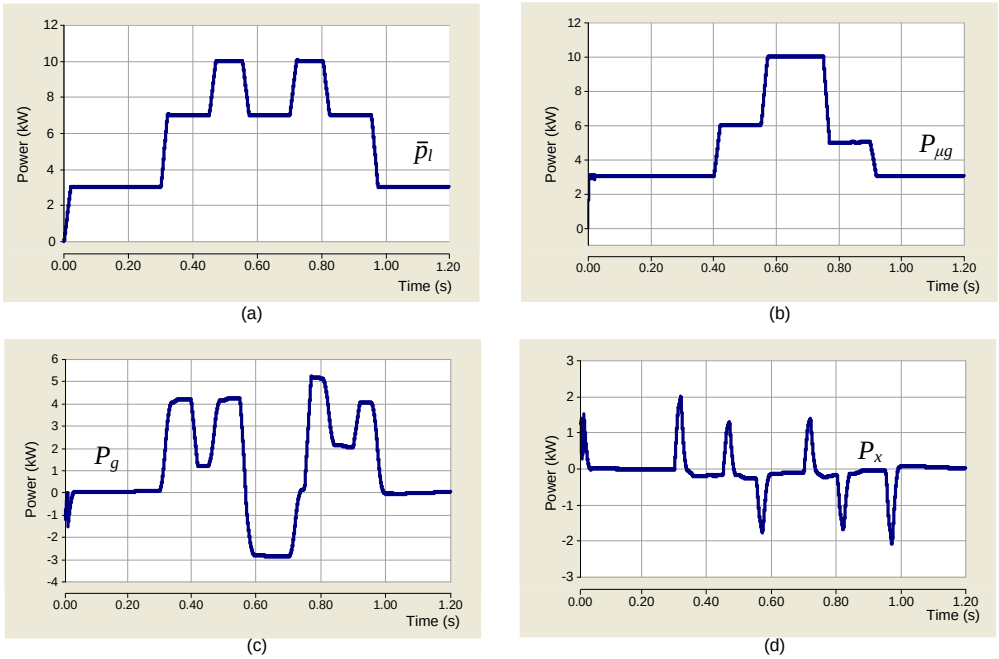

Fig. 5.6 (a) Load power (b) Main inverter power (c) Utility grid power (d) Auxiliary inverter power

the load and main inverter matches with that of the reference profiles. Fig. 5.6(d) is the power drawn from auxiliary inverter which should be ideally zero as per this control strategy. It can be observed that the auxiliary inverter power is negligible, apart from the transient periods (load step variations). Then another quantity which adds on to auxiliary inverter power is P_{loss} during transients. P_{loss} will be drawn from the auxiliary inverter immediately after the step variations of microgrid power, till the change is tracked by the PI controller. This also accounts for the variations of auxiliary inverter power from zero. Once P_{loss} is tracked by the PI controller it will be drawn from the utility grid. Fig. 5.6(c) is the plot of power injected by the utility grid and it the

difference of load power and the main inverter power. It can be observed that from t= 0.6 to$0.7s$, P_g is negative. This is because during this period $P_{\mu g}$ is greater than $\overline{p}$.

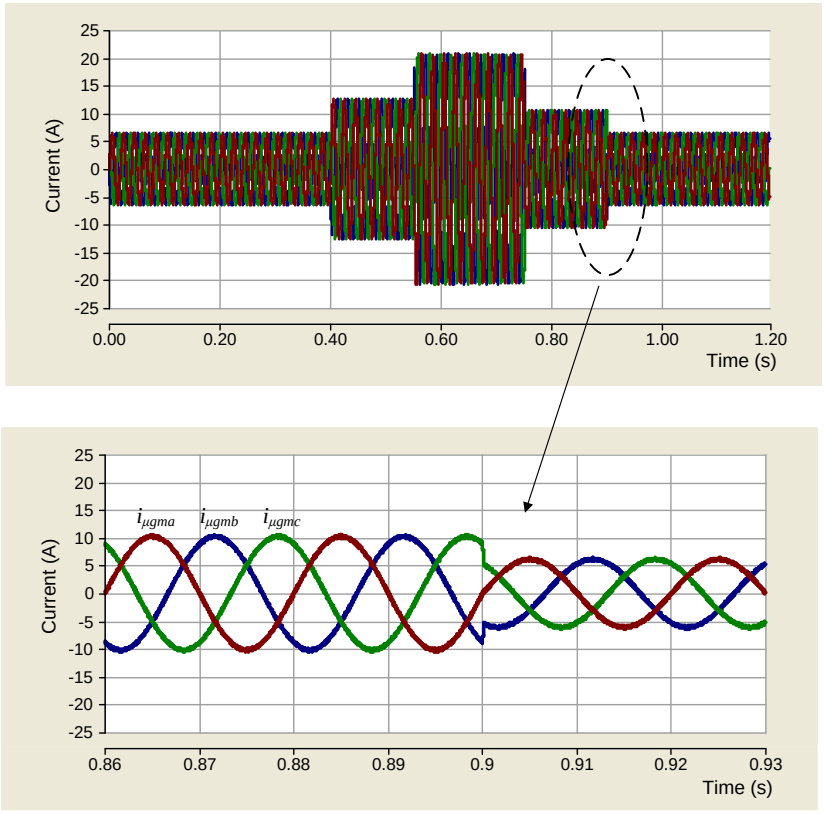

Fig. 5.7 Main inverter currents

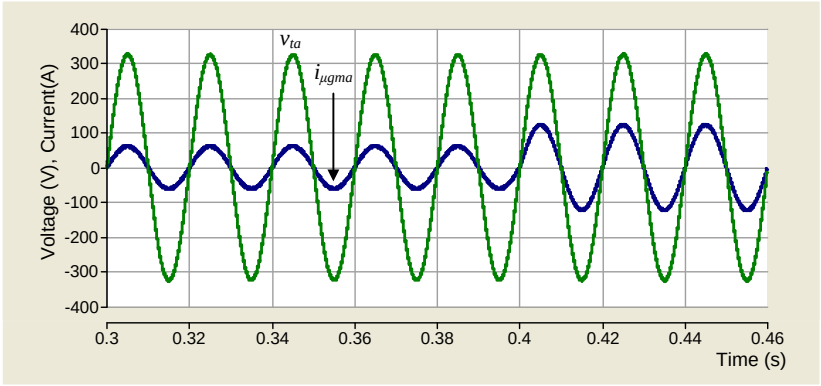

Fig. 5.8 a-phase PCC voltage and main inverter current

Now we will take look on different currents flowing in the system. Fig. 5.7 shows the current which is drawn out of the main inverter. It shows two plots, the one shown below is a enlarged view of main inverter current of a small area in the whole simulation, which is shown in the plot above. It can be seen that main inverter current is balanced

and sinusoidal as per the strategy. The magnitude of the current varies as per the step variation in available microgrid power. The PCC voltage and the main inverter currents are shown together in 5.8, current is multiplied by a factor of 10 for proper visibility. It can be seen that the main inverter currents are in phase with PCC voltage.

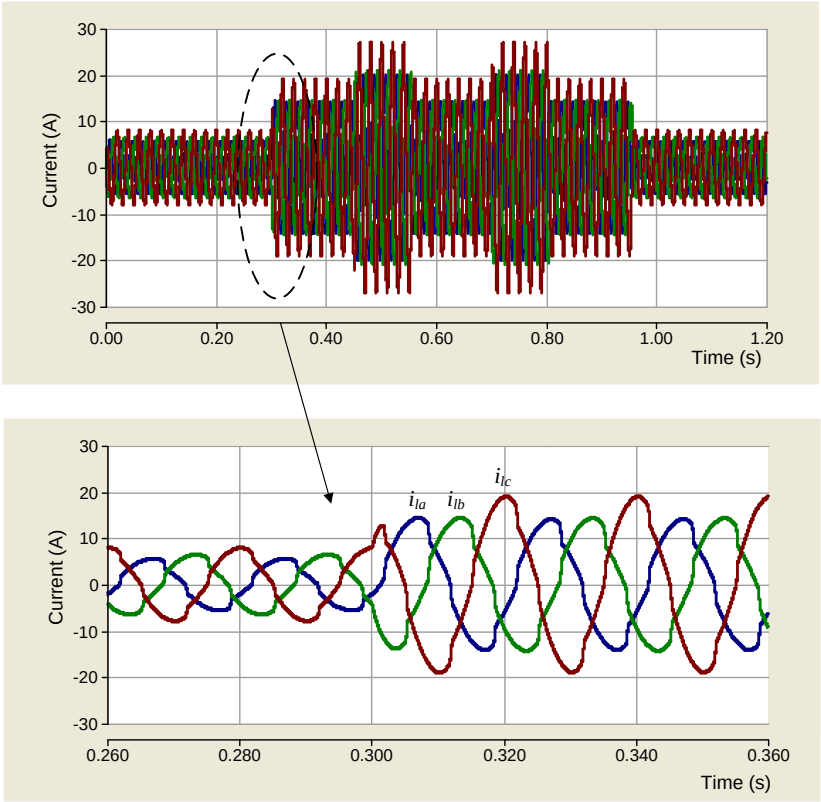

Fig. 5.9 Load currents

The load currents is shown in Fig. 5.9. The load currents are unbalanced and it include harmonics, this can be understood from the enlarged view given. These unbalance and harmonics should be compensated. The magnitude of the load current varies according to the defined load profile. The main inverter currents are balanced and sinusoidal because it is only sharing average active power demanded by load.

Fig. 5.10 shows the currents drawn from utility grid, the currents drawn from utility grid are also balanced and sinusoidal when ever power is shared. It can be seen that till t=$0.3\,s$, the currents drawn from the utility grid is negligible. This is because the microgrid power is equal to the load power and only P_{loss} is drawn from the utility, which is a very small fraction of the load. The magnitude of the utility grid currents varies depending upon the quantity of load power shared by the utility grid. The utility grid currents

are either in phase or out of phase by 180° depending upon whether $P_{\mu g} < (\overline{p}_l + P_{loss})$ or $P_{\mu g} > (\overline{p}_l + P_{loss})$ respectively. $P_{\mu g} < (\overline{p}_l + P_{loss})$, this mode of operation of the system can be called as grid supporting mode because the utility grid and microgrid shares the average active power demand by the load or it can be said that microgrid is supporting the utility grid in meeting the load demand. In the grid supporting mode, the utility

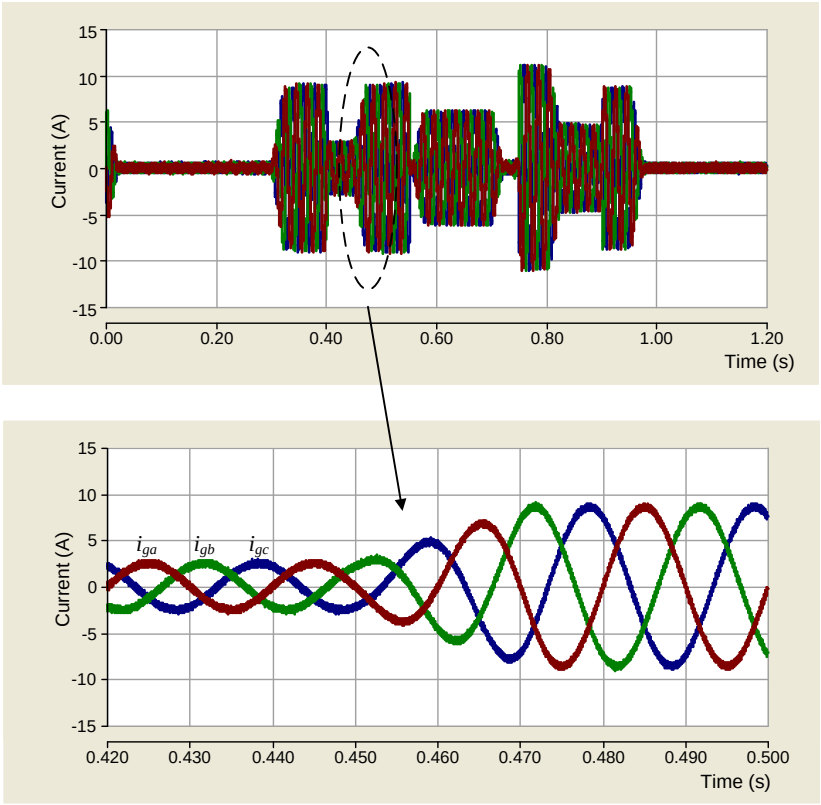

Fig. 5.10 Utility grid currents

grid current and the PCC voltage are in phase with each other. $P_{\mu g} > (\overline{p}_l + P_{loss})$, this mode of operation of the system can be called as the grid injecting mode because the microgrid available power is more than the load demand so the excess power is injected into the system. n the grid injecting mode, the utility grid current and the PCC voltage are in phase-opposition with each other. Figs. 5.11 (a) and (b) shows the PCC volatge and utility grid current of phase a during grid supporting mode and grid injecting mode respectively. Auxiliary inverter currents are shown in Fig. 5.12, these currents compensates the unbalance and harmonics in the load current. The auxiliary inverter current ideally comprises of only reactive and harmonic components. These currents delivers the reactive power and the oscillating component of the active power demanded by the

load, average active power supplied due to these currents is ideally zero.

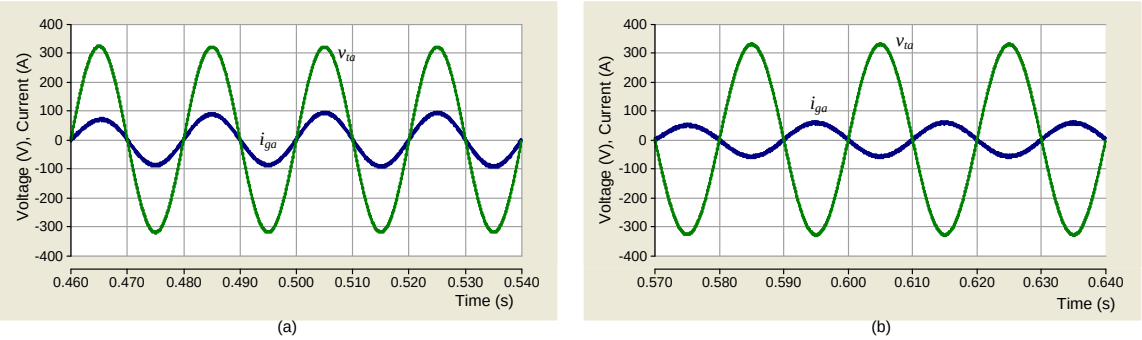

Fig. 5.11 (a) PCC voltage and utility grid current during grid supporting mode (b) PCC voltage and utility grid current during grid injecting mode

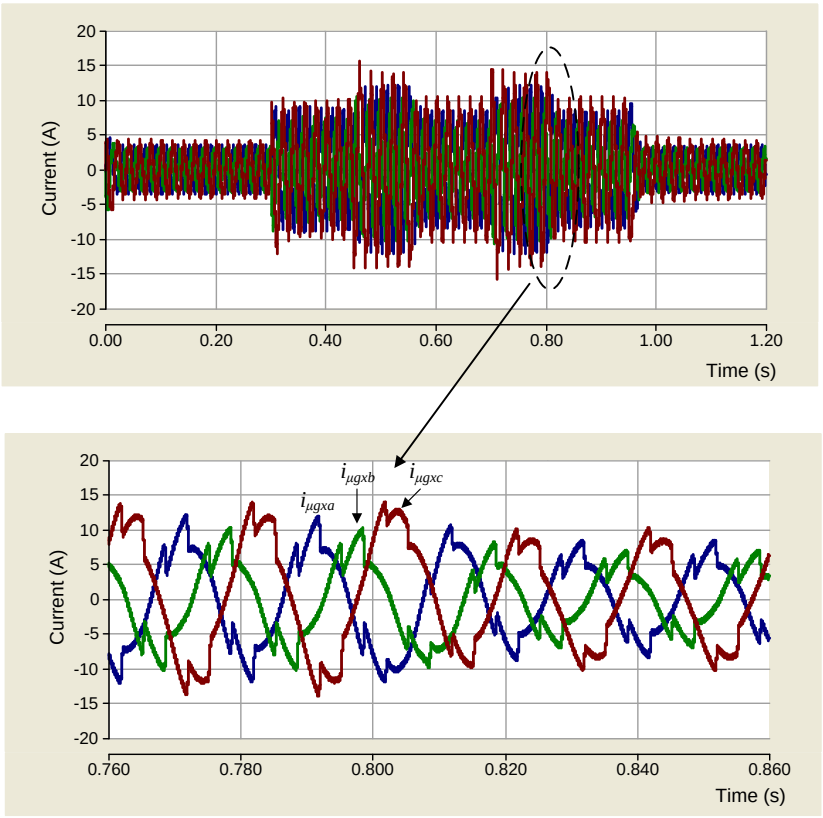

Fig. 5.12 Auxiliary inverter currents

The magnitude of the currents vary depending upon the step variations of the load which are already defined. The plots of the PCC voltage (v_{ta}) and main inverter current ($i_{\mu gma}$) of phase A are shown in Fig. 5.13. It can be observed that the voltage and current and exactly in phase or the utility grid is now operating in unity power factor (UPF).

The DC capacitor voltage (v_{dc}) is shown in Fig. 5.14. The DC capacitor voltage of

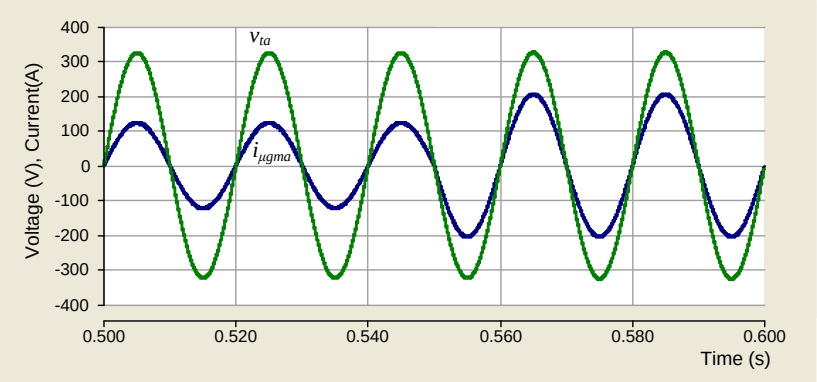

Fig. 5.13 Phase - *a* PCC voltage and main inverter current

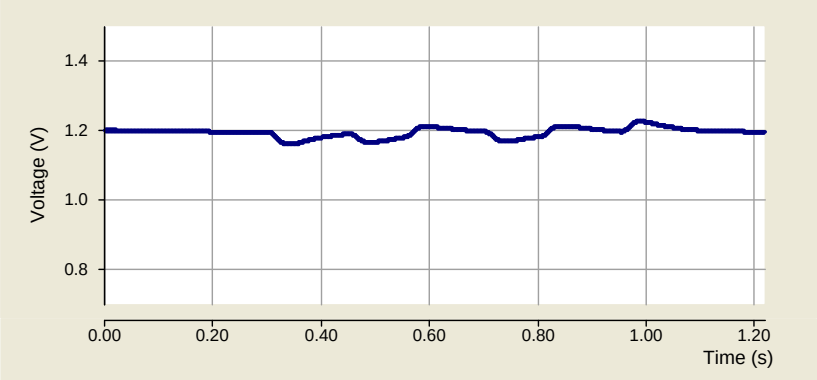

Fig. 5.14 DC capacitor voltage of auxiliary inverter

the auxiliary inverter should be a constant irrespective of the load variations, for proper operation. Therefore we should have a strategy to stabilize the DC link voltage. This is achieved with the help of a PI controller, the value of K_p and K_i are selected as 15 and 0.005 respectively. It can be seen that it is constant at 1200 V apart from transients due to load variations. It can be seen that at t=0.3 s when an additional load (L1) is switched on, the DC capacitor voltage dips, but the PI controller tracks the deviation of voltage from the reference value (1200 V) and brings it back to reference value. At t= 0.95 s, when $L1$ is switched off the DC capacitor voltage rises from the reference value but it is brought back to the reference value by the controller. The instantaneous reactive power demanded by the load and the instantaneous reactive power supplied by the auxiliary inverter are shown in Figs. 5.15 (a) and (b) respectively. It can be observed that both are identical plots, from which it is evident that the entire reactive power demanded by

the load is supplied by auxiliary inverter. Thus various modes of operation of the DVSI scheme for microgrid are studied using the simulations

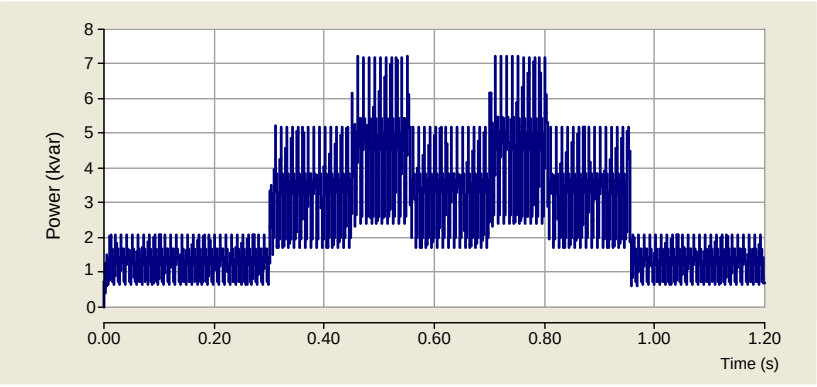

(a)

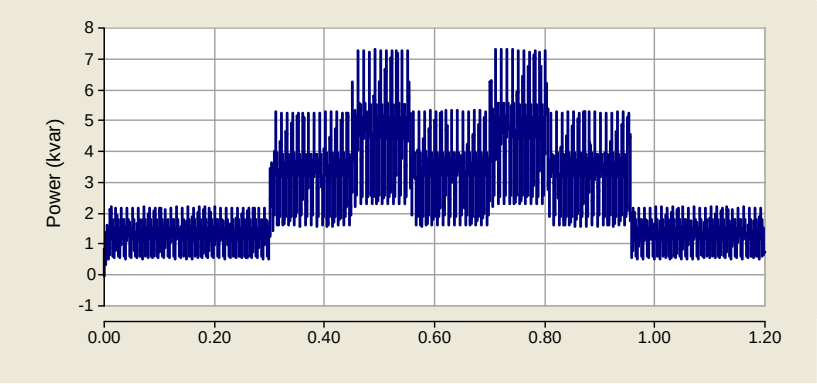

(b)

Fig. 5.15 (a) Load reactive power (b) Reactive power supplied by the auxiliary inverter

5.4 Modified Control Strategy for a System with Non Stiff Utility Grid

Transmission lines form an integral part of the power system. When the loads are at a long distance from the generation system, they will be interconnected with transmission lines which will introduce some impedance, which is termed as feeder impedance. The value of feeder impedance decides whether the utility grid is stiff or non stiff. When the feeder impedance is relatively more, it makes the utility grid non stiff or weak. If the utility grid is weak, the voltages at PCC will no more be balanced and sinusoidal. The unbalance and harmonics in the currents get reflected on the PCC voltages. The feeder impedance can be represented between the utility grid and PCC as shown in Fig. 5.16.

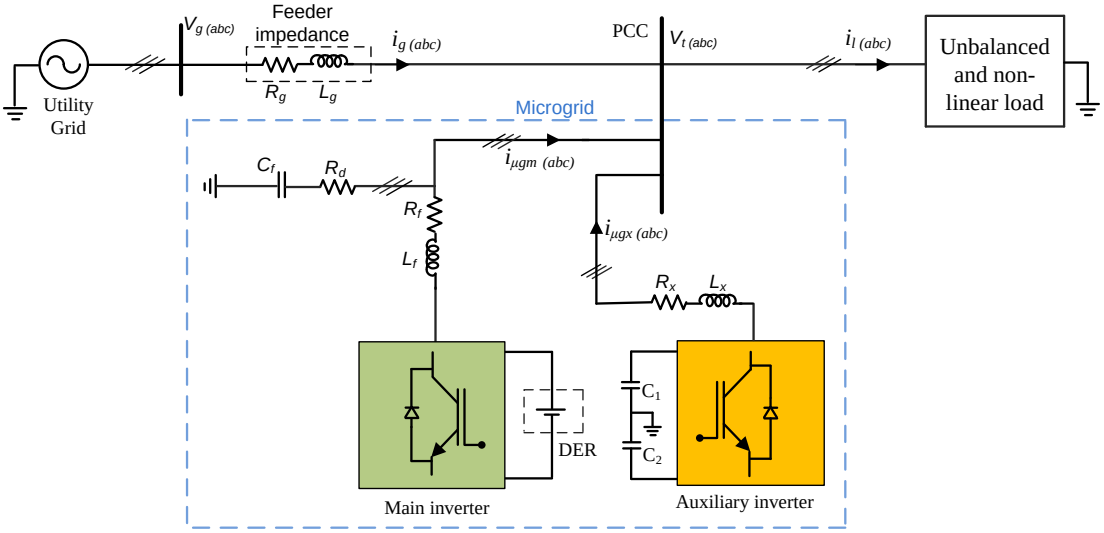

Fig. 5.16 System with non stiff utility grid

When the utility grid is weak, application of the control strategy which was discussed previously will not give desired results. A modification is required in the reference current generation schemes of the inverters for achieving the desired objectives. The system has an additional capacitor (C_f) and a resistance (R_d) as shown in Fig. 5.16, to filter out the switching components which are present in the PCC voltages.

5.4.1 Modified Control Strategy

This modified strategy involves extraction of fundamental component from the PCC voltages which contain unbalance and harmonics. In other words, conversion of the PCC voltages into balanced sinusoidal quantities and use these sinusoidal voltages for the reference current generation. To convert the PCC voltages to balanced sinusoidal voltages *dq0* transformation is made used [24]. The PCC voltages in natural reference frame are transformed into *dq0* reference frame as given below,

$$\begin{bmatrix} v_{td} \\ v_{tq} \\ v_{t0} \end{bmatrix} = \sqrt{\frac{2}{3}} \begin{bmatrix} \cos\theta & \cos(\theta + \frac{2\pi}{3}) & \cos(\theta - \frac{2\pi}{3}) \\ -\sin\theta & -\sin(\theta + \frac{2\pi}{3}) & -\sin(\theta - \frac{2\pi}{3}) \\ \frac{1}{\sqrt{2}} & \frac{1}{\sqrt{2}} & \frac{1}{\sqrt{2}} \end{bmatrix} \begin{bmatrix} v_{ta} \\ v_{tb} \\ v_{tc} \end{bmatrix}. \tag{5.11}$$

θ is a function of ωt depending upon the reference frame chosen, ω used for the transformation above is the fundamental frequency of operation. The average components

of d-axis and q-axis when inverse transformed will give us the fundamental component of the PCC voltages. Thus, v_{td} and v_{tq} are separated into an average component and oscillatory component,

$$v_{td} = \overline{v}_{td} + \widetilde{v}_{td}, \;\; v_{tq} = \overline{v}_{tq} + \widetilde{v}_{tq}. \tag{5.12}$$

Now the fundamental of the PCC voltage in natural reference frame can be obtained

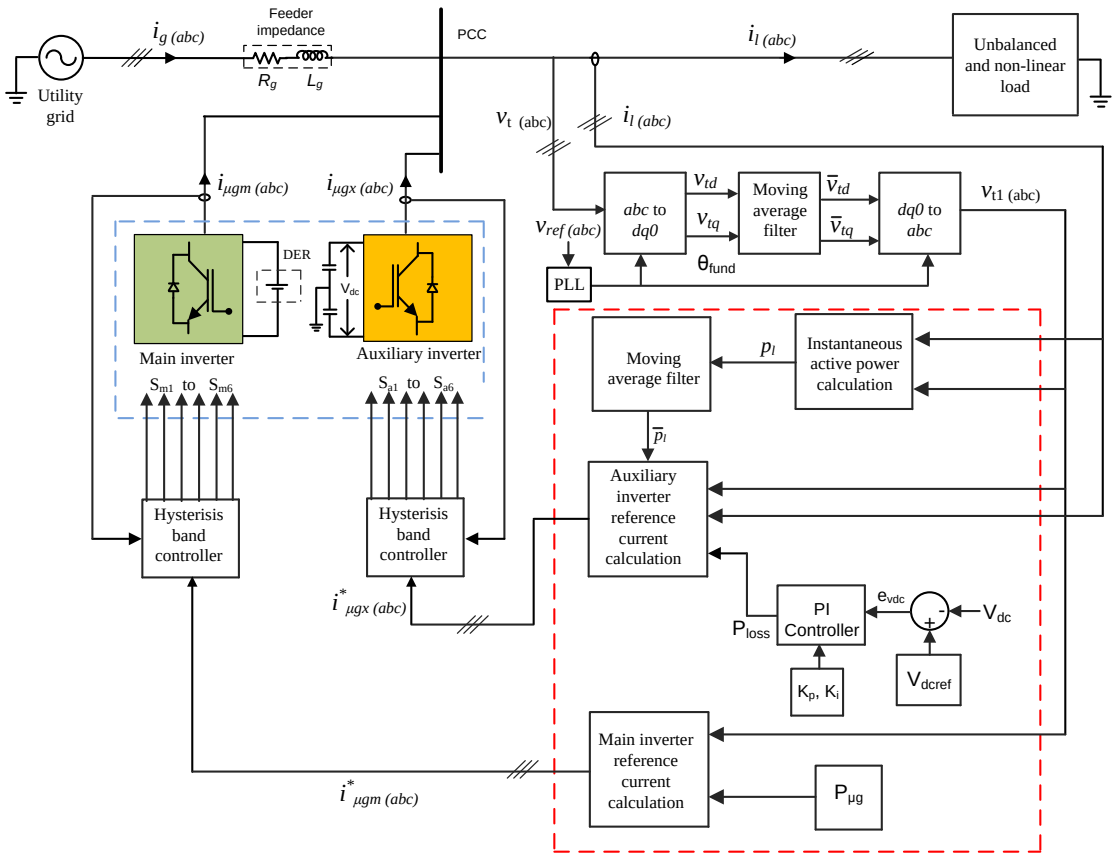

Fig. 5.17 Control strategy for system with non stiff utility grid

with help of inverese *dq0* transformation as given below

$$\begin{bmatrix} v_{ta1} \\ v_{tb1} \\ v_{tc1} \end{bmatrix} = \sqrt{\frac{2}{3}} \begin{bmatrix} \cos\theta & -\sin\theta & \frac{1}{\sqrt{2}} \\ \cos(\theta + \frac{2\pi}{3}) & -\sin(\theta + \frac{2\pi}{3}) & \frac{1}{\sqrt{2}} \\ \cos(\theta - \frac{2\pi}{3}) & -\sin(\theta - \frac{2\pi}{3}) & \frac{1}{\sqrt{2}} \end{bmatrix} \begin{bmatrix} \overline{v}_{td} \\ \overline{v}_{tq} \\ 0 \end{bmatrix}. \tag{5.13}$$

The voltages $v_{ta1}, v_{tb1}, v_{tc1}$ should be used in the reference current generation algorithms for main inverter and the auxiliary inverter discussed sections 5.2.1 and 5.2.2. This strategy will make sure that the currents drawn from the utility grid and main inverter

are balanced and sinusoidal and meet all other objectives of the dual inverter scheme even in the presence of feeder impedance.

5.4.2 Simulation Studies

All the simulation parameters chosen are same as that mentioned in Table. 5.3, with an addition of feeder impedance $R_g = 0.5\ \Omega$ and $L_g = 4$ mH, the filter capacitance C_f= 5 μF, R_d= 10Ω. Fig. 5.18(a) shows the PCC voltages, with presence of feeder impedance in the system. It can be observed that the PCC voltages are affected with

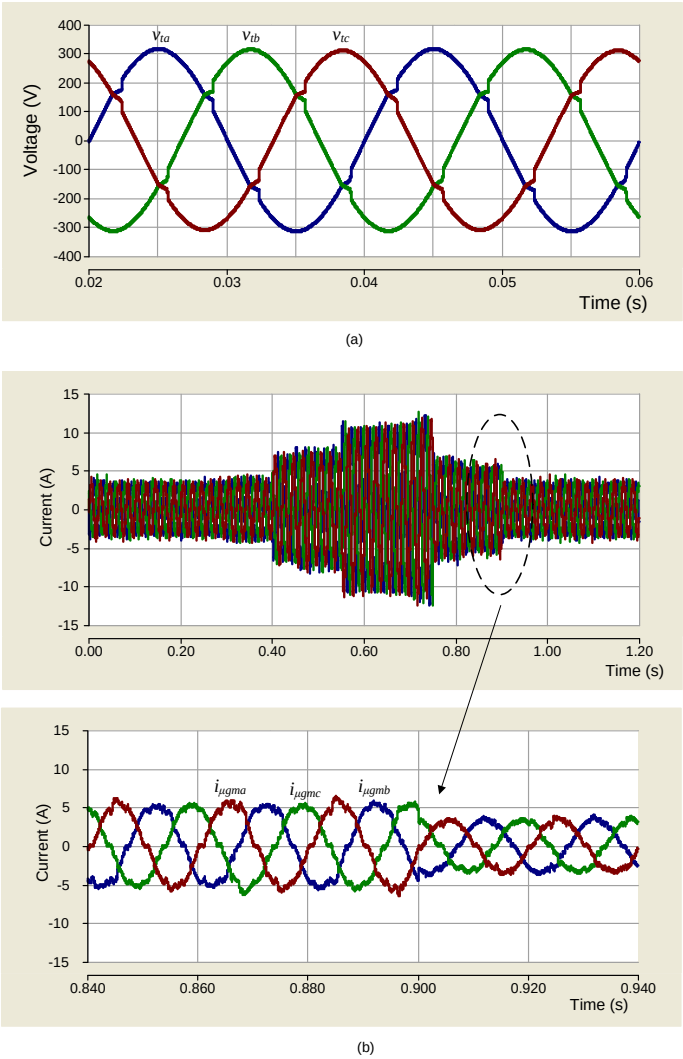

Fig. 5.18 (a) PCC voltage with presence of feeder impedance (b) Main inverter currents without using modified algorithm for reference current generation

unbalance and harmonics. This is because the feeder impedance in the system transfers the unbalance and harmonics in the load currents on to the PCC voltage. Fig.

5.18(b), shows the main inverter currents, when the PCC voltages are directly used for the reference current generation. It is evident that the main inverter currents are neither balanced nor sinusoidal which is undesirable. The control strategy defined in Section 5.2 performs effectively only if the PCC voltages are balanced and sinusoidal. When the utility grid is non stiff the PCC voltages gets distorted and this strategy will not perform effectively. Therefore, we make use of the modified algorithm in case of systems with non stiff utility grids. Let us observe the various powers obtained, which is shown in Fig. 5.19. Fig. 5.19 (a) is the plot of load average active power demand ($\overline{p}_l$).

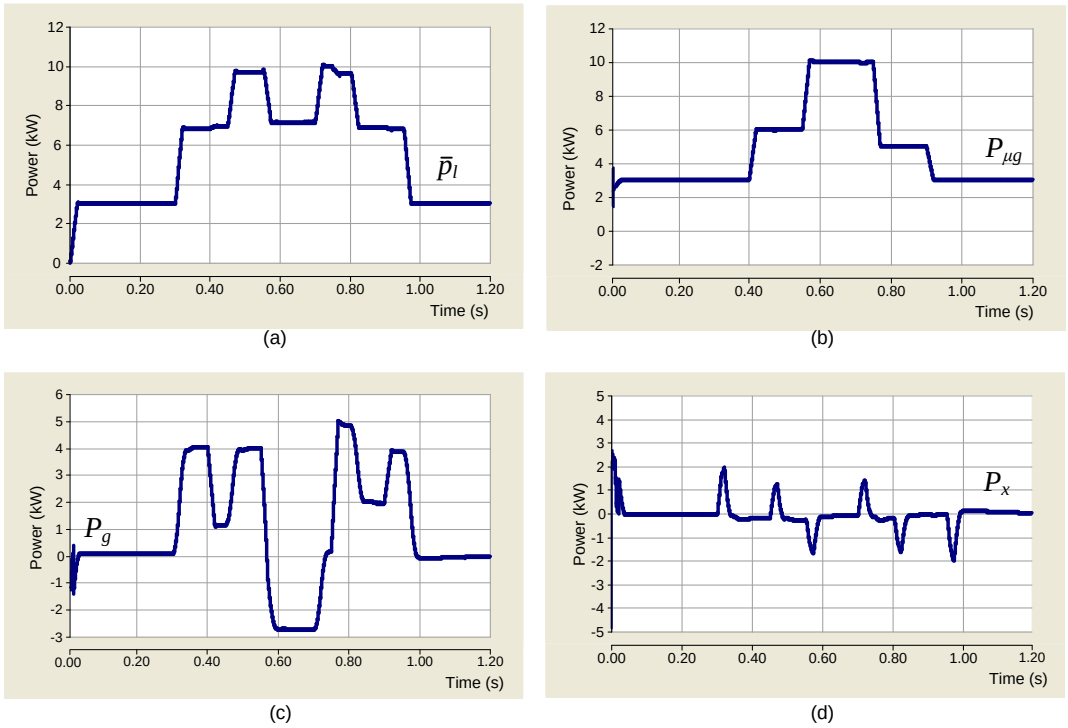

Fig. 5.19 (a) Load power (b) Main inverter power (c) Utility grid power (d) Auxiliary inverter power

A close observation will discover that there are small deviations ($t = 0.75\ s$) from a constant value in $\overline{p}_l$, this is because of the slight variation in PCC voltage. PCC voltage variation occurs due to variation in the voltage drop in the feeder impedance, which in turn is dependent on the current drawn from the utility grid. Whenever there is a change in the available power from the microgrid, the share from the utility grid changes accordingly. The relation between the utility grid voltage (v_g) and PCC voltage (v_t) can be expressed as given below,

$$v_t = v_g - i_g R_g + i_g L_g \frac{di_g}{dt}. \tag{5.14}$$

Figs. 5.19(b), (c), (d) shows the main inverter power, utility grid power and auxiliary inverter power respectively. The utility grid supplies the difference between the average active power demand by the load and the available power from the microgrid. The auxiliary inverter power is ideally zero, but it deviates at transients (load step variation).

Fig. 5.20 shows the currents drawn from the main inverter. It can be observed that

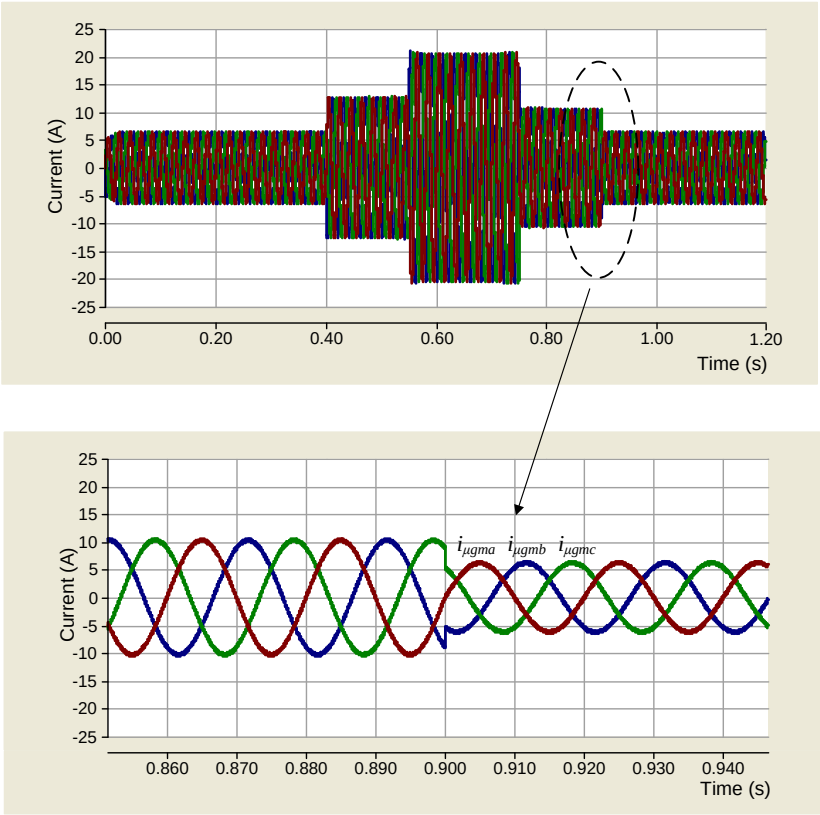

Fig. 5.20 Main inverter currents, when modified algorithm is used for reference current generation

the currents are perfectly balanced and sinusoidal which is a desired result of the dual inverter scheme. The modified reference current has enabled us to draw a balanced and sinusoidal current from the main inverter even when the system has a weak utility grid. The magnitude of the current varies depending upon the available microgrid power ($P_{\mu g}$). The currents injected by the main inverter will always be in phase with the v_{ta1}, which of the PCC voltages. Fig. 5.21 shows the utility grid currents, as desired the utility currents are also balanced and sinusoidal. The main inverter currents are always in phase with the of the PCC voltages, this is shown in Fig. 5.22, the current is scaled by a factor of 10 for better visibility.

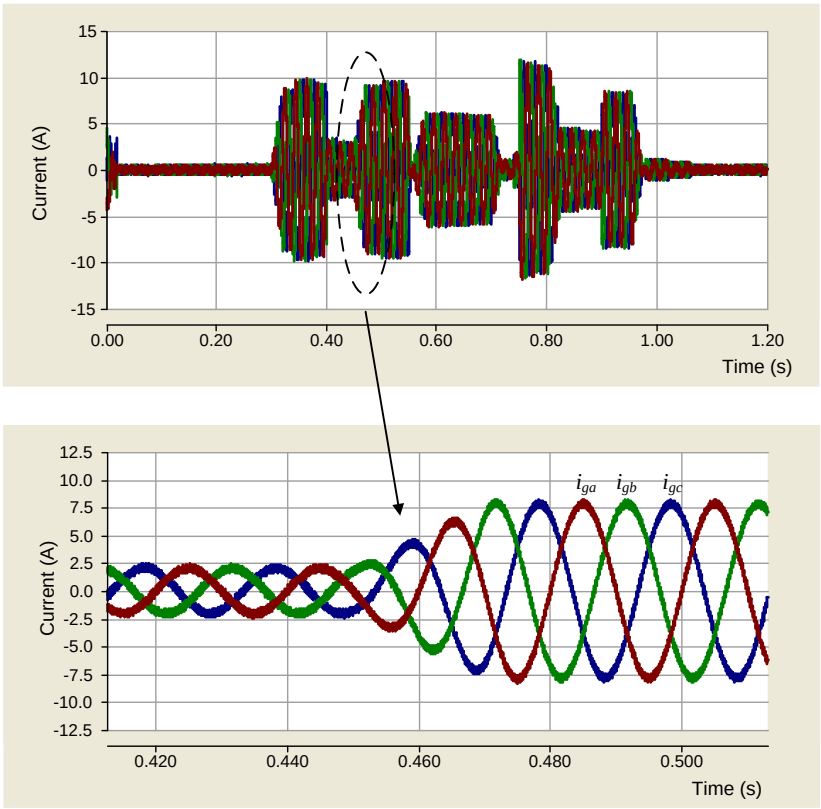

Fig. 5.21 Utility grid currents, when modified algorithm is used for reference current generation

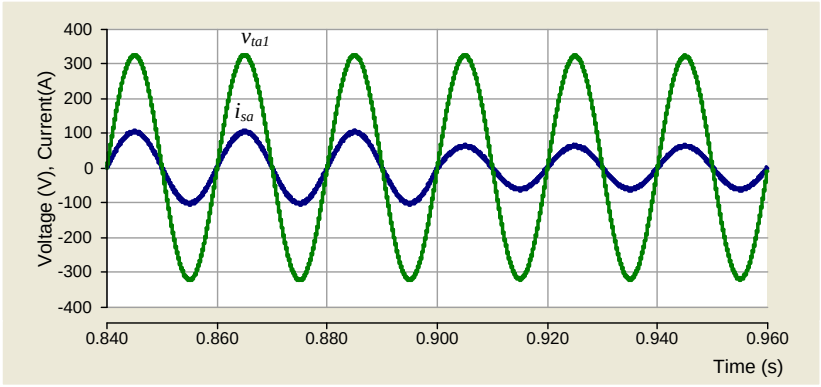

Fig. 5.22 Fundamental PCC voltage and the main inverter current

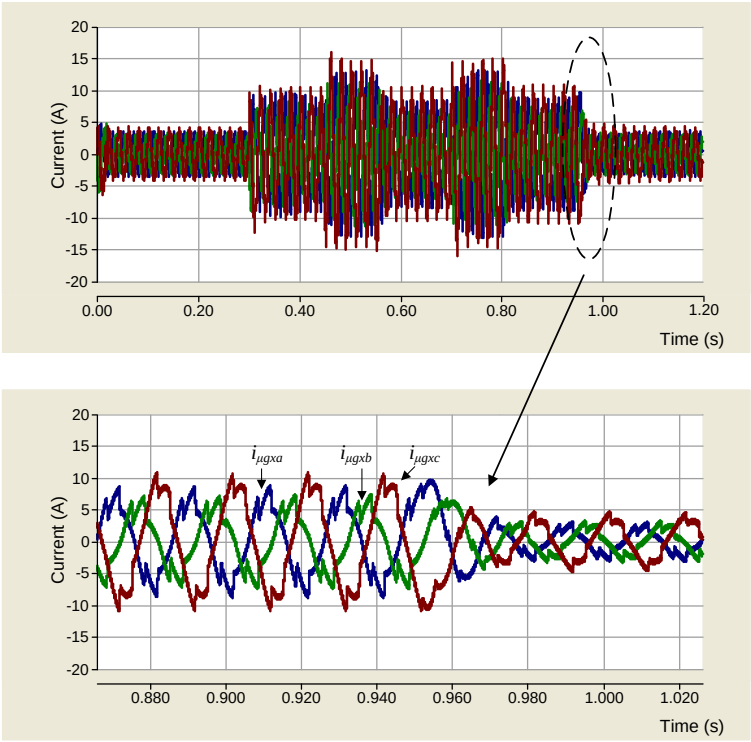

Fig. 5.23 Auxiliary inverter currents

Fig. 5.23 shows the plot of the currents which are drawn from the auxiliary inverter. These currents comprises of only reactive component and harmonic components. The fundamental powers delivered due to these currents are zero in steady state. Fig. 5.24,

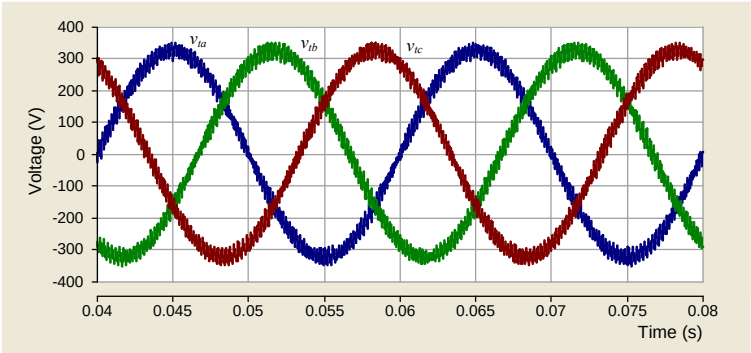

Fig. 5.24 PCC voltages, with modified algorithm

shows the PCC voltages with the usage of modified control strategy. It can be observed that we the voltages are balanced and sinusoidal with presence of switching frequency components, the THD of this waveform is 1.5% which is within acceptable limits.

5.5 Islanded Operation of DVSI Scheme

A microgrid system is said to be operating in islanded mode when it is disconnected from utility grid and operate as an autonomous entity. The system can be lead into islanded mode either intentionally or unintentionally. Intentional islanding occurs due to a planned maintenance in the utility grid, unintentional islanding occurs due to faults in the system i.e, variation in voltage or frequency. The voltage magnitude and frequency should be regulated between the specified limits in the grid codes. A voltage magnitude regulation limit of of 1.1 pu to 0.88 pu is mentioned in [25]. The loads connected to the system is supplied lonely by the microgrid in islanded operation. A DVSI scheme

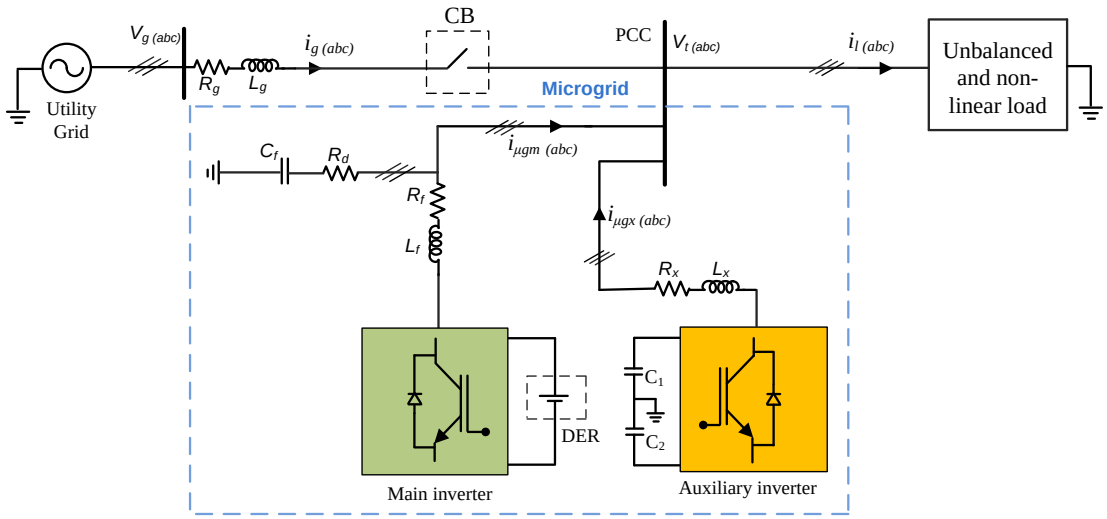

Fig. 5.25 DVSI scheme capable of islanded operation

capable of islanded mode operation is shown in Fig. 5.25. The system gets into islanded mode if Circuit Breaker (CB), is opened. In grid connected mode, the voltage and frequency at PCC is regulated by the utility grid voltage, irrespective of the microgrid. Therefore in grid connected mode, both the inverters in DVSI scheme operates in current controlled mode. Since most of the loads are voltage sensitive, the PCC voltage ($v_{t\,(abc)}$) and frequency should be regulated even in islanded mode. Therefore one of the inverters should operate in voltage control mode in order to regulate the voltage and frequency at PCC. Since the auxiliary inverter is acting as a load compensator, the main inverter is chosen to operate in voltage control mode.

5.5.1 Operation of Main Inverter in Voltage Controlled Mode

The main inverter slips into voltage controlled mode once the microgrid system is islanded. In voltage controlled mode the main inverter is made to track a reference voltage (desired magnitude and frequency), with the help of a hysteresis band controller. Thereby regulating the magnitude and frequency of the PCC voltages. The reference voltage are chosen as given in the below equation,

$$\begin{aligned} v_{taref} &= V_m sin\omega t \\ v_{tbref} &= V_m sin(\omega t - 120^\circ) \\ v_{tcref} &= V_m sin(\omega t + 120^\circ) \end{aligned} \tag{5.15}$$

Where, V_m is the desired peak value and ω is the desired frequency, of the PCC voltage. Then the error signal which is to be fed into the hysteresis controller is obtained as given in (5.16)

$$\begin{aligned} v_{ea} &= v_{ta} - v_{taref} \\ v_{eb} &= v_{tb} - v_{tbref} \\ v_{ec} &= v_{tc} - v_{tcref}. \end{aligned} \tag{5.16}$$

The voltage controlled mode operation of the main inverter can be schematically represented as shown in Fig. 5.26. During islanding, the auxiliary inverter still continues to operate in current controlled mode, thereby providing compensation to the non linear load. Therefore no modification of control strategy is required for the auxiliary inverter and it will follow the same operation as discussed in Section . Since the auxiliary inverter is compensating the unbalance and harmonics, only balanced current will be drawn from the main inverter. Therefore, in both grid connected mode and in islanded mode, the main inverter has to deliver only balanced sinusoidal current. The average active power demanded by the load will be supplied by the main inverter. The DC link voltage of the auxiliary inverter should be kept constant, for satisfactory operation of the auxiliary inverter. Therefore, the P_{loss} component required to maintain the DC link voltage of the auxiliary inverter will also be drawn from the main inverter during the

islanded mode. This summarizes the operation of both the inverters in islanded mode.

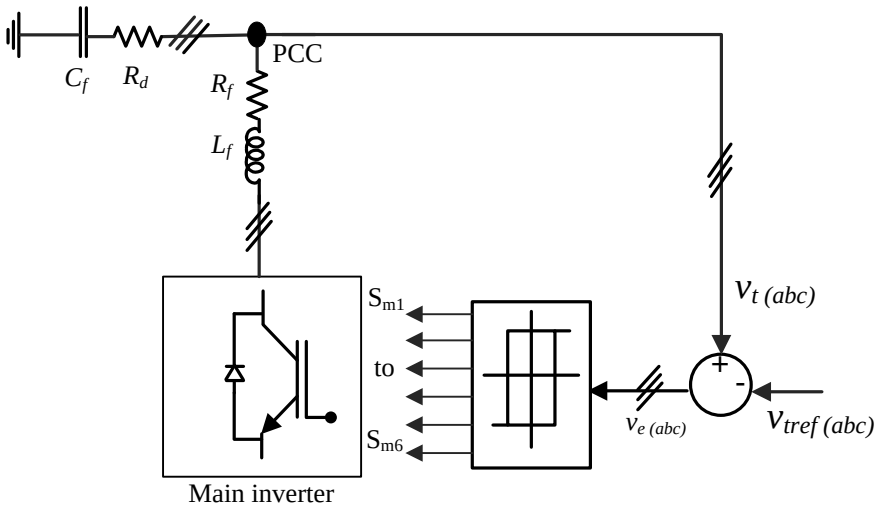

Fig. 5.26 Voltage controlled mode operation of main inverter

5.5.2 Simulation Results

The simulation study makes use of the parameters given in Table 5.3. Here the islanding operation is simulated by creating a sag in the utility voltage. At t= 0.3 s, a 20% sag is created in the utility grid voltages. This sag is detected by the system and the system changes to islanded mode. The simulation will show the grid connected mode operation and the transition into islanded operation (CB is opened). The available microgrid power is assumed to be 4 kW.

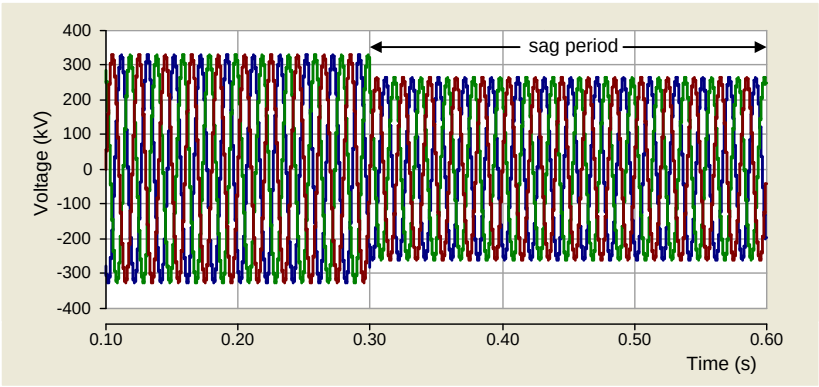

Fig. 5.27 Utility grid voltage

In grid connected mode two loads are connected to the system, critical load (CL)

of 3kW and non critical load (L_1) of 4KW. The system is simulated in such a way that the non critical load (L_1) is shed off when the system is islanded. The microgrid supplies only CL when operating in islanded mode. The utility grid voltages are shown in Fig. 5.27. It can be seen that a sag is created at t= 0.3 s. The average active powers of the load, the main inverter, the utility grid and the auxiliary inverter are shown in Figs. 5.28(a), (b), (c) and (d) respectively. It can be seen that the load average active power demand is 7 kW in grid connected mode and in islanded mode it goes down to 3 kW, since L_1 is shed off after islanding. The main inverter is generating a power of 10 kW

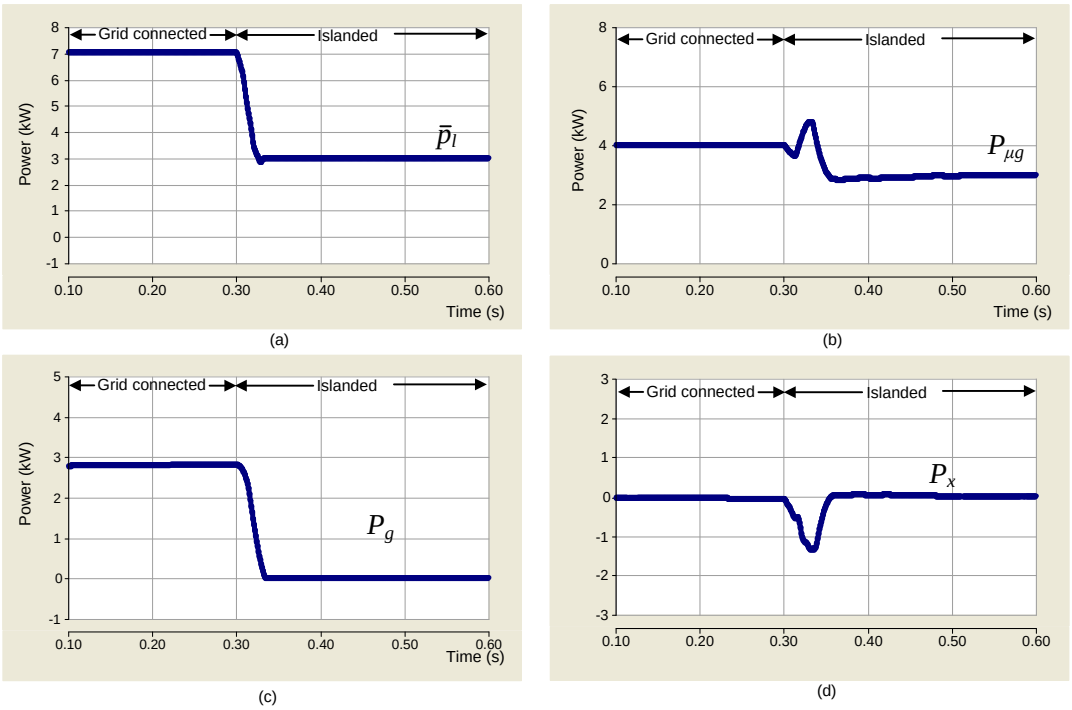

Fig. 5.28 (a) Load average active power (b) Main inverter active power (c) Utility grid active power (d) Auxiliary inverter average active power

in grid connected mode, since the power generated by main inverter is less than the load demand (grid sharing mode), the utility power is positive, it can be observed that the utility power is almost near to 3 kW. In islanded mode the main inverter changes to voltage control mode and generates the power demanded by the load and P_{loss} component, it can be observed that the power demanded by the load and the power generated by main inverter are almost same. The utility grid power share is zero in islanded mode, as it is disconnected from the system. The average active power of the auxiliary inverter is zero during the whole simulation, irrespective of the operating mode, apart from transient periods.

Now we will take a look at the various currents flowing in the system. The plot of the utility grid currents are shown in Fig. 5.29. It can be seen that the utility grid currents are balanced and sinusoidal in grid connected mode and the it falls down to zero once the islanding operation has been carried out. Fig. 5.30 shows the plots of the main

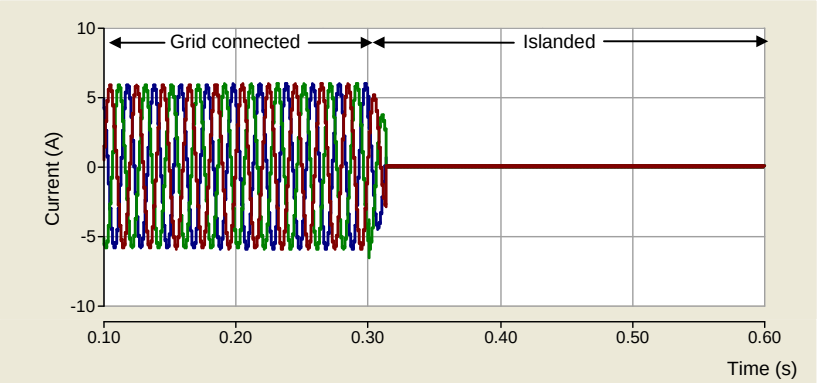

Fig. 5.29 Utility grid currents

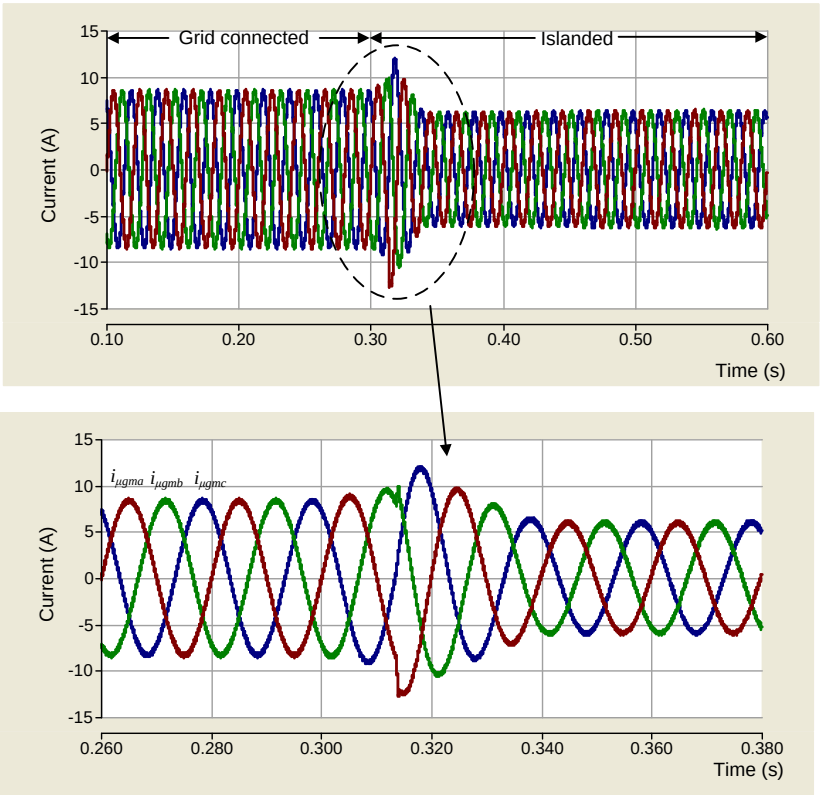

Fig. 5.30 Main inverter currents

inverter currents. It is observed that the main inverter currents are always balanced and sinusoidal, irrespective of the mode of operation. The main inverter therefore has to track only the fundamental component of the load current as desired. Since the main

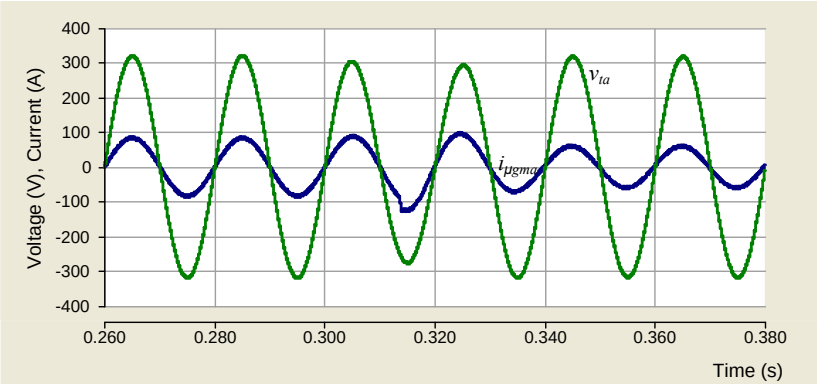

Fig. 5.31 Phase-*a* PCC voltage and main inverter current

inverter only tracks fundamental irrespective of the mode of operation, the switching frequency of the switches in main inverter will be comparatively less and this can increase the life of the switches in main inverter. The main inverter currents are always in phase with PCC voltage, it can be observed from Fig. 5.31. The current is multiplied by a factor of 10 for proper visibility. Therefore the main inverter is operating in UPF condition. The plot of the load currents are shown in Fig. 5.32. It is evident that the

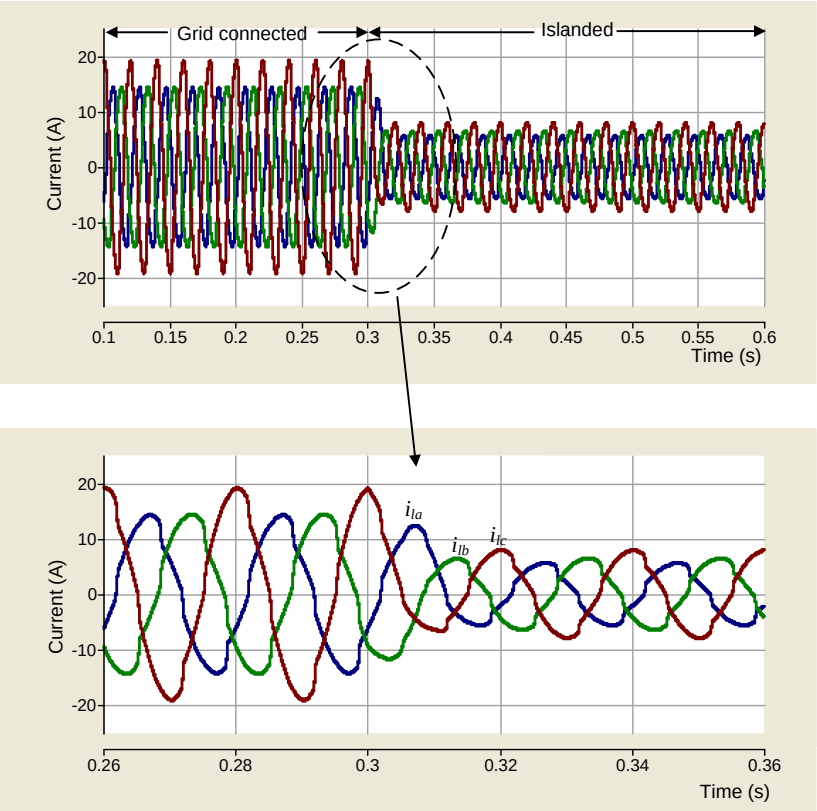

Fig. 5.32 Load Currents

currents are unbalanced and it contain harmonics. The fundamental component of these

currents are entirely supplied by the main inverter (since the system is operating in grid injecting mode), the unbalance and harmonics are supplied by the auxiliary inverter. The magnitude of the load currents are reduced after islanding, this occurs due to the shedding of load L_1 at the islanding instant.

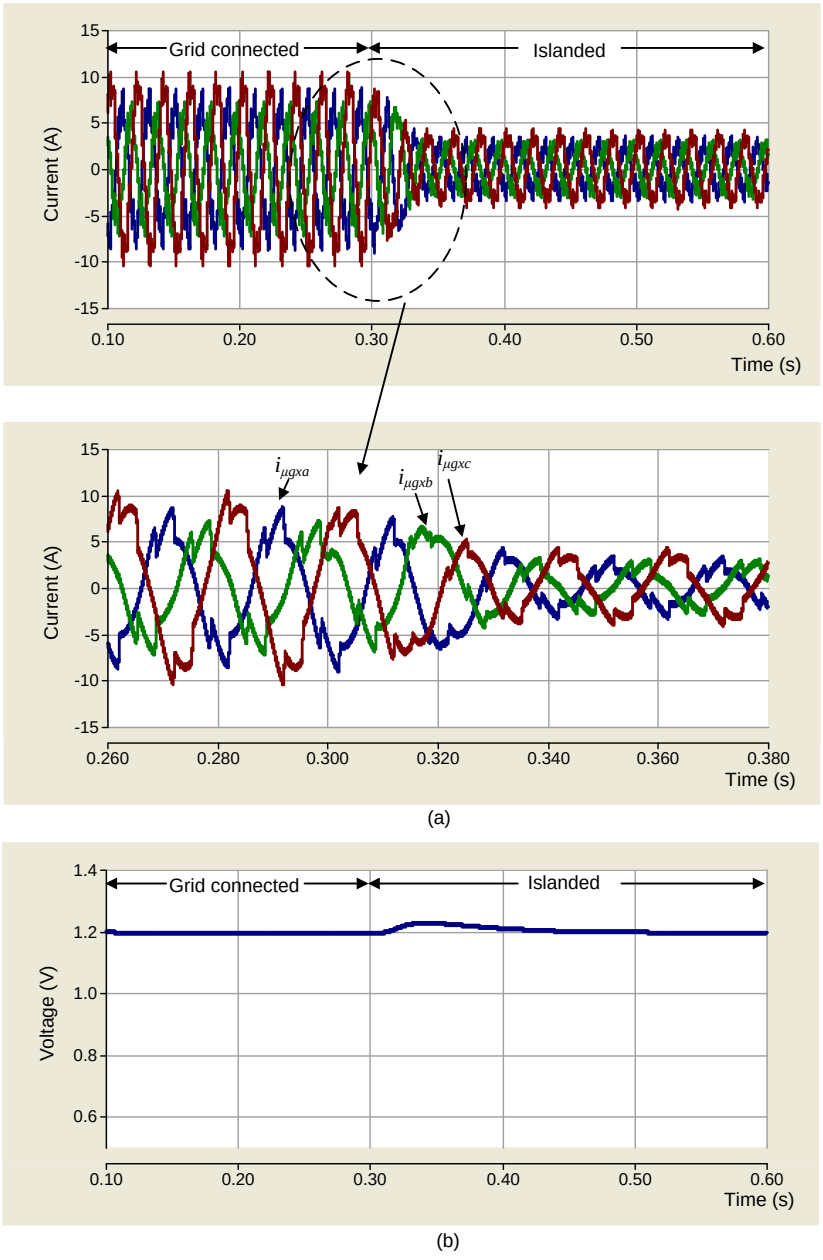

Fig. 5.33 (a) Auxiliary inverter currents (b) DC link voltage of auxiliary inverter

Fig. 5.33(a) shows the auxiliary inverter currents. These currents are responsible for the unbalance and non linear load compensation. The magnitude of the auxiliary inverter currents reduces at the islanding instant due the reduction in the load demand

(load shedding). The DC link voltage of the auxiliary inverter should be a constant to achieve the desired operation of the auxiliary inverter. The DC link voltage of the auxiliary inverter is shown in Fig. 5.33(b). It can be observed that it remains at 1200 V, it swells at the islanding instant, but it is tracked and brought back to the refernce value by the PI controller.

Fig. 5.34 shows the PCC voltage during the simulation. It is very evident from the magnified view that the PCC voltage is well regulated and also we have a very smooth transition.

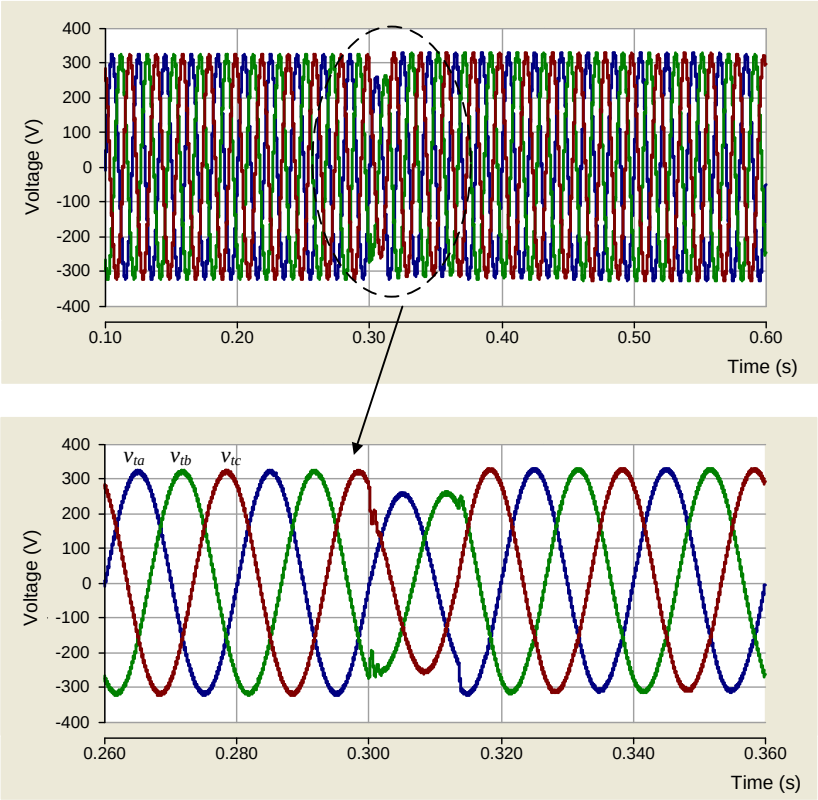

Fig. 5.34 PCC voltages

5.6 Advantages of DVSI Scheme

DVSI scheme makes use of an additional inverter when compared to a single inverter system. The usage of this additional inverter can be justified by the additional advantages due to the DVSI scheme, which are listed below,

Reliability: DVSI scheme has two inverters, which adds more reliability to the system.

Reliability increases as we are not forcing a single inverter to generate, fundamental, unbalance and harmonic components of load current. The main inverter is tracking only balanced sinusoidal current, the auxiliary inverter is tracking the entire harmonic and unbalance components demanded by the load current. This reliability makes it suitable for supplying very critical loads.

Flexibility: Both the inverters are fed from separate DC links which allows the operate independently, thus increasing the flexibility of the system. For instance, if the DC link of the main inverter is taken down for any maintenance and the main inverter is disconnected from the system, still you can utilize the the load compensation capability of the auxiliary inverter.

Better utilization of microgrid power: This DVSI scheme helps to transfer the entire power generated by the DERs into active power, since we have a separate provision for reactive power compensation . Thus increasing the active power injection capability of the system.

Reduced DC grid rating: Since the main inverter is not delivering zero sequence quantities, there is no need of split topology in main inverter. Therefore the DC grid rating of the microgrid is reduced, when compared to single inverter system.

Reduction in losses: The losses in the single inverter system and DVSI scheme are compared. The losses compared is based on the simulation studies in Section 5.3 and a similar simulation using single inverter system. The On state resistance of switch is, 0.01 Ω and the filter resistance is 0.5Ω. The losses in single inverter ($LOSS_{SI}$) is calculated using the equation 5.17.

$$Loss_{SI} = V_{dc}\, I_{dc} - \frac{1}{T}\int \left(v_{ta} i_{\mu ga} + v_{tb} i_{\mu gb} + v_{tc} i_{\mu gc}\right) dt \tag{5.17}$$

Where V_{dc} is the DC link voltage and I_{dc} is the current through the DC link.
The losses in the DVSI scheme will involve two components, losses in main inverter and losses in auxiliary inverter. The loss in main inverter ($LOSS_{MI}$) and auxiliary

inverter ($LOSS_{AI}$) can be found out as follows,

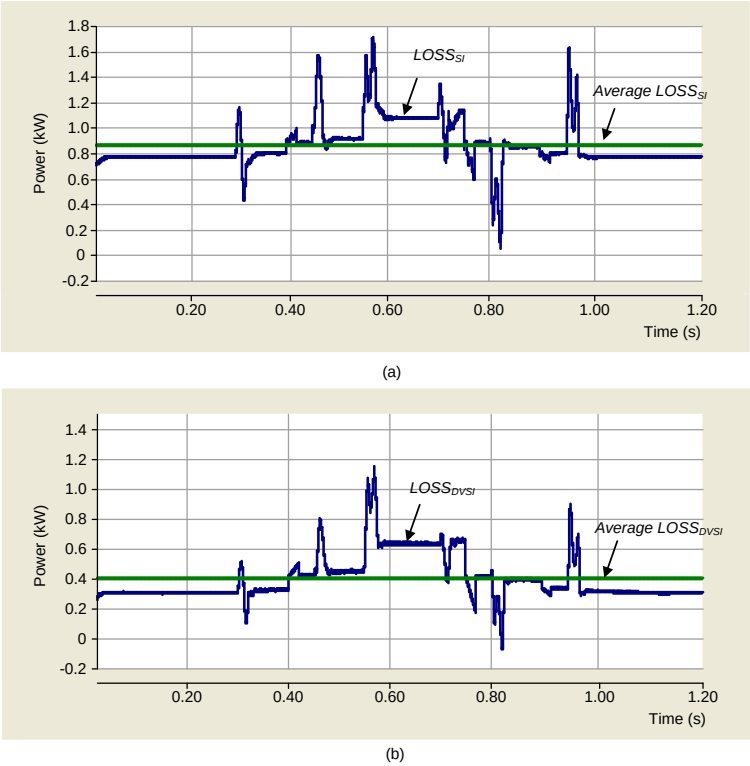

Fig. 5.35 (a) $LOSS_{SI}$ and average$LOSS_{SI}$ for entire day (b) $LOSS_{DVSI}$ and average $LOSS_{DVSI}$ for entire day

$$Loss_{MI} = V_{dcm}\, I_{dcm} - \frac{1}{T}\int (v_{ta} i_{\mu gma} + v_{tb} i_{\mu gmb} + v_{tc} i_{\mu gmc})\, dt \tag{5.18}$$

$$Loss_{AI} = V_{dc}\, I_{dc} - \frac{1}{T}\int (v_{ta} i_{\mu gxa} + v_{tb} i_{\mu gxb} + v_{tc} i_{\mu gxc})\, dt \tag{5.19}$$

The total losses in DVSI scheme($LOSS_{DVSI}$) can be found out as given below,

$$Loss_{DVSI} = Loss_{MI} + Loss_{AI} \tag{5.20}$$

Fig. 5.35(a) and (b) shows the plots of $LOSS_{SI}$ and $LOSS_{DVSI}$ respectively for the simulation in Section 5.3.3. The average of $LOSS_{SI}$ and $LOSS_{DVSI}$ for the entire day also has been found out, they are 861 W and 396 W respectively. This clearly shows that there is a considerable amount of reduction in losses when DVSI scheme is chosen.

5.7 Summary

A dual voltage source inverter scheme is proposed for microgrid systems with enhanced power quality. This scheme has two separate inverters with different responsibilities. Control algorithms were developed for grid connected and islanded mode of operations considering non stiff utility grid. In grid connected mode, there are two types of operation grid supporting mode and grid injecting mode. The two inverters operates in current controlled mode while grid connected operation as the voltage and frequency is regulated by the utility grid. In islanded mode the main inverter switches to voltage controlled mode to regulate the voltage and frequency at PCC. The existence of two inverters make the scheme more reliable and main inverter is free from supplying unbalanced or harmonic components.

CHAPTER 6

CONCLUSION AND FUTURE SCOPE

6.1 Conclusion

Conducted a detailed study on *abc* to $\alpha\beta 0$, *abc* to *dq0* and *abc* to symmetrical component transformations as they were identified to be useful in developing efficient control algorithms for microgrid systems. It was found that, depending upon the reference frames there is a variation in the elements of the transformation matrices of *abc* to $\alpha\beta 0$ and *abc* to *dq0* transformations. Therefore a generalized *abc* to $\alpha\beta 0$ and *abc* to *dq0* transformation matrix has been developed which helps to obtain the transformation matrix directly without performing any analysis on the chosen reference frame.

Control algorithms for power quality enhanced microgrid are formulated using studied transformations. The algorithms formulated enabled the grid interactive inverter to export power generated by the DG's and in addition to this, it also act as a non linear load compensator. It was observed that all the transformations were giving desired results. Then a comparative study was conducted among the algorithms and identified instantaneous symmetrical component theory as the suitable theory for conducting further studies.

A dual voltage source scheme is proposed for microgrid systems. This scheme has two separate inverters with different responsibilities. Control algorithms were developed for grid connected and islanded mode of operations. A modified control strategy is discussed for system with non stiff utility grids. In grid connected mode, there are two types of operation grid supporting mode and grid injecting mode. Both inverters are supplied from different DC links as their functionalities are different. The two inverters operates in current controlled mode while grid connected operation as the voltage and frequency is regulated by the utility grid. In islanded mode the main inverter switches to voltage controlled mode to regulate the voltage and frequency at PCC. The existence of

two inverters make the scheme more reliable. The main inverter is free from supplying unbalanced or harmonic components. It is observed that there are many more additional advantages while using DVSI scheme.

6.2 Future Scope

In this study, one main inverter and one auxiliary inverter are considered. There can be many inverters paralleled in real time microgrid system . But it is not necessary that for every main inverter there is a corresponding auxiliary inverter. There can be multiple main inverters and a corresponding auxiliary inverter. Therefore systems with multiple main inverters and single auxiliary inverter, with main inverters sharing the load demand can be subjected to future studies.

The power quality enhancement feature considered in this study focus on non linear load compensation. Voltage compensation at PCC during sag/swell is another area that should be looked upon. Incorporating voltage compensation will alleviate the problem of frequent islanding. Therefore incorporating voltage compensation at PCC is another future prospect.

REFERENCES

[1] F. Katiraei, R. Iravani, N. Hatziargyriou, and A. Dimeas, "Microgrids management," *Power and Energy Magazine, IEEE*, vol. 6, no. 3, pp. 54 –65, May-June 2008.

[2] W. Yang, A. Xin, and G. Yang, "Microgrid's operation-management containing distributed generation system," in *Electric Utility Deregulation and Restructuring and Power Technologies (DRPT), 2011 4th International Conference on*, July-2011, pp. 703–707.

[3] H. Zhou, T. Bhattacharya, D. Tran, T. Siew, and A. Khambadkone, "Composite energy storage system involving battery and ultracapacitor with dynamic energy management in microgrid applications," *Power Electronics, IEEE Transactions on*, vol. 26, no. 3, pp. 923–930, Mar, 2011.

[4] M. Delghavi and A. Yazdani, "Islanded-mode control of electronically coupled distributed-resource units under unbalanced and nonlinear load conditions," *Power Delivery, IEEE Transactions on*, vol. 26, no. 2, pp. 661–673, April, 2011.

[5] B. Kroposki, C. Pink, R. DeBlasio, H. Thomas, M. Simoes, and P. Sen, "Benefits of power electronic interfaces for distributed energy systems," *Energy Conversion, IEEE Transactions on*, vol. 25, no. 3, pp. 901–908, Sept.2010.

[6] M. Schonardie, R. Coelho, R. Schweitzer, and D. Martins, "Control of the active and reactive power using dq0 transformation in a three-phase grid-connected pv system," in *Industrial Electronics (ISIE), 2012 IEEE International Symposium on*, 28-31, May, 2012, pp. 264–269.

[7] R. S. Bajpai and R. Gupta, "Voltage and power flow control of grid connected wind generation system using dstatcom," in *Power and Energy Society General Meeting - Conversion and Delivery of Electrical Energy in the 21st Century, 2008 IEEE*, 20-24, July, 2008, pp. 1–6.

[8] Z. Chen, F. Blaabjerg, and J. Pedersen, "A multi-functional power electronic converter in distributed generation power systems," in *Power Electronics Specialists Conference, 2005. PESC '05. IEEE 36th*, 16 June, 2005, pp. 1738–1744.

[9] M. Goyal and R. Gupta, "Power flow control in distributed microgrid with wind energy system," in *Engineering and Systems (SCES), 2012 Students Conference on*, March, 2012, pp. 1–5.

[10] M. Marei, E. El-Saadany, and M. M. A. Salama, "A novel control algorithm for the dg interface to mitigate power quality problems," *Power Delivery, IEEE Transactions on*, vol. 19, no. 3, pp. 1384–1392, July, 2004.

[11] R. Majumder, A. Ghosh, G. Ledwich, and F. Zare, "Load sharing and power quality enhanced operation of a distributed microgrid," *Renewable Power Generation, IET*, vol. 3, no. 2, pp. 109–119, June.2009.

[12] J. Guerrero, P. C. Loh, T.-L. Lee, and M. Chandorkar, "Advanced control architectures for intelligent microgrids ;part ii: Power quality, energy storage, and ac/dc microgrids," *Industrial Electronics, IEEE Transactions on*, vol. 60, no. 4, pp. 1263–1270, 2013.

[13] M. Azizi, A. Fatemi, M. Mohamadian, and A. Varjani, "Integrated solution for microgrid power quality assurance," *Energy Conversion, IEEE Transactions on*, vol. 27, no. 4, pp. 992–1001, 2012.

[14] Y. Li, D. Vilathgamuwa, and P. C. Loh, "Microgrid power quality enhancement using a three-phase four-wire grid-interfacing compensator," *Industry Applications, IEEE Transactions on*, vol. 41, no. 6, pp. 1707–1719, Nov-Dec, 2005.

[15] P. Rodriguez, A. Luna, R. Mun andoz Aguilar, I. Etxeberria-Otadui, R. Teodorescu, and F. Blaabjerg, "A stationary reference frame grid synchronization system for three-phase grid-connected power converters under adverse grid conditions," *Power Electronics, IEEE Transactions on*, vol. 27, no. 1, pp. 99 –112, Jan. 2012.

[16] M. Schonardie and D. Martins, "Three-phase grid-connected photovoltaic system with active and reactive power control using dq0 transformation," in *Power*

Electronics Specialists Conference, 2008. PESC 2008. IEEE, June 2008, pp. 1202 –1207.

[17] A. Ghosh and A. Joshi, "A new approach to load balancing and power factor correction in power distribution system," *Power Delivery, IEEE Transactions on*, vol. 15, no. 1, pp. 417 –422, Jan 2000.

[18] W. C. Duesterhoeft, M. W. Schulz, and E. Clarke, "Determination of instantaneous currents and voltages by means of alpha, beta, and zero components," *American Institute of Electrical Engineers, Transactions of the*, vol. 70, no. 2, pp. 1248 – 1255, July 1951.

[19] Y. Zhu, X. Shi, and Y. Dan, "Deduction of coordinate transform for instantaneous reactive power theory and analysis on relationship between $\alpha - \beta$ and dq0 transformation," in *Electronic Measurement Instruments, 2009. ICEMI '09. 9th International Conference on*, Aug. 2009, pp. 4–922 –4–925.

[20] R. H. Park, "Two-reaction theory of synchronous machines generalized method of analysis-part i," *American Institute of Electrical Engineers, Transactions of the*, vol. 48, no. 3, pp. 716 –727, July 1929.

[21] C. L. Fortescue, "Method of symmetrical co-ordinates applied to the solution of polyphase networks," *American Institute of Electrical Engineers, Transactions of the*, vol. XXXVII, no. 2, pp. 1027 –1140, July 1918.

[22] H. Akagi, Y. Kanazawa, and A. Nabae, "Instantaneous reactive power compensators comprising switching devices without energy storage components," *Industry Applications, IEEE Transactions on*, vol. IA-20, no. 3, pp. 625 –630, May 1984.

[23] U. Rao, Mahesh.K.Mishra, and A. Ghosh, "Control strategies for load compensation using instantaneous symmetrical component theory under different supply voltages," *Power Delivery, IEEE Transactions on*, vol. 23, no. 4, pp. 2310–2317, 2008.

[24] E. Ozmedir, M. Kale, and S. Ozmedir, "A novel control method for active power

filter under non-ideal mains voltage," in *Control Applications, 2003. CCA 2003. Proceedings of 2003 IEEE Conference on*, vol. 2, June 2003, pp. 931 – 936 vol.2.

[25] I. Balaguer, Q. Lei, S. Yang, U. Supatti, and F. Z. Peng, "Control for grid-connected and intentional islanding operations of distributed power generation," *Industrial Electronics, IEEE Transactions on*, vol. 58, no. 1, pp. 147–157, Jan, 2011.